1994

Evidence For A Continuum Model Of Diffusion In Lipid Bilayer Membranes: Synthesis And Studies Of Macrocyclic Polyamides In Monolayer And Lipid Bilayer Systems

Patricia Alison Paprica

Evidence for a Continuum Model of Diffusion in Lipid Bilayer Membranes:

Synthesis and Studies of Macrocyclic Polyamides in Monolayer and Lipid Bilayer Systems

by

Patricia Alison Paprica

Department of Chemistry

Submitted in partial fulfilment
of the requirements for the degree of
Doctor of Philosophy

Faculty of Graduate Studies
The University of Western Ontario
London, Ontario
December, 1993

ISBN 0-315-90554-9

Canada

ABSTRACT

This research project is directed towards establishing the relationship between the surface areas of intermediately sized molecules (50-300Å^2) and their lateral diffusion coefficients in lipid bilayer membranes. Synthetic methods were developed to allow for the preparation of two series of macrocyclic polyamide amphiphiles, with and without fluorescent nitrobenzoxadiazole (NBD) labels, using macrocyclic polyamine aza-crown ethers as starting materials.

The geometry of the macrocyclic polyamides were determined using variable temperature NMR, which has indicated that both the C(O)-N bond and NBD-N bond in the smallest, labelled macrocyclic polyamide exhibit partial double bond character. As a consequence of this restricted bond rotation, both the amide groups and the NBD-N groups of macrocyclic polyamides can be considered as rigid planar moieties.

The surface areas occupied by the macrocyclic polyamides at the air−water interface were determined using a Langmuir film balance, and were found to be in agreement with surface area measurements of computer molecular models based on the assumption that the amide and NBD-N groups are rigid and planar. Both monolayer and computer experiments have shown that there is a systematic trend of increasing surface area throughout the two

series of macrocyclic polyamides.

Finally, the lateral diffusion coefficients of labelled macrocyclic polyamides were determined using Fluorescence Photobleaching Recovery (FPR), and the lateral diffusion coefficients of the amphiphiles were correlated with their surface areas. This correlation has shown that there is a significant dependence of lateral diffusion on the size of amphiphiles with surface areas between 30-250 $Å^2$, and is the first demonstrated dependence of lateral diffusion on surface area for amphiphiles in this size regime.

Analysis of the dependence of lateral diffusion on surface area has indicated that the lateral diffusion of macrocyclic polyamides which have surface areas smaller than or equal to that of the phospholipids which comprise the bilayer are best modelled using Free Area theory, which states that amphiphiles which are smaller than phospholipids will diffuse at the rate of lipid self diffusion. In contrast, the lateral diffusion of amphiphiles which have surface areas which are larger than that of phospholipids are best modelled using Sackman-Evans Continuum theory applied to a diffusant which does not span the bilayer membrane. This novel finding suggests that Continuum theory can be applied to the diffusion of molecules which are only slightly larger than the molecules which form the continuum.

No single thing abides; but all things flow

Fragment to fragment clings - the things thus grow

Until we know and name them.

By degrees they melt,

And are no more the things we know.

Titus Lucretius Carus

ACKNOWLEDGEMENTS

When starting new experiments during this research project, I often found myself in unfamiliar territory. I owe many thanks to the individuals who have taken the time to share what they know and help me along. For example, John Vanstone and Warren Lindsay were always supportive in the most desperate instances of instrument failure, and Dr. Harold Dick's expertise with monolayer experiments was much appreciated.

In addition, past and present Graduate Students of the Petersen group; Dr. Bruce Balcolm, Dr. Dave Bjarneson, Dr. Paul St. Pierre, Paul Wiseman, Glenn Munro, Mamta Srivastava and Claire Brown, have improved the quality of this research project and the quality of my life while I was working on it.

I owe many thanks to all the friends who have supported me during the tryin; times associated with completing a Ph.D.; Dr. Markus Kuhn, Artur Bzowski, Marci Vernon, Dr. Vince Quiquero, Tim Pope and Steve Naftel. Likewise external support from my family, my sister Diana and my significant other, Adam Di Carlo has been invaluable.

Finally, and most importantly, I wish to thank Dr. Nils Petersen. Without Dr. Petersen's creative initiative, this research project would not have started. Without Dr. Petersen's guidance and scientific talent, it would not have been finished either.

TABLE OF CONTENTS

CHAPTER 3: DETERMINATION OF MOLECULAR STRUCTURE: VARIABLE TEMPERATURE NMR AND MOLECULAR MODELLING ANALYSES

CHAPTER 4: SURFACE AREA DETERMINATION OF MACROCYCLIC POLYAMIDES AT THE AIR-WATER INTERFACE

CHAPTER 5: DETERMINATION OF LATERAL DIFFUSION COEFFICIENTS

CHAPTER 6: CONCLUSIONS

APPENDICES

LIST OF TABLES

LIST OF SCHEMES

LIST OF FIGURES

LIST OF EQUATIONS

NUMERICAL LIST OF COMPOUNDS

No.	Name(s)
1	piperazine, 1,4-diazacyclohexane
2	triaza-9-crown-3, 1,4,7-triazacyclononane
3	tetraaza-12-crown-4, cyclen, 1,4,7,10-tetrazacyclododecane
4	pentaaza-15-crown-5, 1,4,7,10,13-pentaza-cyclopentadecane
5	hexaaza-18-crown-6, hexacyclen, 1,4,7,10,13,16-hexaza-cyclooctadecane
6	1,4-dilauroyl-1,4-diazacyclohexane
7	1,4,7-trilauroyl-1,4,7-triazacyclononane
8	1,4,7,10-tetralauroyl-1,4,7,10-tetrazacyclododecane
9	1,4,7,10,13-pentalauroyl-1,4,7,10,13-pentaazacyclopentadecane
10	1,4,7,10,13,16-hexalauroyl-1,4,7,10,13,15-hexaaza-cyclooctadecane
11	dimethylaminopyridine, para-dimethylaminopyridine, DMAP
12	Proton Sponge, 8-bis(dimethylamino)-napthalene
13	NBD-Cl, nitrobenzoxadiazoyl chloride, 7-chloro-4-nitrobenz-2-oxa-1,3-diazole
14	1-(nitrobenzoxadiazoyl)-4-lauroyl-1,4-diazacyclohexane
15	1-(nitrobenzoxadiazoyl)-4,7-dilauroyl-1,4,7-triaza-cyclononane
16	1-(nitrobenzoxadiazoyl)-4,7,10-trilauroyl-1,4,7,10-tetra-azacyclododecane
17	1-(nitrobenzoxadiazoyl)-4,7,10,13-tetralauroyl-1,4,7,10,13-pentaaza-cyclopentadecane
18	1-(nitrobenzoxadiazoyl)-4,7,10,13,16-pentalauroyl-1,4,7,10,13,16-hexaaza-cyclooctadecane
19	NBD-piperazine, 1-(nitrobenzoxadiazoyl)-1,4-diazacyclohexane
20	1-(nitrobenzoxadiazoyl)-1,4,7-triaza-cyclononane
21	1-(nitrobenzoxadiazoyl)-4-lauroyl-1,4,7-triaza-cyclononane
22	1,4-diacetyl-1,4-diazacyclohexane

GLOSSARY OF ABBREVIATIONS

DMAP	para-dimethylaminopyridine
DMF	dimethylformamide
DMPC	dimyristoylphosphatidylcholine
DPPC	dipalmitoylphosphatidlylcholine
FPR	Fluorescence Photobleaching Recovery (also FRAP)
FRAP	Fluorescence Photobleaching After Recovery
N_2L_2	di-amide **6**, 1,4-dilauroyl-1,4-diazacyclohexane
N_3L_3	tri-amide **7**, 1,4,7-trilauroyl-1,4,7-triazacyclononane
N_4L_4	tetra-amide **8**, 1,4,7,10-tetralauroyl-1,4,7,10-tetrazacyclododecane
N_5L_5	penta-amide **9**, 1,4,7,10,13-pentalauroyl-1,4,7,10,13-pentaazacyclopentadecane
N_6L_6	hexa-amide **10**, 1,4,7,10,13,16-hexalauroyl-1,4,7,10,13,16-hexaaza-cyclooctadecane
N_2L[NBD]	labelled mono-amide **14**, 1-(nitrobenzoxadiazoyl)-4-lauroyl-1,4-diazacyclohexane
N_3L_2[NBD]	labelled di-amide **15**, 1-(nitrobenzoxadiazoyl)-4,7-dilauroyl-1,4,7-triaza-cyclononane
N_4L_3[NBD]	labelled tri-amide **16**, 1-(nitrobenzoxadiazoyl)-4,7,10-trilauroyl-1,4,7,10-tetra-azacyclododecane
N_5L_4[NBD]	labelled tetra-amide **17**, 1-(nitrobenzoxadiazoyl)-4,7,10,13-tetralauroyl-1,4,7,10,13-pentaaza-cyclopentadecane
N_6L_5[NBD]	labelled penta-amide **18**, 1-(nitrobenzoxadiazoyl)-4,7,10,13,16-pentalauroyl-1,4,7,10,13,16-hexaaza-cyclooctadecane
NBD	4-nitrobenz-2-oxa-1,3-diazoyl
NBD-Cl	7-chloro-4-nitrobenz-2-oxa-1,3-diazole
NBD-PE	nitrobenzoxadiazoyl-egg-phosphatidylcholine
NMR	Nuclear Magnetic Resonance
THF	tetrahydrofuran
TMS	tetramethylsilane

Chapter 1

INTRODUCTION

1.1 The Fluid Mosaic Model of Lipid Bilayer Membranes

The cell is the basic structural unit of all living organisms, and all cells are encompassed by lipid bilayer membranes. Phospholipids, which are the major component of most biological membranes, have distinct hydrophilic (polar) head groups and hydrophobic (non-polar) tail regions (Figure 1-1). Lipid bilayer membranes with hydrophilic exteriors and hydrophobic interiors spontaneously assemble from phospholipids in aqueous environments. This assembly is driven by entropy according to the hydrophobic effect.[1]

Our current understanding of biological membranes is based on the fluid mosaic model proposed by Singer and Nicolson in 1972[2] (Figure 1-2). According to this model, the phospholipids of the bilayer membrane form a continuous fluid sheet, within which proteins and phospholipids undergo rapid (two-dimensional) lateral diffusion. Diffusion of phospholipids from one face of the membrane to the other is also possible, but much slower, with a half-life on the order of hours.[3]

The dynamic nature of biological membranes, first proposed by Singer and Nicolson, is now considered to be a fundamental property of membranes which is associated with many essential biological functions. Numerous

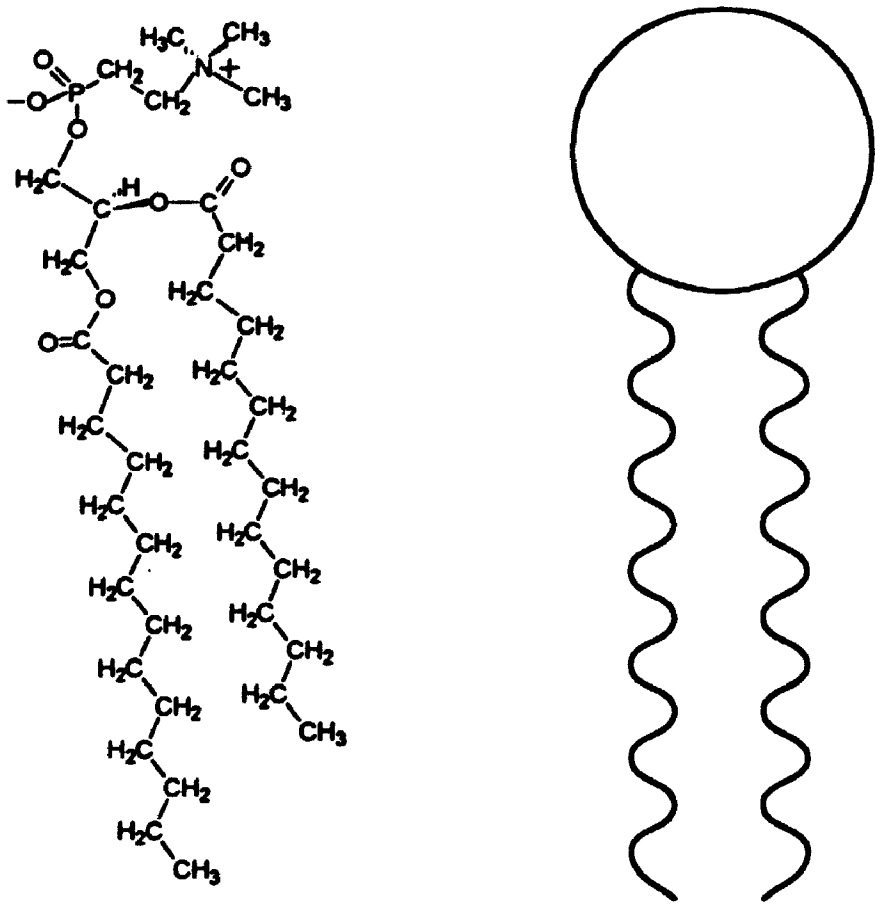

(a) (b)

Figure 1-1: Molecular Structure of a Phospholipid
(a) chemical structure of dimyristoylphosphatidylcholine
(b) schematic representation showing polar head group (O) and non-polar hydrocarbron tail groups (~)

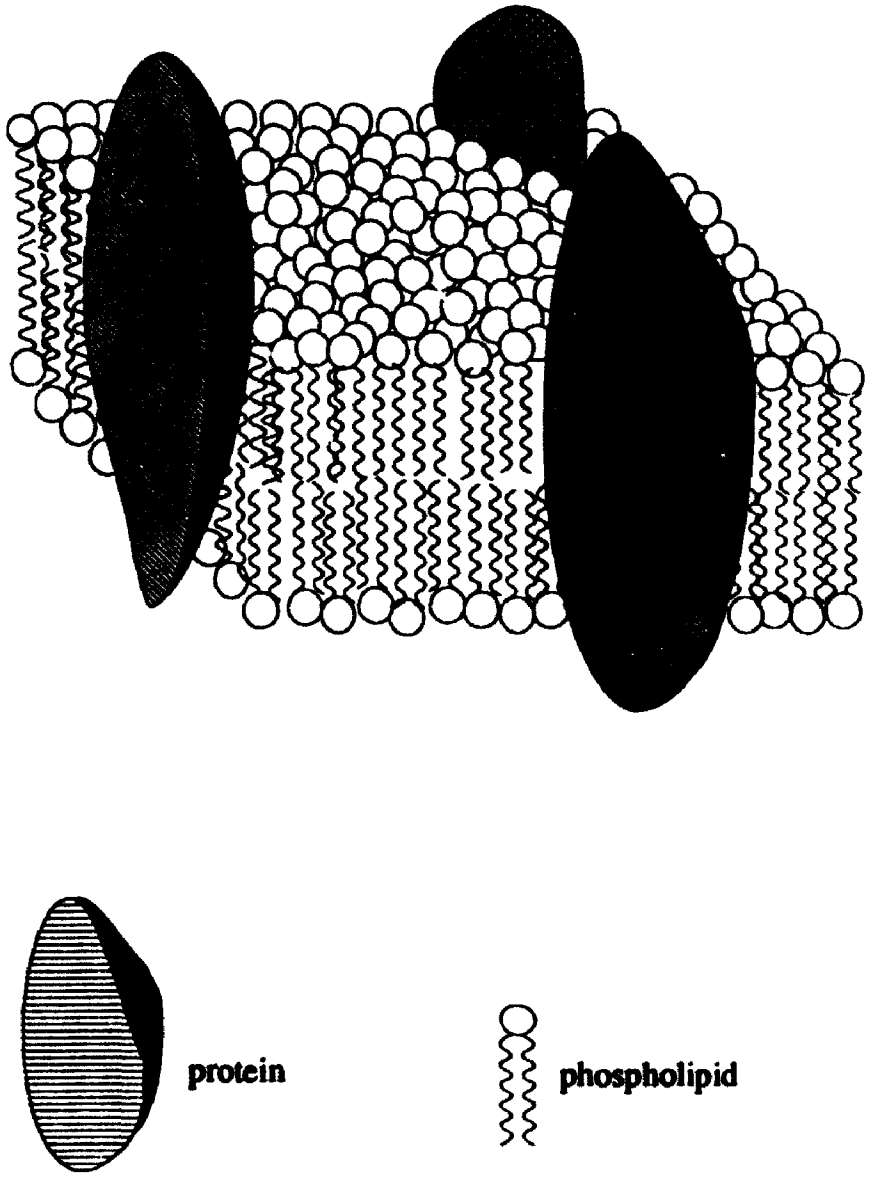

Figure 1-2: The Singer-Nicolson Fluid Mosaic Model of Cell Membranes

experiments have shown that receptor proteins in biological membranes can respond to external stimuli by moving laterally within the membrane to form specialized aggregate structures at the cell surface.[4,5,6] Receptor proteins span biological membranes, and have the ability to react with extra-cellular and intra-cellular components. The tendency of receptors to form aggregates in response to extra-cellular stimuli can be correlated to the processes by which intra-cellular reactions are triggered in response to hormone-cell interactions and cell-cell communication. Thus, the lateral mobility of membrane components is a key property which allows cells to interact with other cells and external chemical signals. Receptor clustering,[4] ligand-receptor interactions,[7] and electron transfer reactions involved in energy conversion processes[8,9] all have the potential to be limited by the rate of two-dimensional lateral diffusion at the cell surface. Our research objective was to study the dynamic nature of biological membranes, specifically lateral diffusion, with the ultimate goal of increasing our understanding of the biochemical roles of biological membranes and membrane components.

It has been shown experimentally that the lateral diffusion coefficient for diffusants in the plane of cellular membranes ranges from zero to 10^{-9} cm^2/sec, depending on the size of the diffusant, and the presence of restrictive membrane components.[10] Numerous membrane proteins have been identified and implicated with essential biochemical processes.[10] Investigation of the

lateral diffusion of membrane proteins (or lack thereof), and the effect of membrane proteins on the lateral diffusion of other cell membrane components is currently an active area of biochemical research.

Even in the absence of restrictive membrane proteins, the rate of lateral diffusion in pure phospholipid membranes exhibits a dependence on the size of the diffusant.[11] Lateral diffusion in model membrane systems composed of pure phospholipid can be as much as one order of magnitude faster than that in cell membranes. Many researchers utilize model membrane systems in order to investigate the rate of lateral diffusion in lipid bilayer membranes in the absence of macroscopic membrane structures which inhibit lateral diffusion. This thesis also focusses on model membrane systems because of their relatively simple structure compared to that of cell membranes.

1-2 Free-Area Theory: Lateral Diffusion of Small Diffusants

The rate of lateral diffusion of molecules which are comparable in size to phospholipids can be explained using Free Area theory. Free Volume theory states that the rate of diffusion of a solute is governed by the rate at which vacancies in solution are created by the diffusion of solvent molecules.[12] By analogy, Free Area theory states that diffusants which have areas smaller than, or equal to, that of phospholipids, will diffuse at the rate of lipid self diffusion.[11] The process is illustrated diagrammatically in Figure 1-3.

According to Free Area theory, once the size of the diffusant exceeds the size of the phospholipids which comprise the bilayer, a rapid exponential decrease in the rate of lateral diffusion is predicted according to Equation 1−1

Equation 1-1

$$D = A e^{\frac{-\zeta a^*}{a_f(T)}}$$

D = lateral diffusion coefficient
A = pre-exponential factor
ξ = numerical constant
a^* = close packed area of diffusant molecule
$a_f(T)$ = the mean free area per phospholipid molecule at a given temperature

Of course, this analysis of lateral diffusion is simplified, since both phospholipid molecules and diffusant molecules will fill vacant areas created by diffusion of phospholipids. Nevertheless, there is experimental evidence in support of Equation 1-1. Specifically a linear relationship between $a_f(T)^{-1}$ and log D has been noted for several phospholipids at various temperatures.[13,14] Furthermore, Balcolm and Petersen have recently demonstrated that the rate of lateral diffusion of linear hydrophobic polymers is independent of the size of the hydrophobic region of amphiphiles,[15] and have thus suggested that lateral diffusion may be predominantly surface area dependent. The predicted dependence of the lateral diffusion coefficient on the radius of the diffusant is shown graphically in Figure 1-4.

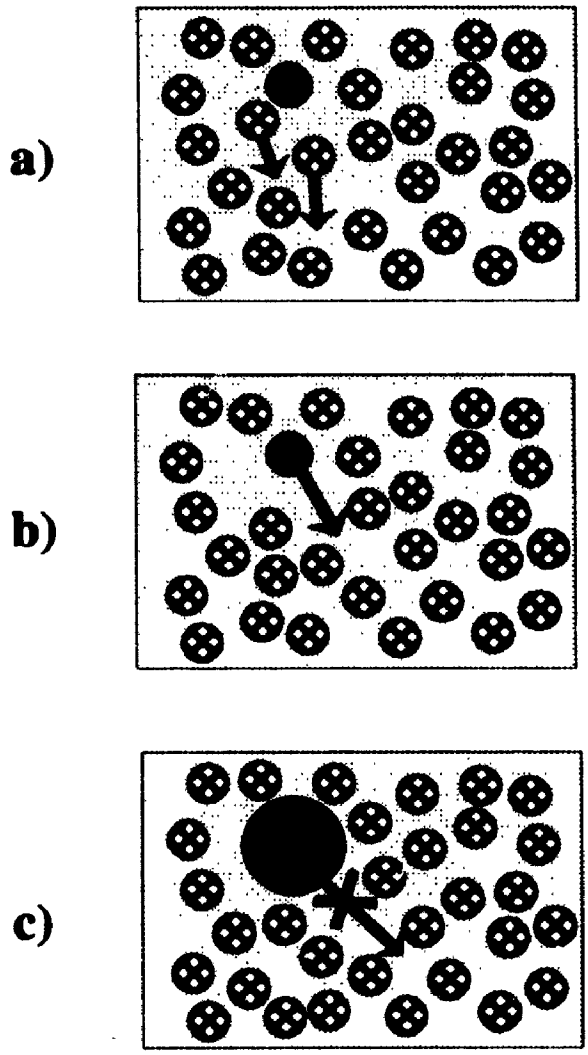

Figure 1-3: Free Area Theory of Lateral Diffusion in Lipid Bilayer Membranes

a) Lateral diffusion of phospholipid molecules creates vacant space on the surface of the bilayer membrane
b) Molecules with surface area equal to, or smaller than that of the phospholipids fill vacant spaces via lateral diffusion
c) Molecules which are have surface areas greater than phospholipids may be too large to diffuse into spaces created by the lateral diffusion of phospholipids

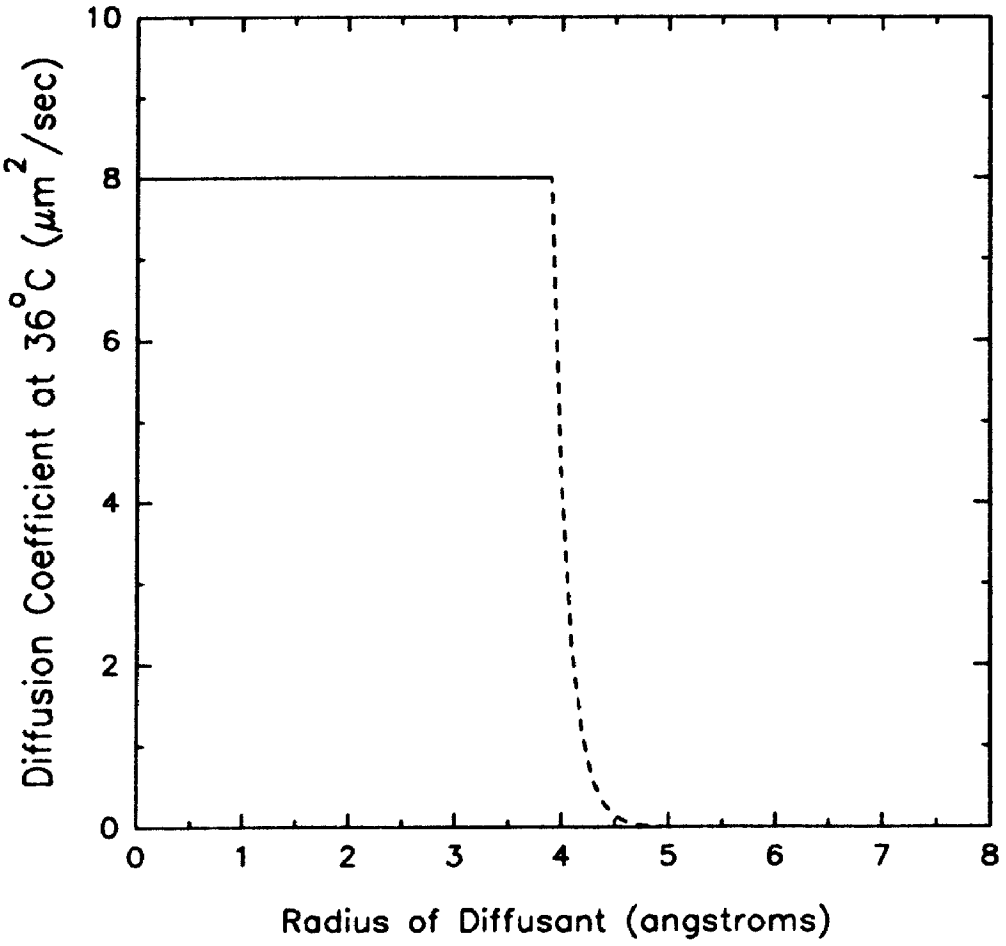

Figure 1-4: Graphical Representation of Free Area Theory

According to Free Area Theory, diffusants with surface areas less than or equal to that of the phospholipids which comprise the bilayer, diffuse at the rate of lipid self-diffusion (——). Once the size of the diffusant exceeds the size of phospholipids in the bilayer, a rapid exponential decrease in the rate of lateral diffusion is predicted (- - - -).

1.3 Continuum Theory: Lateral Diffusion of Proteins

The Stokes Einstein equation predicts the three dimensional diffusion coefficient for a spherical diffusant with radius a in a medium of viscosity η. According to this well known equation, the diffusion coefficient of a spherical particle is inversely proportional to the radius of the diffusant and the viscosity of the medium;

Equation 1-2

$$D = \frac{kT}{6\pi\eta a}$$

k = Boltzman constant
T = temperature

Saffman and Delbrück have extended the Stokes Einstein equation so that it applies to lateral diffusion in lipid bilayer membranes;[16]

Equation 1-3

$$D = \frac{kT}{6\pi\eta_m h}\ln\left[\frac{\eta_m h}{\eta_w a} - 0.5772\right]$$

η_m = viscosity of the membrane
η_w = viscosity of bathing phase (usually water)
a = radius of diffusant
h = membrane thickness

According to Saffman-Delbrück theory, proteins are treated as rigid cylinders with height h which move through a viscous, membrane sheet. Saffman-Delbrück theory is also called Continuum theory because the phospholipids which comprise the bilayer are treated as a continuum with characteristic viscosity instead of as individual molecules (Figure 1-5a).

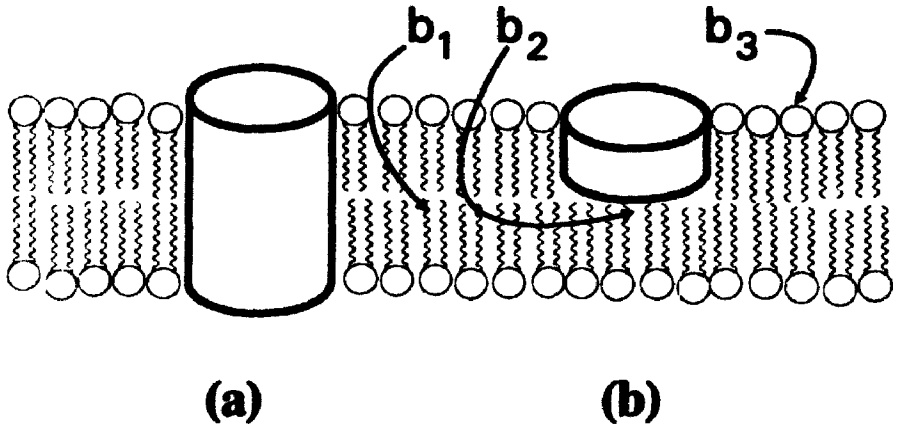

Figure 1-5: Continuum Models of Lateral Protein Diffusion in Phospholipid Membranes

(a) The diffusant (cylinder) spans the membrane (Saffman-Delbruck and Sackman-Evans theories)
(b) The diffusant (cylinder) partially penetrates the membrane (Sackman-Evans theory only)

The surfaces where frictional coefficients (b_1 , b_2 , and b_3) for Sackman-Evans theory apply are indicated

Recently, Sackman and Evans have developed a new theory to describe diffusion in lipid bilayer membranes.[17] This theory allows for differential drag on different surfaces of the diffusing amphiphile, and it is therefore possible to describe the lateral diffusion of amphiphiles which do not span the lipid bilayer using Sackman-Evans theory (Figure 1-5b). Tamm has recently applied Sackman-Evans theory to the lateral diffusion of a signal peptide which does not span the lipid bilayer.[18] According to Sackman-Evans theory, the lateral diffusion of a cylinder with height h which extends into the lipid bilayer is described according to Equation 1-4;

Equation 1-4

$$D = \frac{kT}{4\pi\eta_m} \times \left[\frac{\epsilon^2}{4} \times \left(1 + \frac{b_1}{b_2}\right) + \epsilon \times \frac{K_1}{K_0}\right]^{-1}$$

η_m is the viscosity of the membrane multiplied by the height of the diffusant and ϵ is related to the radius of the diffusant (a) according to Equation 1-5;

Equation 1-5

$$\epsilon = a\sqrt{\frac{b_2 + b_3}{\eta_m}}$$

K_1 and K_0 are first and second order modified Bessel functions of ϵ. The parameters b_1, b_2 and b_3 are frictional coefficients for the frictional force between the two layers of the membrane, the frictional force applied by the bathing phase (water) on the membrane (and the diffusant), and the frictional force applied by the membrane on the diffusant respectively.

The parameter b_1 has been estimated to be approximately equal to the frictional coefficient between two fluid lipid monolayers which has been calculated to be less than or equal to 3 x 10^5 Poise/cm.[19] If the aqueous bathing phase is considered to be semi-infinite, then the drag of the aqueous phase on the membrane, b_3, can be approximated as $b_3 \approx \mu_w^2/\eta_m$ where μ_w is the viscosity of water. As an approximation, the frictional drag of the membrane on the substrate, b_2, can be set equal to the frictional drag between the two sheets of the membrane (b_1).

For molecules such as proteins which span the lipid bilayer, the predictions for lateral diffusion from the Sackman-Evans model exhibit approximately the same size dependence as is predicted by Saffman-Delbrück theory, though the absolute values for lateral diffusion coefficients are slightly smaller. Both theories can be considered examples of Continuum theory, since both theories treat the phospholipid membrane as a continuous fluid sheet with characteristic viscosity; however, Sackman-Evans theory allows one to assume different frictional forces in different regions of the lipid bilayer.

Experimental data collected thus far support Saffman-Delbrück theory and Sackman-Evans theory[11, 12] within the normal limits of membrane viscosity (0.75-1.5 Poise)[11] for membrane protein diffusants with radii greater than 10Å. These results are illustrated graphically in Figure 1-6. In contrast with Free Area theory, Continuum theory predicts that the rate of lateral diffusion

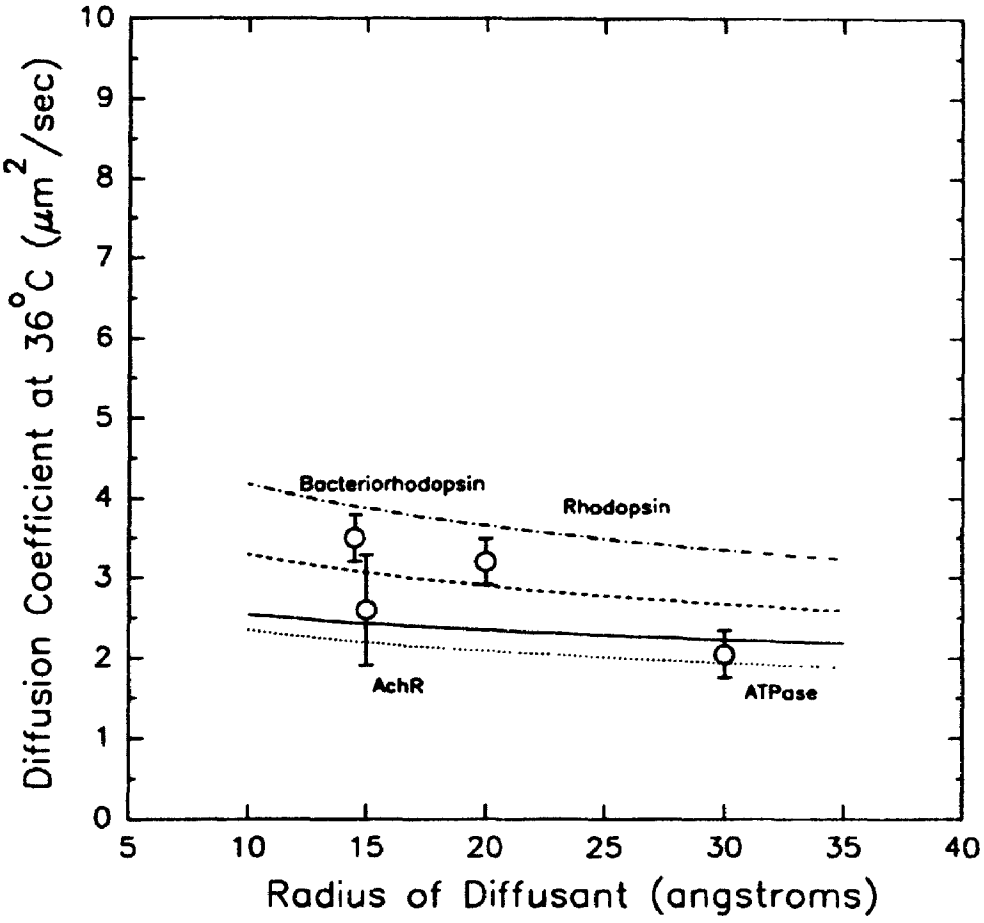

Figure 1-6: Graphical Representation of Continuum Theory

All curves are constructed based on a lipid bilayer with thickness 60 angstroms, assuming the viscosity of water is 0.01 Poise.
The predictions from Saffman Delbruck theory are shown for membrane viscosities of 1.5 Poise (·····), 1.0 Poise (- - - - -) and 0.75 Poise (- · - · -).
The predicted curve for Sackman-Evans theory (——)was constructed on $b_1=b_2=3 \times 10^{-5}$ Poise, and a membrane viscosity of 1.0 Poise.
Data points (O) were taken from Vaz et al. (reference #11, and references therein).

Both theories predict a weak dependence of lateral diffusion on surface area for amphiphiles with radii less than 10 angstroms.

exhibits a weak dependence on the radius of the diffusant.

1.4 Summary and Experimental Approach

If one plots the equations for Free Area theory and Continuum theory of lateral diffusion on the same graph, the inconsistency of the predictions of the two types of theories for molecules with surface areas between 50 and 300Å^2 is immediately apparent (Figure 1-7). These results are not surprising given the disparate treatment of phospholipids by the two theories;

- According to Free Area theory, for a given diffusant, phospholipid size is the single most important factor which determines the rate of lateral diffusion
- According to Continuum theory, phospholipids are not treated as individual molecules. Rather, the bilayer formed by phospholipids is treated as a continuous sheet with a characteristic viscosity

Our research goal was to explore the region of the graph which lies between the domains which have been experimentally correlated to Free Area and Continuum theory respectively. In addition to the theoretical interest of this region, knowledge of the lateral diffusion coefficients of intermediately sized molecules may provide insight into biochemical mechanisms involving molecules with surface areas between 50 and 300Å^2, many of which are thought to be diffusion controlled.

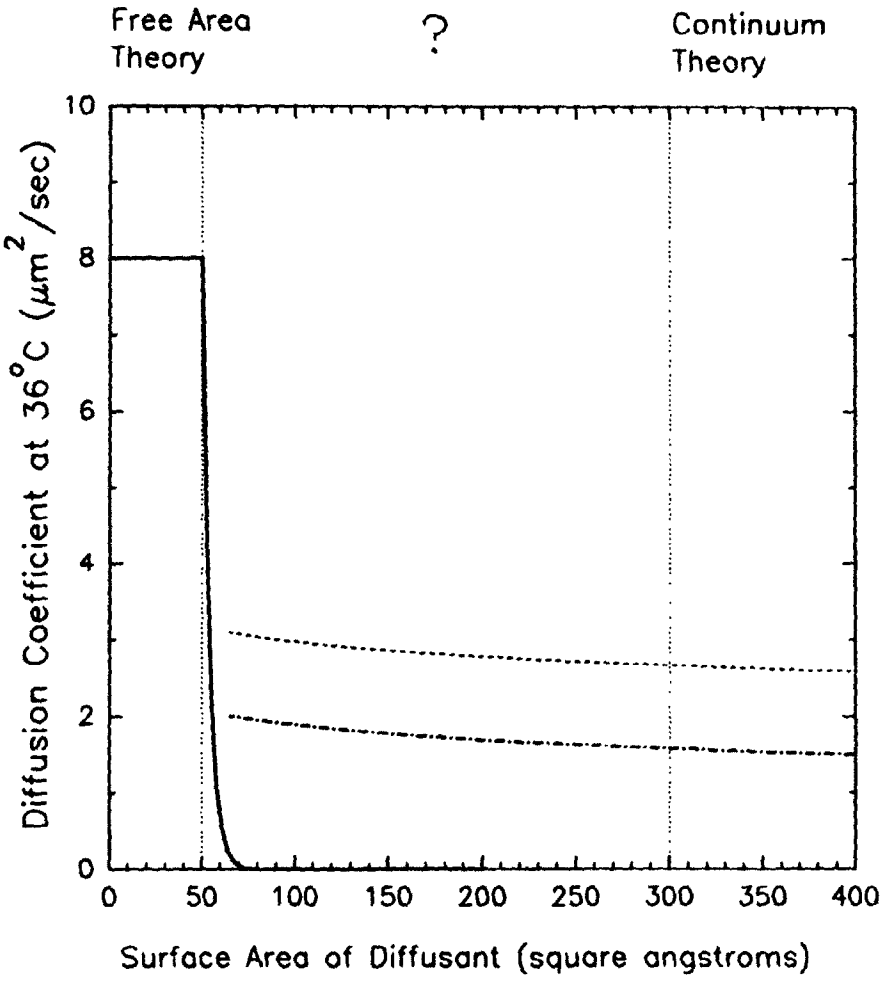

Figure 1-7: Graphical Representation of Free Area Theory and Continuum Theory

There is experimental evidence to support Free Area theory (——) for molecules with surface areas less than or equal to 50 square angstroms, and Continuum theory [Saffman-Delbruck theory (·····) and Sackman-Evans theory (·-·-·)], for molecules with surface areas greater than or equal to 300 square angstroms. Free Area theory and Continuum theory predict different trends for diffusants with surface areas in the range of 50-300 square angstroms.

Graphs for Continuum theory were generated based on a viscosity of 0.01 Poise for the aqueous phase, and a viscosity of 1.0 Poise for the membrane which is estimated to be 60 angstroms thick.

Our approach to this problem is experimental. The initial step was the synthesis of amphiphilic probes which are predicted to have surface areas which fall within the region of interest (Chapter 2), and characterization of these molecules (Chapter 3). The surface areas of the molecules of interest were determined in pure and mixed monolayers (Chapter 4). Finally, the lateral diffusion coefficients of the probes were determined in model membrane systems (Chapter 5). A summary of our findings for these experiments and directions for further research are presented in the last chapter of this thesis.

Though our experimental objective involved obtaining information about a biological question, our approach to the question was fundamentally chemical. The interdisciplinary nature of this research project has thus produced results which have significance in the disciplines of organic synthesis, physical surface chemistry, and molecular structure analysis, in addition to providing insight into the biophysical properties of phospholipid membranes.

1.5 References

1. Tanford, C., *The Hydrophobic Effect*, Wiley, New York, 1973.
2. Singer, S.J., Nicolson, G.L., The Fluid Mosaic Model of the Structure of Cell Membranes, *Science*, 1972, *175*, 720-729.
3. Zachowski, A., and Devaux, P.F., Transmembrane Movements of Lipids, *Experientia*, 1990, *46*, 644-653.
4. Schlessinger, J., The Mechanism and Role of Hormone-Induced Clustering of Membrane Receptors, *Trends. Biochem. Sci.*, 1980, 5, 210-214.
5. Petersen, N.O., Johnson, D.C., and Schlessinger, M.J., Scanning Fluorescence Correlation Spectroscopy, II., Application to Virus Glycoprotein Aggregation, *Biophys. J.*, 1986, *49*, 817-820.
6. Waugh, S.M, Willardson, B.M., Kannan, R., Labotka, R.J., and Low, P.S., Heinz Bodies Induce Clustering of Band 3, Glycophorin and Ankyrin in Sickle Cell Erythrocytes, *J. Clin. Invest.*, 1986, *78*, 111-115.
7. Dower, S.K., Titus, J.A., and Segal, D.M., The Binding of Multivalent Ligands to Cell Surface Receptors, in *Cell Surface Dynamics*, 1984, Perelson, A.S., DeLisi, C. and Wiehel, F.W., Editors, Marcel Dekker, New York, 277-328.

8. Strittmatter, P., and Rogers, M.J., Apparent Dependence of Interaction Between Cytochrome b5 and Cytochrome b5 Reductase upon Translational Diffusion in Dimyristoyl Lecithin Liposomes, *Proc. Natl. Acad. Sci*, **1975**, *72*, 2658-2661.

9. Gupte, S., Wu, E.S., Hoechli, L., Jacobson, K., Sowers, A.E. and Hackenbrock, C.R., Relationship Between Lateral Diffusion, Collision Frequency and Electron Transfer of Mitochondrial Inner Membrane Oxidation-Reduction Components, *Proc. Natl. Acad. Sci*, **1984**, *91*, 2606-2610.

10. Edidin, M., Rotational and Lateral Diffusion of Membrane Proteins and Lipids, *Current Topics in Membranes and Transport*, **1989**, *29*, 91-127, and references therein.

11. Vaz, W.L.C., Goodsaid-Zalduondo, F., and Jacobson, K., Lateral Diffusion of Lipids and Proteins in Bilayer Membranes, *FEBS Letters*, **1984**, *174*, 199-207 and references therein.

12. Cohen, M.H., Turnbull, D., Molecular Transport in Liquids and Gases, *J. Chem. Phys.*, **1959**, *31*, 1164-1169.

13. McCown, J.T., and Galla, H.J., Pressure Variation of the Lateral Diffusion in Lipid Bilayer Membranes, *Biochim. Biophys. Acta*, **1983**, *733*, 291-294.

14. Vaz, W.L.C., Clegg, R.M., Hallman, D., Translational Diffusion of Lipids in Liquid Crystalline Phase Phosphatidylcholine Multibilayers, *Biochem.*, **1984**, *24*, 781-786.

15. Balcolm, B.J., and Petersen, N.O., Lateral Diffusion in Model Membranes is Independent of the Size of the Hydrophobic Region of Molecules, *Biophys. J.*, **1993**, *65*, 630-637.

16. Saffman, P.G., and Delbrück, M., Brownian Motion in Biological Membranes, *Proc. Natl. Acad. Sci. USA*, **1975**, *73*, 3111-3113.

17. Evans, E., and Sackman, E., Translational and Rotational Drag Coefficients for a Disk Moving in a Liquid Membrane Associated with a Rigid Substrate, *J. Fluid Mech.*, **1988**, *194*, 553-561.

18. Tamm, L, Membrane Insertion and Lateral Mobility of Synthetic Amphiphilic Signal Peptides in Lipid Model Membranes, *Biochim. Biophys. Acta*, **1991**, *1071*, 123-148.

19. Merkel, R., Sackman, E., and Evans, E., Molecular Friction and Epitactic Coupling Between Monolayers in Supported Bilayers, *J. de Physique*, **1989**, *50*, 1535-1555.

Chapter 2

SYNTHESIS

2.1 Introduction

2.1.1 Necessary Criteria for Target Molecules

According to the problem outlined in Chapter 1, the first step in this research project was the synthesis of molecules which can be used to study the relationship between the lateral diffusion coefficients and the surface areas of intermediately sized molecules in lipid bilayer membranes. The synthetic target molecules must posses certain features in order for this project to be successful.

i) Primarily, the target molecules must be a series of compounds which have common structural features at the molecular level. This is an absolute requirement if one hopes to unequivocally link changes in the lateral diffusion coefficient throughout the series to changes in the surface area of the molecules (and not other factors associated with change in molecular structure).

ii) The molecules synthesized must be amphiphiles, i.e. molecules which contain distinct polar (hydrophilic) and non-polar (hydrophobic) domains.

iii) The geometry of the polar domain of each amphiphile should have restricted conformational motion, such that the geometry and surface area of the polar group can be determined without too much ambiguity.

iv) The predicted surface areas of the target molecules in bilayer phospholipid membranes must span the theoretical region in question, i.e. the range of 50Å^2 to 300Å^2 (Figure 1-7).[1]

v) In order to approximate the surface areas of the amphiphiles, the molecules must form stable monolayers at the air-water interface. These monolayers may consist either of pure amphiphile, or of amphiphile mixed with a phospholipid of known surface area.

vi) The molecules synthesized must be capable of incorporating into bilayer membranes.

vii) In order to determine the lateral diffusion coefficients of the molecules in lipid bilayer membranes, the molecules must contain a fluorescent moiety. This fluorophore should preferably be well characterized in biological membranes, and small compared to the difference between the surface areas of different molecules in the series. A maximum of one fluorophore per molecules is desired.

Of the criteria listed above, only (i)-(iv) and (vii) can be determined before a molecule has been synthesized. We postulated that if criteria (i)-(iv) and (vii) were fulfilled, then there would be a high probability that criteria (v) and (vi) would also be met.

In order for this project to succeed, it is essential that the geometry and surface areas of the labelled amphiphiles be determined accurately. Unfortunately this is not necessarily a simple procedure for large amphiphiles; however, the task can be made less daunting if a second analogous series of unlabelled amphiphiles is also prepared. Our general approach for determination of surface area was to determine the general structure and surface area of each compound in the series using unlabelled amphiphiles with the expectation that subsequent analysis of the surface areas of labelled amphiphiles, should allow one to identify the effect of fluorophore on the surface areas of large amphiphiles.

In summary, we determined that in order to fulfil our goal of correlating the surface areas and lateral diffusion coefficients of intermediately sized molecules in lipid bilayer membranes, it would be necessary to produce two series of target molecules. According to the criteria listed above, the target molecules for this project were established as:

(a) A series of amphiphiles with a common empirical formula, large enough to have predicted surface areas of 50-300Å^2.

(b) An analogous series of amphiphiles which contain one fluorescently bound molecule per amphiphile.

2.1.2 Macrocyclic Polyamines as Starting Materials

Five macrocyclic polyamines, (also called azacrowns) which have the molecular formula $(CH_2CH_2NH)_n$, n=2,3,4,5,6 (**1**, **2**, **3**, **4**, **5**) are commercially available (Figure 2-1). Characterization of the metal cation binding properties of macrocyclic polyamines,[2,3] and derivatives prepared from them,[4,5,6,7] is an active area of research which spans the disciplines of inorganic chemistry, organic chemistry and biochemistry. Extensive research has been done focussing on the pK_a[8,9] values of azacrown ethers, and pH controlled reactions of macrocyclic polyamines. [9,10] Most of the derivatives of macrocyclic polyamines which have been prepared thus far are N-alkylated macrocyclic poly-aza crown ethers. Research in the discipline of analytical chemistry has indicated that mono-N-alkylated macrocyclic polyamines can be incorporated into liquid membranes.[11]

Recent experiments have shown that certain macrocyclic polyamine derivatives which are completely N-alkylated, or N-acylated, form stable monolayers at the air-water interface.[12,13] Lehn launched this area of research which was undertaken with the initial goal of trying to synthesize ion channels which span the thickness of biological membranes.[14]

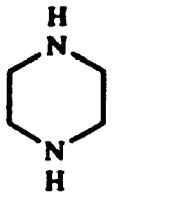

piperazine, **1**

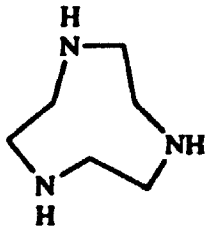

tri-aza-9-crown-3, **2**

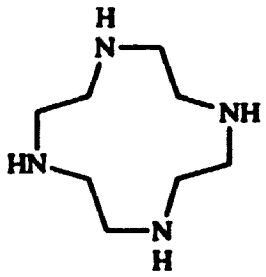

tetra-aza-12-crown-4, **3**

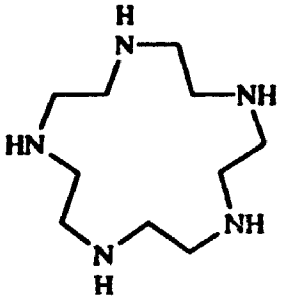

penta-aza-15-crown-5, **4**

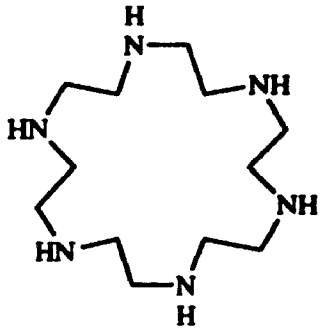

hexa-aza-18-crown-6, **5**

Figure 2-1: Commercially Available Macrocyclic Polyamines

Lehn prepared several alkyl macrocyclic polyamides and determined their surface areas in monolayers at the air-water interface.[12] Among the molecules synthesized was 1,4,7,10,13,16-hexalauroyl-1,4,7,10,13,16-hexaazacyclodecane (Figure 2-2, **10**), which had a measured surface area of 235 ± 5 Å^2 that lies within the desired range of 50-300Å^2. Though the surface areas of Lehn's macrocyclic polyamides were only recorded to very low surface pressures (compared to those in biological membranes), Lehn's data suggested that other poly-lauroyl macrocyclic polyamides may also form stable monolayers. Furthermore, Lehn's results suggested that macrocyclic hexalauroyl-hexa-amide (**10**) has a predictable disk-structure at the surface of the air-water interface.

Though many molecules can be classified as amphiphiles, a much smaller subset of this group is predicted to form stable monolayers at the air-water interface. Lehn's findings were, therefore, the single most important factor taken into consideration when determining which organic syntheses to pursue. Macrocyclic polyamides were thus selected as the unlabelled target molecules for this research project (Figure 2-2).

The abbreviation beneath each compound in Figure 2-2 is intended to represent its structure. For example, tri-amide **7** is given the abbreviation N_3L_3; N_3 indicates that the molecule is derived from tri-aza cyclononane, L_3 indicates that the molecule is the tri-lauroyl derivative. All compounds,

$R = (CH_2)_{10}CH_3$

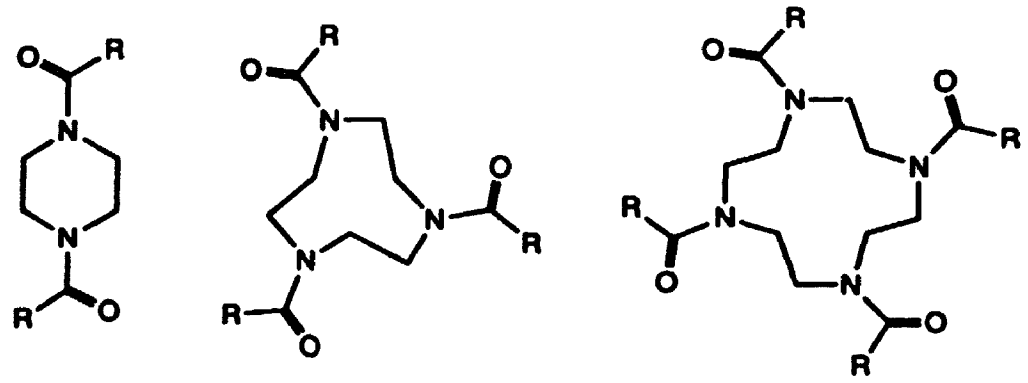

6, N_2L_2 **7**, N_3L_3 **8**, N_4L_4

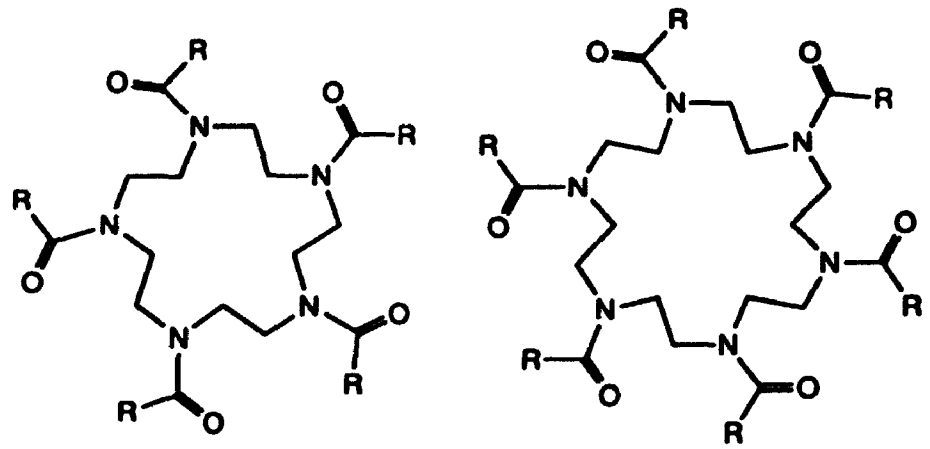

9, N_5L_5 **10**, N_6L_6

Figure 2-2: Macrocyclic Polyamide Target Molecules

including those containing less than 13 atoms in the ring, are referred to as macrocycles to emphasize the fact that the compounds comprise a series.

2.2 Synthesis of Macrocyclic Polyamides

Initially our synthetic efforts focussed on using the method developed by Lehn[12] to prepare macrocyclic polyamides with the molecular formula $(CH_2CH_2NC(O)(CH_2)_{10}CH_3)_n$, where n=2,3,4,5,6. (**6**, **7**, **8**, **9**, **10**) Lehn's method for preparation of hexa-amide **10** (N_6L_6) involves allowing the hexa-amine **5** to react with six equivalents of lauroyl chloride in dry refluxing N,N'-dimethylacetamide. Six equivalents of dimethyl-aminopyridine (DMAP, **11**) were used as a hyper-acylation catalyst and as a base to react with the HCl produced during the reaction (Scheme 2-1).

A key step in the purification procedure of Lehn's method is the addition of water to the crude reaction mixture, which is reported to result in precipitation of the amide product. In our hands, this step was not always successful even in the preparation of hexa-amide **10** (N_6L_6). Furthermore, tetra-amide **8** (N_4L_4) only formed a precipitate when NaCl was added to the solution, and the precipitate which did form contained greater than 50% (m/m) N,N'-dimethylacetamide, which was very difficult to remove. Our lack of success with Lehn's method, and variations of it which had been published elsewhere,[15] prompted us to explore alternative reaction conditions.

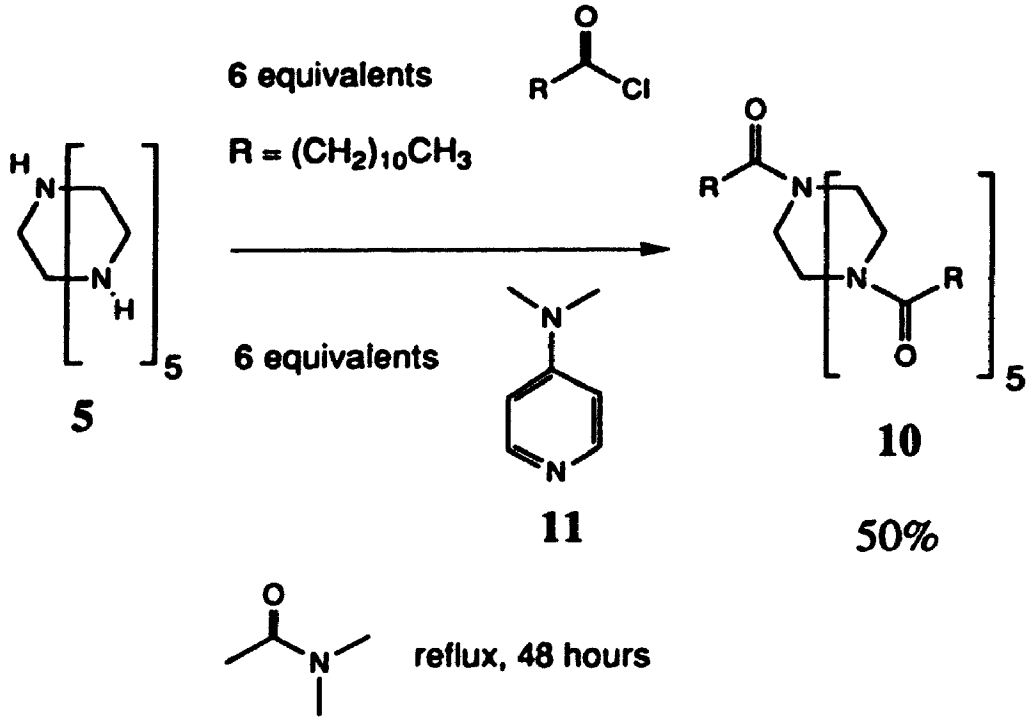

Scheme 2-1: Lehn's Method for Synthesis of Macrocyclic Polyamides

In our hands, the yield of hexa-amide **10** (N_6L_6) prepared by Lehn's method was consistently less than 50%; however, sufficient material was prepared and purified to perform solubility studies. These experiments indicated that both hexa-amine **5** and hexa-amide **10** (N_6L_6) were soluble in warm tetrahydrofuran (THF), and subsequent synthetic efforts focussed on using THF as the reaction solvent. In addition to being less toxic than N,N'-dimethyl-acetamide, THF is easily removed from reaction mixtures by rotary evaporation. The use of THF as a cosolvent in the preparation of derivatized macrocyclic polyamines has since been reported elsewhere.[13]

Because amines and acid chlorides generally react very quickly[16], it was surprising that the method used by Lehn required 48 hours reaction time. We postulated that one reason for the long reaction time might be the fact that DMAP (**11**), which has a pK_a value of 9.7,[17] is not sufficiently basic to prevent extensive protonation of macrocyclic polyamines in solution. A review of the literature indicated that the pK_1 values[10,8] of macrocyclic polyamines are in fact higher than that of DMAP (Table 2-1). Accordingly, we sought a non-nucleophilic base with a pK_a higher than 10.85, so that the equilibration in solution would favour the free base form of macrocyclic polyamine.

Proton sponge [1,8-bis(dimethylamino)-napthalene (**12**)], is a non-nucleophilic sterically hindered base with a pK_a of 12.37.[18] Proton sponge is less expensive than DMAP and less toxic. Furthermore, the free base form

	pK_1	pK_2	pK_3	pK_4	pK_5	pK_6
piperazine (1)[10]	9.83	5.56	—	—	—	—
triaza-9-crown-3 (2)[10]	10.42	6.82	<2	—	—	—
tetraaza-12-crown-4 (3)[8]	10.7	9.6	<2	<2	—	—
pentaaza-15-crown-5 (4)[10]	10.85	9.65	6.0	<2	<2	—
hexaaza-18-crown-6 (5)[10]	10.07	9.11	8.61	3.97	<2	<2

Table 2-1: pK_a Values of Macrocyclic Polyamines

of proton sponge is soluble in most organic solvents (including THF) but the protonated base is not. Therefore, removal of protonated proton sponge from the reaction mixture is achieved by simple filtration.

Based on this information we established new reaction conditions. The series of macrocyclic polyamides $(CH_2CH_2N\text{-}C(O)(CH_2)_{10}CH_3)_n$, n=2,3,4,5,6 (**6, 7, 8, 9, 10**) were prepared by reacting macrocyclic polyamines with lauroyl chloride in THF using proton sponge as base (Scheme 2-2). Initially all products were purified using silica chromatography; however, later work indicated that the white solids obtained after two recrystalizations were equally pure.

The FTIR spectrum of each of the macrocyclic polyamides exhibits characteristic Amide I, and $-CH_2-$ scissoring bands. The NMR spectra for the series of macrocyclic polyamides is consistent with a series of compounds with a common empirical formula $(CH_2CH_2N\text{-}C(O)(CH_2)_{10}CH_3)_n$, n=2,3,4,5,6 (Table 2-2, 2-3).

When evaluating stepwise reactions of the type;

$$(A\text{-}H)_n + n\ B\text{-}Y \rightarrow (A\text{-}B)_n + n\ H\text{-}Y$$

the overall yield can be calculated as the product of the yields for each step. It follows that one can calculate the average yield per step of a multi-step reaction which has n steps using a geometric mean calculation;

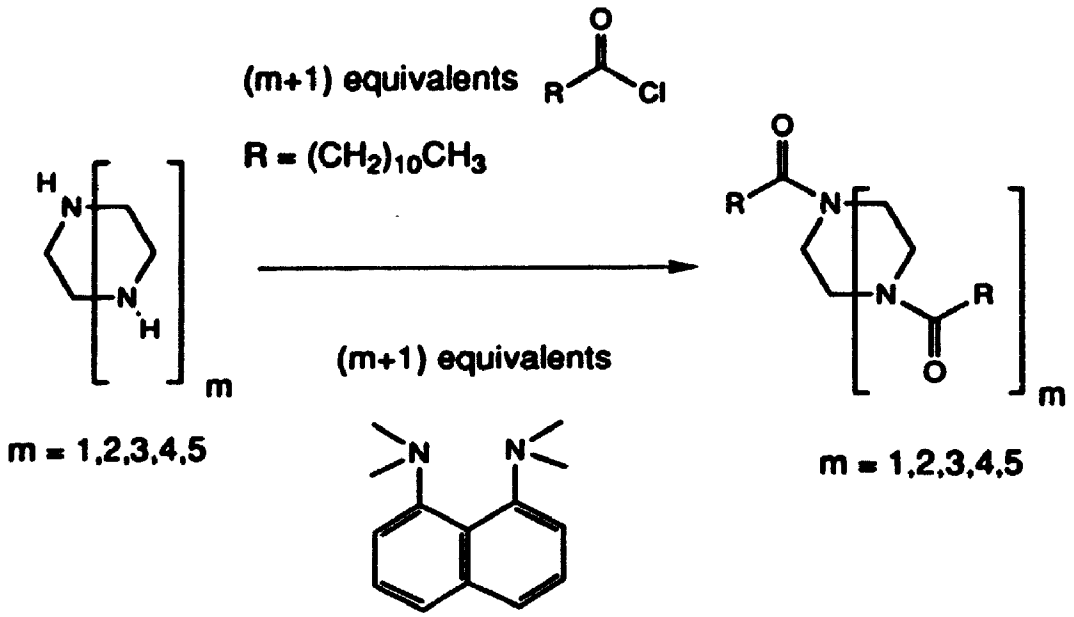

Scheme 2-2: Improved Method for Synthesis of Macrocyclic Polyamides

	δ $CDCl_3$				
	di-amide **6** (N_2L_2)	tri-amide **7** (N_3L_3)	tetra-amide **8** (N_4L_4)	penta-amide **9** (N_5L_5)	hexa-amide **10** (N_6L_6)
$C\underline{H}_2C\underline{H}_2NC(O)$	3.61 3.47 (mult, 8H)	3.69 3.40 (mult, 12H)	3.54 (br.s, 16H)	3.47 3.45 (mult, 20H)	3.57 3.42 (mult, 24H)
$C\underline{H}_2C(O)$	2.34 (t, 4H)	2.27 (t, 6H)	2.29 (br.t, 8H)	2.46 (t, 10H)	2.4 (mult, 12H)
$C\underline{H}_2CH_2C(O)$	1.63 (quint, 4H)	1.60 (quint, 6H)	1.63 (br.s, 8H)	1.64 (quint, 10H)	1.61 (br. quint, 12H)
$C\underline{H}_3CH_2$	0.88 (t, 6H)	0.88 (t, 9H)	0.88 (t, 12H)	0.88 (t, 15H)	0.88 (t, 18H)
$(C\underline{H}_2)_n$	1.26 (mult, 32H)	1.26 (mult, 48H)	1.26 (mult, 64H)	1.26 (mult, 80H)	1.26 (mult, 96H)

Table 2-2: ^1H NMR Spectra of Macrocyclic Polyamides‡

‡ Macrocyclic polyamides with the general formula:

$$(CH_2CH_2N\text{-}C(O)\text{-}(CH_2)_{10}CH_3)_n,\ n=2,3,4,5,6$$

Broad peaks are reported as br

	δ $CDCl_3$				
	di-amide **6** (N_2L_2)	tri-amide **7** (N_3L_3)	tetra-amide **8** (N_4L_4)	penta-amide **9** (N_5L_5)	hexa-amide **10** (N_6L_6)
$\underline{C}H_2\underline{C}H_2NC(O)$	45.15 41.33	51.10 48.58	~49 (br)	~48-52 (br)	~48-52 (br)
$\underline{C}H_2C(O)$	33.09	33.72	not detected	32.71	32.91 32.77 (br)
$\underline{C}H_2CH_2C(O)$	25.05	25.24	25.20	25.28	25.26
$\underline{C}H_3CH_2$	13.91	14.08	14.08	14.11	14.09
$N\underline{C}(O)$	171.81	174.46	not detected	174.15	174.32
$\underline{C}H_2)_n$	31.70 29.41(2) 29.30(2) 29.24 29.13 22.48	31.87 29.59(3) 29.51(2) 29.31 22.65	31.89 29.61(3) 29.51(2) 29.31 22.66	31.95 29.62(3) 29.54(2) 29.50 22.68	31.90 29.63(2) 25.60(2) 25.54 25.37 22.67

Table 2-3: ^{13}C NMR Spectra of Macrocyclic Polyamides[‡]

[‡] Macrocyclic polyamides with the general formula:

$$(CH_2CH_2N\text{-}C(O)\text{-}(CH_2)_{10}CH_3)_n,\ n=2,3,4,5,6$$

Broad peaks are reported as br

Equation 2-1 $$\%\ average\ yield\ per\ step = \sqrt[n]{\%\ overall\ yield}$$

This equation was used to calculated the average yield per step for the multistep acylation reactions of macrocyclic polyamines. These calculations indicated that the average yield for each step in macrocyclic polyamide syntheses was ≥89%, even though the overall yields ranged from 51-99%. The total reaction time, yields, and average yield per step are reported for macrocyclic polyamides **6-10** in Table 2-4. The yield obtained for hexa-amide **10** (N_6L_6) was approximately equal to the value reported by Lehn; however, with the new reaction conditions, preparation was faster and easier.

	yield	average yield per step‡
Di-amide **6** (N_2L_2)	99%	99%
Tri-amide **7** (N_3L_3)	77%	92%
Tetra-amide **8** (N_4L_4)	70%	91%
Penta-amide **9** (N_5L_5)	55%	89%
Hexa-amide **10** (N_6L_6)	51%	89%

Table 2-4: Experimental Yields For Macrocyclic Polyamide Syntheses

‡ Calculated as the geometric mean according to equation 2-1

2.3 Synthesis of Labelled Macrocyclic Polyamides

2.3.1 Fluorescently Labelled Target Molecules

With the unlabelled macrocyclic polyamides in hand, we began the task of synthesizing a series of fluorescently labelled analogues. The first step in this process was the determination of a suitable fluorescent probe for our experiments. Nitrobenzoxadiazole (NBD) was the obvious choice for several reasons. Fluorescent NBD derivatives are easily prepared by allowing compounds containing amino groups to react with (non-fluorescent) nitrobenzoxadiazoyl chloride (NBD-Cl, **13**) (Scheme 2-3).[19] The NBD group is one of the smallest fluorescent probes known which has a λ_{max} value in the visible region, and NBD derivatives are among the most commonly used fluorescent probes in biological systems.[20] NBD-nitrogen derivatives also have favourable optical properties, with molar extinction co-efficients of approximately 20,000 $cm^{-1}mol^{-1}L$.[21] Their λ_{max} values typically range between 450-490 nm, and derivatives are therefore readily excited by the 476.5 nm line of argon ion lasers. NBD phosphatidyl ethanolamine (NBD-PE), a NBD-derivatized phospholipid, is the single most commonly used probe for determination of lateral diffusion coefficients in lipid bilayer membranes. Finally, NBD was chosen as the fluorescent probe for this project because our research group has several years experience working with NBD derivatives.[19,21,22] Accordingly, mono-NBD-labelled macrocyclic

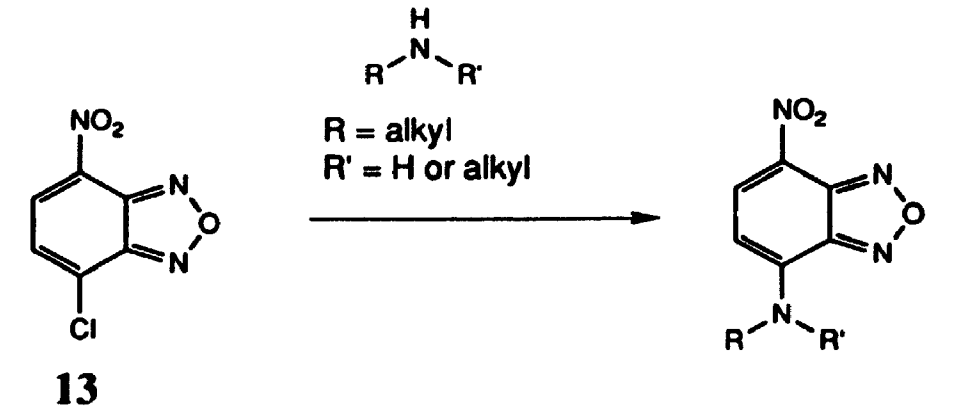

λ_{max} = 330-340 nm

λ_{max} = 450-490 nm

Scheme 2-3: Preparation of Fluorescent Derivatives Using NBD-Cl (13)

poly-lauroyl polyamides were chosen as the labelled target molecules for this research project (Figure 2-3).

2.3.2 Preparation of NBD-labelled Mono-Amide 14

Initially, our goal was to prepare macrocyclic polyamine derivatives which had been covalently linked to a single NBD fluorophore, then react these compounds with an excess of lauroyl chloride to obtain fluorescently labelled macrocyclic polyamides. This approach was ambitious. Traditionally, mono-substituted macrocyclic polyamines are difficult to prepare, because mono-substituted macrocyclic polyamines are generally more reactive than un-substituted macrocyclic polyamines.[5,6,4]

It was therefore encouraging to find that reaction of piperazine with NBD-Cl in diethyl ether at room temperature resulted in the formation of dark orange, insoluble, mono-NBD-labelled piperazine **19** (Scheme 2-4) within minutes, in quantitative yield. Compound **19** (NBD-piperazine) was characterized by NMR (D_2O with HCl) and mass spectrometry.[23] No evidence of a di-NBD-labelled species was detected.

Unfortunately, this low solubility of NBD-piperazine (**19**) which initially seemed fortuitous, eventually proved to be problematic as it became clear that NBD piperazine (**19**) was not very soluble in organic solvents. Attempts to extract NBD piperazine (**19**) from basic aqueous solutions into organic solvents

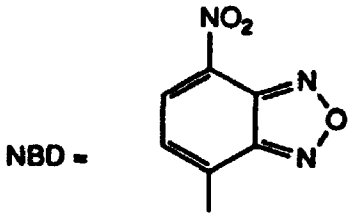

R = $(CH_2)_{10}CH_3$

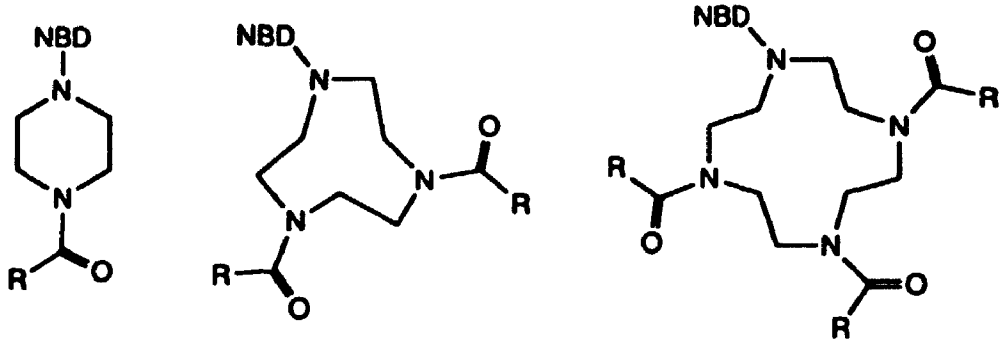

14, N_2L[NBD] **15, N_3L_2[NBD]** **16, N_4L_3[NBD]**

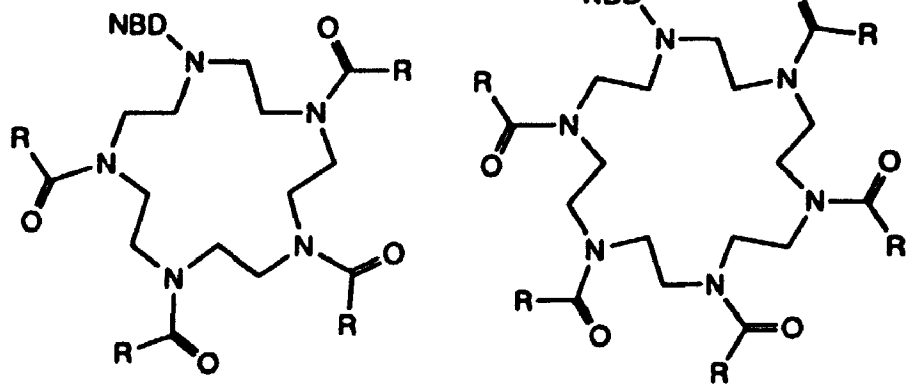

17, N_5L_4[NBD] **18, N_6L_5[NBD]**

Figure 2-3: Labelled Macrocyclic Polyamide Target Molecules

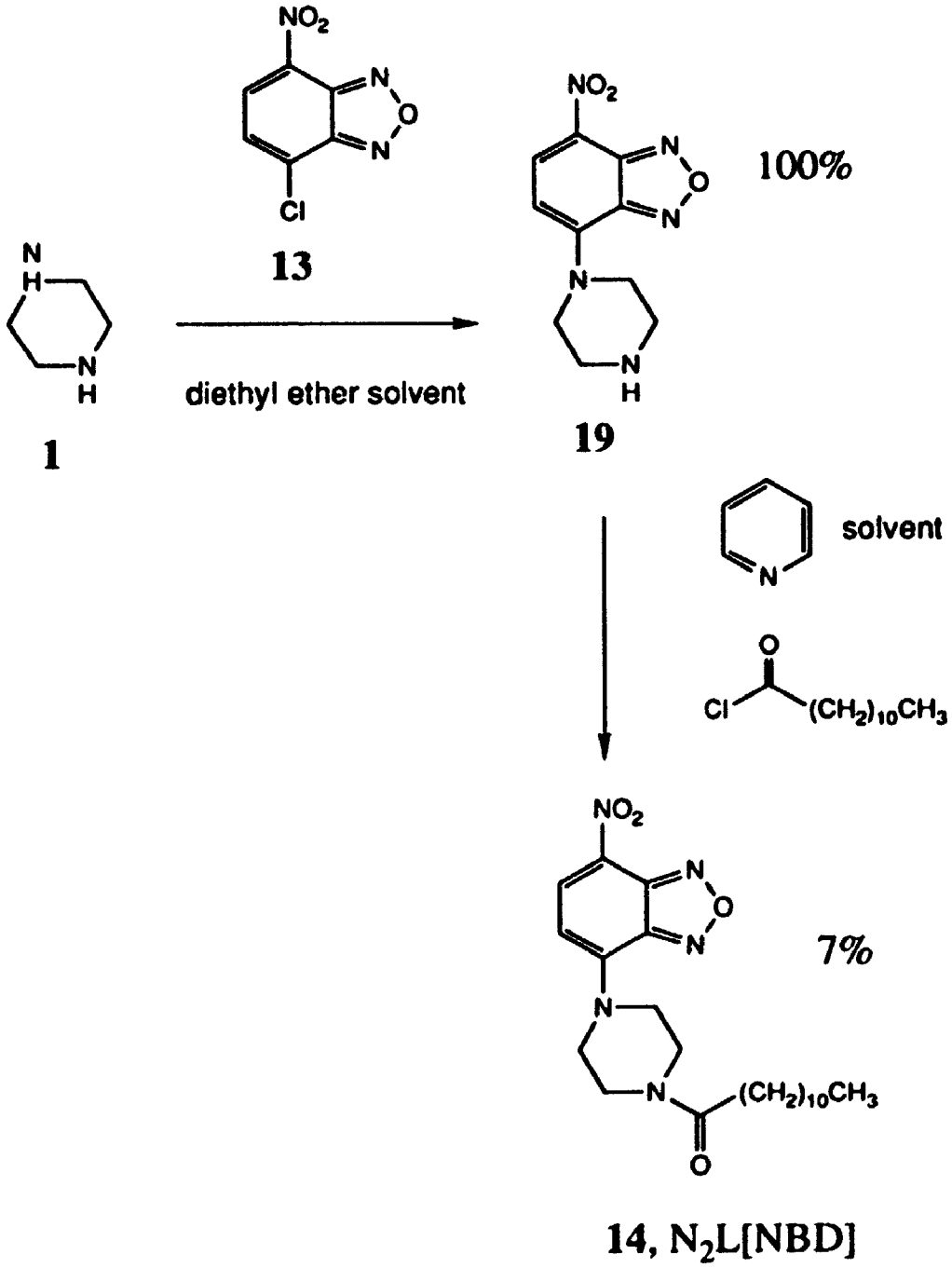

Scheme 2-4: Two-Step Method for the Preparation of Labelled Mono-Amide **14** (N_2L[NBD]

were also unsuccessful. Moreover, the NBD group proved to be unstable over the prolonged time periods at high temperatures which were required to achieve even minimal dissolution of NBD-piperazine (**19**).

Many months were spent trying to find suitable reaction conditions for conversion of NBD-piperazine (**19**) to labelled mono-amide **14** (N_2L[NBD]). Various solvents (including pyridine, DMF, THF, dimethylacetamide, CH_2Cl_2, acetonitrile) and bases (including proton sponge, triethylamine and DMAP) were tried. The best yield of labelled mono-amide **14** (N_2L[NBD]) [7%] was obtained by reacting NBD-piperazine (**19**), and lauroyl chloride in pyridine. Purification of this material was extremely difficult due to the large percentage of oxidized NBD and amine material, which complicated purification procedures (Scheme 2-4). Fortunately, sufficient material was prepared to allow for characterization, which facilitated NMR and TLC analyses of subsequent synthetic strategies for preparation of labelled mono-amide **14** (N_2L[NBD]).

Macrocyclic polyamines $(CH_2CH_2NH)_n$, n=3,4,5,6 were also treated with NBD-Cl in diethyl ether at room temperature, and in each case an orange, insoluble precipitate formed within 30 minutes. These orange solids also exhibited very low solubility in all organic solvents which we tested, and when these compounds were treated with lauroyl chloride in pyridine, none of the desired mono-labelled macrocyclic polyamide products could be isolated.

Once it became apparent that the low solubility of mono-NBD- labelled macrocyclic polyamines precluded the preparation of labelled macrocyclic polyamides by the above method, we focussed our efforts on a statistical method for preparation of labelled macrocyclic polyamides. Typically a solution containing both NBD-Cl and lauroyl chloride in THF was added to a THF solution of piperazine and proton sponge. These experiments indicated that lauroyl chloride was much more reactive than NBD-Cl, and attempts to prepare labelled mono-amide **14** (N_2L[NBD]) by this method invariably resulted in the preparation of large amounts of di-amide **6** (N_2L_2).

Accordingly, a less reactive activated lauric acid derivative was sought. Lauric anhydride is commercially available and predicted to react more slowly than lauroyl chloride with amine groups.[16] We found that when a solution containing lauric anhydride and NBD-Cl was added to a solution containing piperazine and proton sponge, appreciable amounts of labelled mono-amide **14** (N_2L[NBD]) were produced (Scheme 2-5). Di-amide **6** (N_2L_2) and labelled mono-amide **14** (N_2L[NBD]) have similar R_f values on silica gel, but could be separated by selective recrystallization of **14** (N_2L[NBD]) from 4:1 hexane:$CHCl_3$. The ratio of di-amide **6** (N_2L_2) to labelled mono-amide **14** (N_2L[NBD]) was found to vary with concentration of the reagents and the ratio of NBD-Cl to lauric anhydride. Some attempts were made to maximize the percentage yield of labelled mono-amide **14**

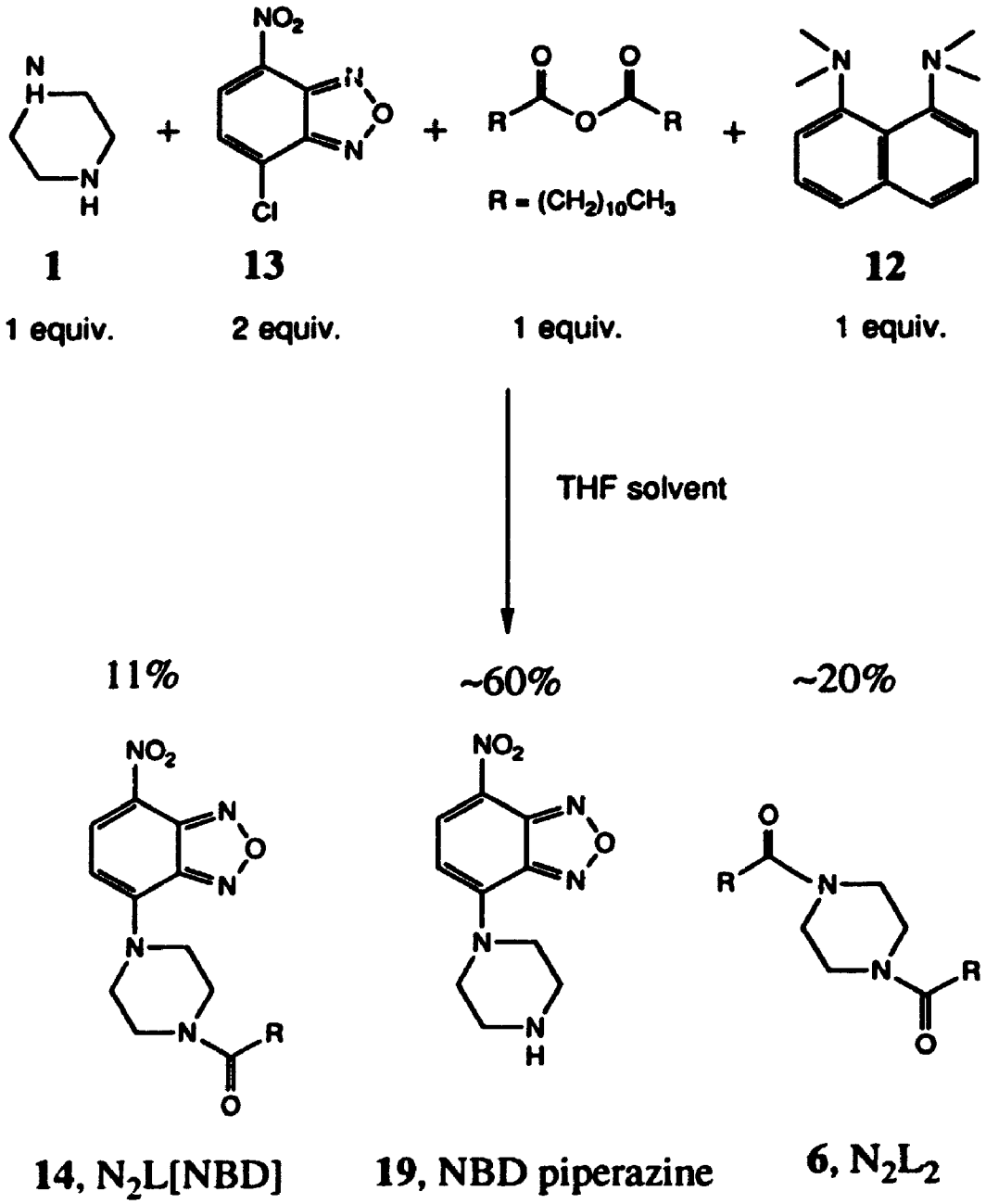

Scheme 2-5: Statistical Method for the Preparation of Labelled Mono-Amide 14 ($N_2L[NBD]$)

(N_2L[NBD]); however, optimizing the yield was not a simple task for several reasons:

(i) If the ratio of lauric anhydride:NBD-Cl was too high, di-amide **6** (N_2L_2) was the major product;

(ii) If the ratio of lauric anhydride:NBD-Cl was too low, insoluble NBD-piperazine (**19**) was the major product;

(iii) The reaction was further complicated by the fact that excess NBD-Cl and proton sponge react to form an unidentified dark-green species in solution.

The best yield of labelled mono-amide **14** (N_2L[NBD]) (11% after two recrystallizations) was obtained by adding a solution of one equivalent lauric anhydride plus two equivalents NBD-Cl in THF to a solution containing one equivalent of piperazine and one equivalent of proton sponge (Scheme 2-5). The low yield was offset by the inexpensive starting materials, and the fact that an entire preparation (excluding recrystallizations) could be performed within 30 minutes.

2.3.2 Preparation of NBD-Labelled Macrocyclic Di-, Tri-, Tetra-, and Penta-amides

When we attempted to prepare labelled di-, tri-, tetra-, and penta-amides (**15**, **16**, **17**, **18**) by the method depicted in Scheme 2-5, the yields of labelled

macrocyclic polyamides were consistently less than 1%. It was possible to prepare a small amount of labelled di-amide **15** (N_3L_2[NBD]) by combining a solution containing 1 equivalent (~0.5 mmol) of tri-amine **2** and 1.5 equivalents proton sponge with a solution containing 1.5 equivalents each of lauric anhydride and NBD-Cl. The product was purified by selective recrystallization from 5:1 hexane:$CHCl_3$ and characterized by NMR and TLC.

Once the R_f value for labelled di-amide **15** (N_3L_2[NBD]) had been determined, it was possible to monitor the reaction kinetics of the statistical, mixed lauric anhydride/NBD-Cl method qualitatively using TLC. Surprisingly, these experiments indicated that a small amount of the desired product, labelled di-amide **15** (N_3L_2[NBD]), formed as soon as the solution of NBD-Cl and lauric anhydride were added to the solution of base and proton sponge. However, most of the fluorescent material formed was present at the baseline of TLC plates developed with 1:1 diethyl ether:ethyl acetate. This material at the baseline was identified as labelled mono-amide **21** (Figure 2-4) which contains one free amino group, based on the fact that free amines are known to have a high affinity for silica gel, which is slightly acidic, and the fact that the compound was THF soluble (and therefore not likely to be mono-NBD-labelled species **20**).

Even after three hours, the relative ratio of labelled di-amide **15** : labelled mono-amide **21** appeared unchanged, and reasons for this phenomenon

were examined. The hypothesis that compound **21** may be protonated, and therefore exhibit diminished nucleophilic activity, was tested by adding a large excess of proton sponge to a small amount of the crude reaction mixture. No change in the ratio of compound **15** : compound **21** was observed.

Alternatively, it was thought that NBD-labelled macrocyclic polyamines may exhibit diminished nucleophilic activity because of the electron withdrawing property of the NBD group.[19] To test this hypothesis a large excess of lauroyl chloride was added to a small amount of the crude reaction mixture, and immediate conversion of all fluorescent material at the baseline of the TLC plate to compound **15** was noted.

From this experiment we concluded that the covalent linkage of NBD to a macrocyclic polyamine must decrease the nucleophilicity of proximate amino groups in the macrocyclic ring (Figure 2-4). Labelled, partially-acylated macrocyclic polyamines would therefore be unable to compete with unlabelled, partially-acylated macrocyclic polyamines for lauric anhydride in solution, and would therefore represent synthetic dead-ends. Based on this evidence, it is not surprising that very little labelled macrocyclic di-, tri-, tetra-, and penta-amide (**15**, **16**, **17**, **18**) could be prepared by the simple statistical approach of adding mixed lauric anhydride and NBD-Cl solutions to macrocyclic polyamine in the presence of proton sponge.

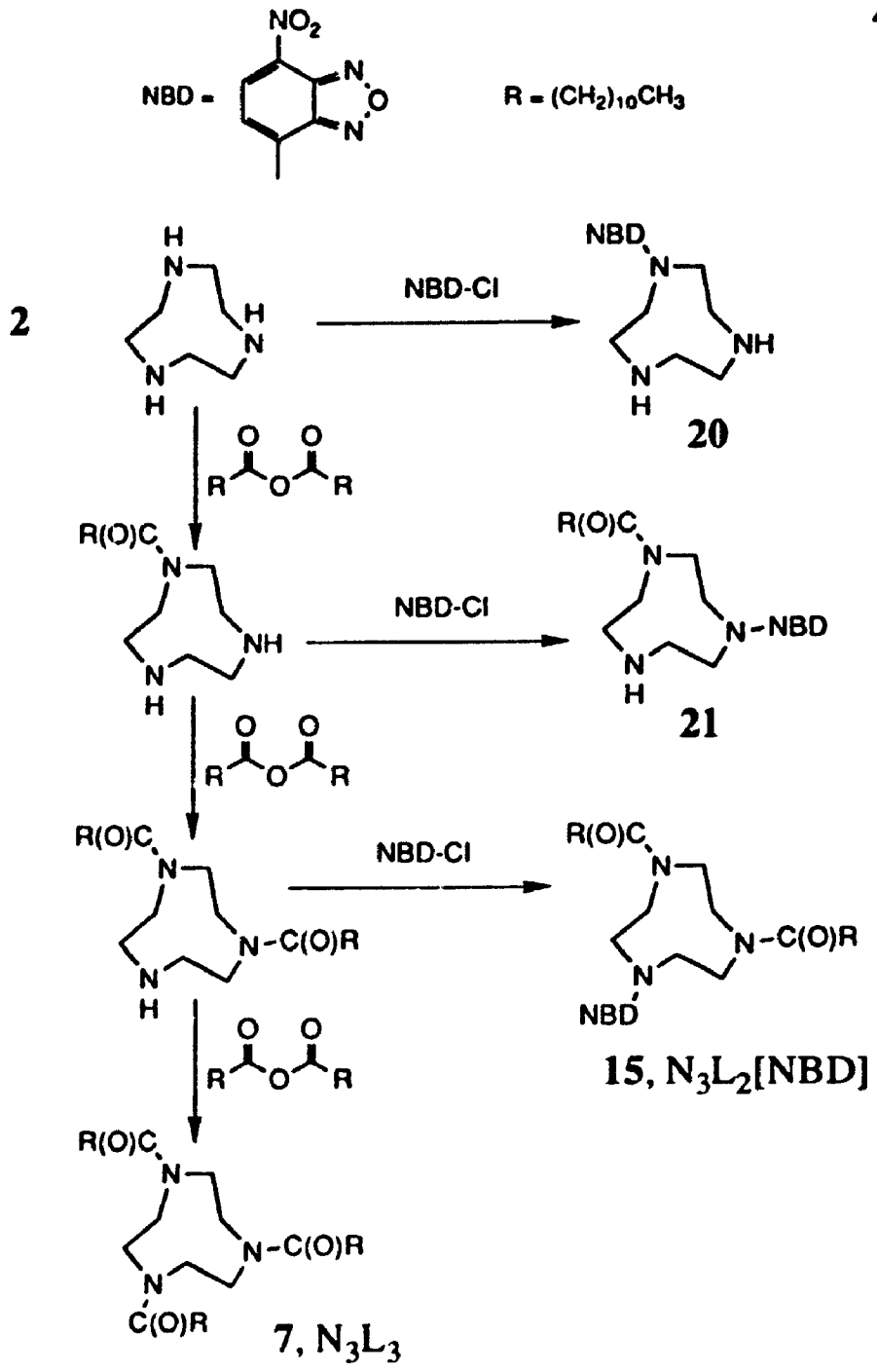

Figure 2-4: Reaction Pathway for the Production of Fluorescently Labelled Di-amide **15**, N_3L_2[NBD]

Since it was not possible to increase the amount of lauric anhydride in the reaction mixture without increasing the percentage yield of unlabelled macrocyclic polyamide, we developed a two-step procedure for the preparation of labelled di-amide **15** (N_3L_2[NBD]). In the first step, a solution containing lauric anhydride and NBD-Cl was added to a solution containing tri-amine **2** and proton sponge. After 3 minutes neat lauroyl chloride was added to the solution dropwise until all fluorescent material at the baseline of a TLC plate developed with 1:1 diethyl ether:ethyl acetate was converted to material which had been previously identified as labelled di-amide **15** (N_3L_2[NBD]) (Scheme 2-6).

The exact quantities of proton sponge, NBD-Cl and lauric anhydride which give the maximum yield of the desired labelled di-amide were hard to determine for the same reasons outlined in the preparation of labelled mono-amide **14** (N_2L[NBD]). In our hands a maximum yield of 15% labelled di-amide **15** (N_3L_2[NBD]) was obtained when a THF solution of one equivalent ($\sim$0.5 mmol for each reaction) of tri-amine **2** and 1.5 equivalents proton sponge were combined with a solution of 1 equivalent lauric anhydride and 1.5 equivalents of NBD-Cl.

Labelled tri-amide **16** (N_4L_3[NBD]), labelled tetra-amide **17** (N_5L_4[NBD]) and labelled penta-amide **18** (N_6L_5[NBD]) were each prepared by the two-step method described above (Scheme 2-6). No solvent system was

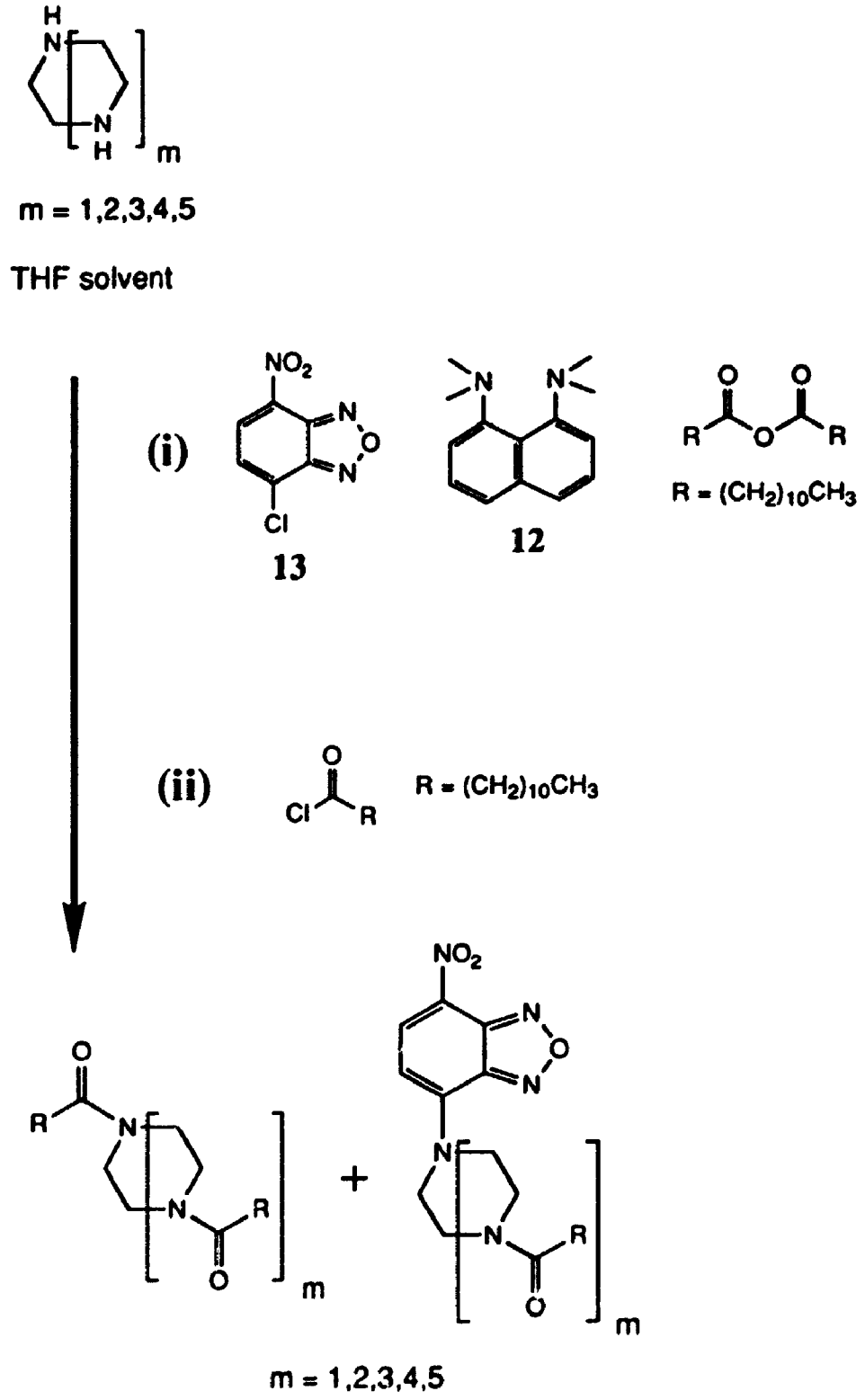

Scheme 2-6: Synthesis of Labelled Macrocyclic Polyamides

See experimental section for exact reaction conditions.

found which allowed for the purification of these compounds by selective recrystallization, nor could the unlabelled and labelled materials produced during each reaction be separated by silica chromatography. Accordingly, these compounds were purified by semi-preparative, reverse-phase HPLC using methanol:THF solvent systems.

All spectral data are consistent with the formation of the desired, labelled, polyamide products. Each compound exhibits a characteristic λ_{max} value of ~480-490 nm. The FTIR spectra of the labelled macrocyclic polyamides each contain peaks corresponding to the NBD-group (NO_2 and C=C,C=N stretching) and amide groups (Table 2-5). It is interesting to note that the peaks corresponding to aromatic C=C and C=N stretching for labelled polyamides **14** and **15** (N_2L[NBD] and N_3L_2[NBD]) are well resolved, but appear as a shoulders on the Amide I peak in larger mono-labelled macrocyclic polyamides **16**, **17**, and **18**, which contain a single NBD group but three or more amide groups.

The ^{1}H NMR data for unlabelled macrocyclic polyamides are presented in Table 2-6. The spectra of the labelled macrocyclic polyamides contain signals due to protons on the alkyl chains and the methylene groups of the macrocyclic ring, which were also present in the spectra of analogous unlabelled macrocyclic polyamides. However, the ^{1}H NMR spectra of NBD-labelled polyamides also contain signals corresponding to protons on the

	FTIR Peaks (cm^{-1})				
	labelled mono-amide **14** (N_2L[NBD])	labelled di-amide **15** (N_3L_2[NBD])	labelled tri-amide **16** (N_4L_3[NBD])	labelled tetra-amide **17** (N_5L_4[NBD])	labelled penta-amide **18** (N_6L_5[NBD])
Amide I stretch (very strong)	1653	1653	1651	1651	1651
Aromatic C=N, C=C stretch (strong)	1613	1623	1618 (shoulder on Amide I)	1617 (shoulder on Amide I)	1618 (shoulder on Amide I)
Aromatic -NO_2 antisymmetric stretch (very strong)	1558	1557	1557	1557	1558
-CH_2- scissoring (very strong)	1472	1472	1472	1472	1473
Aromatic -NO_2 symmetric stretch (very strong)	1332	1337	1338	1339	1317

Table 2-5: FTIR Spectra of Labelled Macrocyclic Polyamides

	δ $CDCl_3$				
	labelled mono-amide **14** (N_2L[NBD])	labelled di-amide **15** (N_3L_2[NBD])	labelled tri-amide **16** (N_4L_3[NBD])	labelled tetra-amide **17** (N_5L_4[NBD])	labelled penta-amide **18** (N_6L_5[NBD])
CH=C<u>H</u>-NO_2	8.40 (AB pattern, 1H, 9Hz)	8.46 (AB pattern, 1H, 9Hz)	8.50 (AB pattern, 1H, 9Hz)	8.60 (AB pattern, 1H, 9Hz)	8.50 (AB pattern, 1H)
C<u>H</u>=CH-NO_2	6.30 (AB pattern, 1H, 9Hz)	6.20 (AB pattern, 1H, 9Hz)	6.55 (br. AB pattern, 1H)	7.02 (AB pattern, 1H, 9Hz)	not detected
$C\underline{H}_2C\underline{H}_2N$	3.75-4.46 (mult, 8H) peaks at 4.28 4.03 3.97 3.84	3.27-4.38 (mult, 12H) peaks at 4.31 4.13 3.74 3.36	3.22-4.50 (br.mult, 16H) peaks at 3.72 4.09	3.48-4.45 (mult, 20H) peaks at 4.24 3.78 3.53 3.44	3.15-4.18 (mult, 24H) peaks at 4.13 3.64 3.47 3.43
$C\underline{H}_2C(O)$	2.40 (t, 2H)	2.27 (mult, 4H)	2.31 (br.t, 6H)	2.53 (mult, 8H)	2.40 (mult, 10H)
$C\underline{H}_2CH_2C(O)$	1.68 (quint, 4H)	1.60 (br. mult, 4H)	1.63 (br. mult, 6H)	1.64 (br. mult, 8H)	1.61 (br. mult, 10H)
$C\underline{H}_3CH_2$	0.88 (t, 3H)	0.88 (t, 6H)	0.88 (t, 9H)	0.88 (t, 12H)	0.88 (t, 15H)
$(C\underline{H}_2)_n$	1.26 (mult, 16H)	1.26 (mult, 32H)	1.26 (mult, 48H)	1.26 (mult, 64H)	1.26 (mult, 80H)

Table 2-6: ^{1}H NMR Spectra of Labelled Macrocyclic Polyamides‡

‡ broad peaks are reported as br

NBD group, and methylene groups of the macrocyclic ring that are adjacent to the NBD group, which are downfield of the signals corresponding to analogous methylene groups adjacent to the amide group.

Though it was not possible to obtain exact molecular weights from the molecular ions of labelled tri-amide **16** (N_4L_3[NBD]), labelled tetra-amide **17** (N_5L_4[NBD]) and labelled penta-amide **18** (N_6L_5[NBD]), in each case the molecular ion corresponding to the macrocyclic polyamide minus the NBD group was observed. Since our HPLC purification of each of the these labelled macrocyclic polyamides allowed for complete removal of unlabelled macrocyclic polyamide side products, these molecular ions are attributed to the labelled macrocyclic polyamides.

The percentage yields of labelled macrocyclic polyamides and unlabelled macrocyclic polyamide side products are indicated in Table 2-7. Though the experimental yields are low, each reaction is complete within 30 minutes. Furthermore, none of the reaction conditions have been systematically optimized, and it is is therefore likely that experimental yields can be improved in the future.

	percentage yield‡	
	labelled	unlabelled
Labelled Mono-amide **14** (N_2L[NBD])	11%	52%
Labelled Di-amide **15** (N_3L_2[NBD])	15%	42%
Labelled Tri-amide **16** (N_4L_3[NBD])	13%	27%
Labelled Tetra-amide **17** (N_5L_4[NBD])	6.9%	14%
Labelled Penta-amide **18** (N_6L_5[NBD])	5.8%	13%

Table 2-7: Experimental Yields From Labelled Macrocyclic Polyamide Syntheses

‡ based on macrocyclic polyamine as the limiting reagent, unlabelled macrocyclic polyamides are side products

2.4 Conclusions

The method developed by Lehn for the preparation of poly-lauroyl macrocyclic polyamides was modified. The new method, which involves reaction of macrocyclic polyamines with lauroyl chloride in THF in the presence of proton sponge, allows for faster and easier preparation of macrocyclic polyamides without decreasing the experimental yield. Using this method poly-lauroyl macrocyclic polyamides with the general formula $(CH_2CH_2N\text{-}C(O)\text{-}(CH_2)_{10}CH_3)_n$, n=2,3,4,5,6 were prepared in good yield.

Our attempts to prepare mono-NBD-labelled macrocyclic polyamides by reacting mono-NBD-labelled macrocyclic polyamines with excess lauroyl chloride were unsuccessful due to the low solubility of mono-NBD substituted macrocyclic polyamines and the instability of the NBD fluorophore in basic solutions at high temperatures. Preparation of NBD-labelled mono-amide **14** (N_2L[NBD]) was achieved by reacting piperazine with a mixed solution of lauric anhydride and NBD-Cl in the presence of proton sponge.

Attempts to use this simple statistical method for the preparation of larger labelled macrocyclic polyamides were not successful. Our experiments indicated that NBD substituted macrocyclic polyamines which are partially-acylated have diminished nucleophilicity compared to unlabelled macrocyclic polyamines which are partially-acylated. This decrease in nucleophilicity is attributed to the electron withdrawing properties of the NBD group.

NBD-labelled macrocyclic di-, tri-, tetra-, and penta-amides can be prepared by a two-step procedure which addresses the diminished nucleophilicity of NBD substituted macrocyclic polyamines. The steps in this method are:

(i) The reaction of macrocyclic polyamine with a mixed solution of lauric anhydride and NBD-Cl in the presence of proton sponge, and;

(ii) Subsequent treatment with lauroyl chloride to convert all labelled, partially-acylated macrocyclic polyamine to mono-NBD-labelled macrocyclic polyamide.

The labelled macrocyclic polyamides described in this Chapter are the first fluorescently labelled macrocyclic polyamides which have been prepared. The general statistical method developed for their syntheses should be applicable for the synthesis of numerous other asymmetrically substituted macrocyclic polyamides.

2.5 Experimental

2.5.1 General

7-chloro-4-nitrobenz-2-oxa-1,3-diazole (NBD-Cl, 13) was purchased from Aldrich Chemical Co. Milwaukee, WI, or Lancaster Chemical Co. ,U.K., and used without additional purification. Pentaaza-15-crown-5-penta-hydrochloride was purchased from Parish Chemical Co., Orem, UT. All other reagents were purchased from Aldrich Chemical Co., Milwaukee, WI, or British Drug House, Toronto, ON and used without additional purification.

Glass-distilled, HPLC grade THF was used in all syntheses. All reagents containing free amino groups were stored under 1 atm argon gas. Macrocyclic polyamides (labelled and unlabelled) were stored under vacuum with Drierite. Fluorescently labelled compounds were handled in subdued light.

Reactions and purification procedures were monitored by thin layer chromatography (TLC) using plastic-backed silica gel 60 UV/254 plates (Merck) as the stationary phase. Column chromatography was performed using 230-400 mesh silica gel (E.M. Science, N.J.).

^{1}H NMR and ^{13}C NMR spectra were acquired with a Varian XL-300 300 MHz spectrometer at 300 MHz and 75 MHz respectively. All NMR spectra were obtained using $CDCl_3$ as the solvent and ^{1}H NMR chemical shifts are reported in ppm relative to TMS as an internal standard.

^{13}C NMR chemical shifts are reported in ppm relative to the centre line of the $CDCl_3$ absorption (77.0 ppm). Melting points (uncorrected) were determined using a Thomas, Hoover model Capillary Melting Point Apparatus. Mass spectrometry analyses were performed by Doug Hairsine on a Finnigan MAT 8320 by the chemical ionization (CI) technique. UV spectra were obtained using a Shimadzu UV-160 UV-Visible Recording Spectrophotometer. Fourier transform infrared spectra were recorded using a Perkin Elmer System 2000 FTIR. FTIR samples were prepared as KBr pellets.

Samples for HPLC purification, were prepared as 0.25-0.5 mg /μL solutions in THF and filtered through Gelman 0.2 μm Nylon Acrodisc syringe filters. De-gassed, glass-distilled THF and methanol were used as solvents for HPLC purifications, solvents were pre-mixed using a magnetic stirrer. The solvent flow rate was 2 mL/min, and samples were run at room temperature. The column used for HPLC purifications was a Waters Prep Nova-Pack HR C-18 reverse phase column in the Waters 8x10 Radial Compression Module. 2-10 mg of sample were loaded per injection from a 20 μL loop.

The HPLC system consisted of two Waters 510 pumps controlled by a Waters Automated Gradient Controller. Eluent was monitored at 390 nm and 230 nm with a Waters 490 multi-wavelength detector. A Gilson 231 programmable sample injector and diluter were interfaced to the Waters

system. Samples were collected using a Gilson 201 auto-collector in the program-time mode which was also interfaced to the system.

2.5.2 Preparation of Free Base Macrocyclic Polyamines

Penta-amine **4** and hexa-amine **5** were prepared by the method of Czarnik et al.[5]

Penta-amine **4**

Pentaaza-15-crown-5-pentahydrochloride (173.6 mg, 0.442 mmol) was dissolved in 1 mL of doubly distilled water. 30 mL of 6M NaOH was added and the solution was transferred to a separatory funnel. The aqueous layer was extracted with 5x20 mL of $CHCl_3$, and the organic layer and approximately one half of the emulsion layer at the interface were collected after each extraction. The combined organic and emulsion layers were transferred to a 250 mL Erlenmeyer flask and anhydrous K_2CO_3 was added while stirring until a white gelatinous phase formed at the bottom of the flask and the chloroform solution was completely clear. The solution was filtered and the $CHCl_3$ was removed by rotary evaporation to yield 68.6 mg (0.319 mmol) of penta-amine **4** (74%).

Hexa-amine 5

Hexacyclen trisulphate, (180 mg, 0.325 mmol) was combined with 2 mL of 1.0 M HCl. 6M NaOH was added dropwise until all material had dissolved and the solution was clear and beige coloured. 30 mL of 6M NaOH was added to the solution and the resultant basic solution was transferred to a separatory funnel. 71 mg (0.273 mmol) of hexa-amine **5** was extracted and collected by the same method as penta-amine **4** (84% yield)

2.5.3 Synthesis of Macrocyclic Polyamides

Di-amide **6** (N_2L_2)

Piperazine (**1**, 73.6 mg, 0.854 mmol) and 363 mg (1.69 mmol) of proton sponge (**12**) were dissolved in 20 mL of THF at room temperature. A solution of 373 mg (1.70 mmol) of lauroyl chloride in 2 mL of THF was added to the solution of free base and immediate formation of a white precipitate was noted. The reaction mixture was stirred at room temperature for 30 minutes, then filtered through Whatman #1 filter paper. The THF solvent was removed from the filtrate by rotary evaporation and the resultant white solid was recrystallized from 20 mL of acetone at 7°C. White crystals were collected and recrystallized from 5 mL of CH_3CN at 7°C to furnish 384 mg (0.852 mmol) of di-amide **6** (N_2L_2) (99% yield). ^1H NMR data are presented in Table 2-2. ^{13}C NMR data are presented in Table 2-3. I.R. 1647(vs) amide I,

1472(vs) CH_2 scissoring. Melting point 67°C. Mass spectrum m/e expected 450.4185, found 450.4183 (M^+).

Tri-amide 7 (N_3L_3)

Tri-amine 2 (101.1 mg, 0.782 mmol) and 504 mg (2.35 mmol) of proton sponge (12) were dissolved in 20 mL of THF at room temperature. A solution of 513 mg (2.35 mmol) of lauroyl chloride in 2 mL of THF was added to the solution of free base and immediate formation of a white precipitate was noted. The reaction mixture was stirred at room temperature for 2 hours then filtered through Whatman #1 filter paper. The THF solvent was removed from the filtrate by rotary evaporation and the resultant white solid was recrystallized from 10 mL of ethyl acetate at 0°C. The resultant amorphous white solid was collected by vacuum filtration then recrystallized from 5 mL of CH_3CN at 7°C to furnish 407 mg (0.602 mmol) of tri-amide 7 (N_3L_3) (74% yield). ^1H NMR data are presented in Table 2-2, ^{13}C NMR data are presented in Table 2-3. I.R. 1641(vs) amide I, 1470(vs) CH_2 scissoring. Melting point 74°C. Mass spectrum m/e expected 675.6275, found 675.6262 (M^+).

Tetra-amide 8 (N_4L_4)

Tetra-amine 3 (92.1 mg, 0.244 mmol) and 214.8 mg (1.00 mmol) of proton sponge (12) were dissolved in 20 mL of THF heated to 60°C. A solution of

238 mg (1.09 mmol) of lauroyl chloride in 2 mL of THF was added to the solution of free base and immediate formation of a white precipitate was noted. The reaction mixture stirred at room temperature for 10 hours, then filtered through Whatman #1 filter paper. 154 mg (0.171 mmol) of tetra-amide **8** (N_4L_4) was purified by the same method as tri-amide **7** (70% yield). ^{1}H NMR data are presented in Table 2-2, ^{13}C NMR data are presented in Table 2-3. I.R. 1634(vs) amide I, 1470(vs) CH_2 scissoring. Melting point 135-136°C. Mass spectrum m/e expected 900.8371, found 900.8455 (M^+).

Penta-amide **9** (N_5L_5)

Penta-amine **4** (60.0 mg, 0.279 mmol) and 214 mg (1.40 mmol) of proton sponge (**12**) were dissolved in 20 mL of THF heated to 60°C. A solution of 239 mg (1.40 mmol) of lauroyl chloride in 2 mL of THF was added to the solution of free base and immediate formation of a white precipitate was noted. The reaction mixture was refluxed at 80°C for 12 hours then allowed to cool to 60°C. The warm solution was filtered through Whatman #1 filter paper. The THF solvent was removed from the filtrate by rotary evaporation and the resultant white solid was recrystallized from 5 mL of methanol at 0°C. The resultant amorphous white solid was collected by vacuum filtration then recrystallized from 5 mL of CH_3CN at 7°C to furnish 172 mg (0.153 mmol) of penta-amide **9** (N_5L_5) (55% yield). ^{1}H NMR data are presented in Table 2-2,

^{13}C NMR data are presented in Table 2-3. I.R. 1650(vs) amide I, 1471(vs) CH_2 scissoring. Melting point 104-105°C. Mass spectrum m/e expected 1126.0463, found 1126.0467 (M^+).

Hexa-amide **10** (N_6L_6)

Hexa-amine **5** (27.8 mg, 0.108 mmol) and 138 mg (0.645 mmol) of proton sponge (**12**) were dissolved in 20 mL of THF heated to 60°C. A solution of 154 mg (0.704 mmol) of lauroyl chloride in 2 mL of THF was added to the solution of free base and immediate formation of a white precipitate was noted. The reaction mixture was refluxed at 80°C for 12 hours then allowed to cool to 60°C. The warm solution was filtered through Whatman #1 filter paper. 74.5 mg (0.055 mmol) hexa-amide **10** (N_6L_6) was purified by the same method as penta-amide **9** (51% yield). ^1H NMR data are presented in Table 2-2, ^{13}C NMR data are presented in Table 2-3. I.R. 1649(vs) amide I, 1472(vs) CH_2 scissoring. Melting point 105-106°C. Mass spectrum m/e expected 1351.2556. found 1351.2314 (M^+).

2.5.3 Synthesis of Labelled Macrocyclic Polyamides

Labelled mono-amide **14** (N_2L[NBD])

Piperazine (**1**, 93.6 mg, 1.09 mmol) and 234 mg (1.09 mmol) of proton sponge (**12**) were dissolved in 10 mL of THF at room temperature. A solution

containing 417 mg (1.09 mmol) of lauric anhydride and 435 mg (2.18 mmol) NBD-Cl (**13**) dissolved in 2 mL of THF was added to the solution of free base. Formation of the dark red NBD-piperazine precipitate (**19**) was noted within 1 minute. The reaction mixture was stirred at room temperature for 20 minutes, then filtered through Celite (diatomaceous earth) which had been packed in a disposable pipette. The THF solvent was removed from the filtrate by rotary evaporation and the resultant orange film was dissolved in 20 mL of acetone, then cooled at 7°C for 4 hours. The di-amide **6** (N_2L_2) crystals which formed during the recrystallization were collected by vacuum filtration then recrystallized from CH_3CN to give 256 mg of di-amide **8** (N_2L_2) (52% yield based on piperazine (**1**) as the limiting reagent).

The filtrate from the acetone recrystallization was concentrated by rotary evaporation, and the resultant dark orange film was dissolved in 2.5 mL of $CHCl_3$ in a 25 mL round bottom flask. 600 mg of dry silica gel, then 2.5 mL of hexane were added, and the solution was mixed well. $CHCl_3$ and hexane were then removed from the mixture by rotary evaporation. The compound absorbed onto silica was carefully deposited on 50 g dry silica gel which had been poured into a 60 mL, medium-frit, sintered glass funnel. A layer of silica sand ($\sim$0.5 cm thick) was deposited over the column to protect the surface.

Diethyl ether was poured through the column under vacuum, and the eluent was monitored by TLC. NBD-Cl was the first compound to elute from

the column (1:1 diethyl ether:ethyl acetate R_f =0.97). Elution with diethyl ether was continued until fluorescent material began to elute from the column, at which point the solvent was changed to 3:1 diethylether:ethyl acetate. The desired product was eluted with this solvent until dark brown oxidized material began to elute (~ 175 mL of 3:1 diethyl ether:ethyl acetate).

Fractions containing fluorescently labelled mono-amide **14** (N_2L[NBD]) were identified by TLC (ethyl acetate R_f= 0.57), combined and concentrated by rotary evaporation. The resultant film was recrystallized from 4:1 hexane:$CHCl_3$ to give 51.7 mg labelled mono-amide **14** (N_2L[NBD]) (11% yield based on piperazine (**1**) as the limiting reagent).

FTIR data are presented in Table 2-5. ^{1}H NMR data are presented in Table 2-6. ^{13}C NMR ($CDCl_3$): δ 172 [C(O)]; 144.79, 144.59, 144.42, 123.27 [NBD quaternary carbons]; 134.90, 102.48 [CH=CH]; 48.88, 48.69, 44.48, 40.31 [(CH_2CH_2N-R)$_2$]; 33.22 [CH_2C(O)]; 31.83, 29.54(3), 29.38, 29.26, 22.61 [(CH_2)$_8$]; 25.04 [CH_2CH_2C(O)]; 14.04 [CH_2CH_3]. Compound decomposes at 108°C. λ_{max}(DMF) 481.5 nm. Mass spectrum m/e expected 431.2533, found 431.2534 (M^+).

Labelled Di-amide **15** (N_3L_2[NBD])

Tri-amine **2** (60.4 mg, 0.467 mmol) and 150 mg (0.700 mmol) of proton sponge (**12**) were dissolved in 10 mL of THF at room temperature. A solution

containing 179 mg (0.467 mmol) of lauric anhydride and 140 mg (0.700 mmol) of NBD-Cl (13) dissolved in 2 mL of THF was added to the solution of free base.

The reaction mixture was stirred at room temperature for 3 min, then one drop of lauroyl chloride (~10 mg, 0.046 mmol) was added to the solution. The reaction with lauroyl chloride was allowed to proceed for 10 min, then the THF soluble components of the reaction mixture were analyzed by TLC (1:1 diethyl ether:ethyl acetate solvent). If any fluorescent material remained at the baseline of the TLC plate, another drop of neat lauroyl chloride was added to the solution. Addition of lauroyl chloride was continued in this manner until no fluorescent material was identified at the baseline of a TLC plate developed with 1:1 diethyl ether:ethyl acetate, at which point the reaction was deemed to be complete. A total of 89.7 mg (0.410 mmol) of lauroyl chloride was added to the reaction mixture.

Upon completion of the reaction (based on TLC analysis) a pale orange precipitate was removed from the reaction mixture by filtration through Whatman #1 filter paper, and the THF solvent was removed from the filtrate by rotary evaporation. The resultant orange film was dissolved in 10 mL of 5:1 hexane:$CHCl_3$ at 80°C, then cooled at 0°C for 10 hours. The resultant brown solid precipitate was collected by vacuum filtration and purified as described below. The filtrate contained tri-amide 7 (N_3L_3), which was purified

by two recrystallizations from 5 mL of CH_3CN at 7°C to give 133 mg (N_3L_3) (42% yield based on tri-amine **2** as the limiting reagent).

The solid from the 5:1 hexane:$CHCl_3$ recrystallization was adsorbed onto silica gel and purified by silica chromatography by the same method as described in the purification of compound **14**. Fractions containing fluorescently labelled di-amide **15** (N_3L_2[NBD]) were identified by TLC (1:1 diethyl ether:ethyl acetate R_f=0.41), combined, and concentrated by rotary evaporation. The resultant orange film was recrystallized from 5:1 hexane:$CHCl_3$ to give 89.7 mg of labelled di-amide **15** (N_3L_2[NBD]), (15% yield based on tri-amine **2** as the limiting reagent).

FTIR data are presented in Table 2-5. ^{1}H NMR data are presented in Table 2-6. Melting point 169-170°C. λ_{max} (DMF) 488.0 nm. Mass spectrum m/e expected 656.4625, found 656.4626 (M^+).

Labelled Tri-amide **16** (N_4L_3[NBD])

Tetra-amine **3**, (58.5 mg, 0.341 mmol) and 146 mg (0.682 mmol) of proton sponge (**12**) were dissolved in 10 mL of THF at 60°C. A solution containing 261 mg (0.682 mmol) of lauric anhydride and 136 mg (0.682 mmol) of NBD-Cl (**13**) dissolved in 2 mL of THF was added to the solution of free base. The reaction mixture was stirred at 60°C for 3 min, then lauroyl chloride was added to the solution dropwise by the same method as described

in the preparation of compound **15**. A total of 149 mg (0.681 mmol) of lauroyl chloride was added to the reaction mixture.

Upon completion of the reaction (based on TLC analysis), the crude mixture was filtered, loaded onto silica gel and partially purified using a dry silica gel column by the same method described in the purification of compound **14**, decreasing the ratio of diethyl ether:ethyl acetate as required to elute all fluorescently labelled material from the column. Fractions containing fluorescently labelled tri-amide **16** (N_4L_3[NBD]) were identified by TLC (ethyl acetate Rf= 0.41), combined, and concentrated by rotary evaporation. The resultant orange film was purified by HPLC.

Pre-mixed 95:5 methanol:THF was used as the elution solvent. Tetra-amide **8** (N_4L_4), t_R=11.6 min, was collected over the time range 9.8-14.8 min (? mg, 27% yield based on tetra-amine **3** as the limiting reagent). Labelled tri-amide **16** (N_4L_3[NBD]), t_R=4.9 min, was collected over the time range 3.8-6.1 minutes. The solvent was removed by rotary evaporation and the resultant orange film was recrystallized from 1.5 ml CH_3CN at 0°C to give 39 mg of orange solid (13% yield based on tetra-amine **3** as the limiting reagent).

FTIR data are presented in Table 2-5. ^{1}H NMR data are presented in Table 2-6. Melting point 151°C. λ_{max} (DMF) 482.5 nm. Mass spectrum m/e expected 881.6718 (M^+), 717.6622 (M^+- NBD), found 717.6624 (M^+- NBD).

Labelled Tetra-amide **17** (N_5L_4[NBD])

Penta-amine **4** (61.9 mg, 0.287 mmol) and 154 mg (0.718 mmol) of proton sponge (**12**) were dissolved in 10 mL of THF at 60°C. A solution containing 274 mg (0.718 mmol) of lauric anhydride and 143 mg (0.718 mmol) of NBD-Cl (**13**) dissolved in 2 mL of THF was added to the solution of free base. The reaction mixture was stirred at 60°C for 3 min, then lauroyl chloride was added to the solution dropwise by the same method as described in the preparation of compound **15**. A total of 126 mg (0.576 mmol) of lauroyl chloride was added to the reaction mixture.

Upon completion of the reaction (based on TLC analysis), the crude mixture was filtered, loaded onto silica gel and partially purified using a dry silica gel column by the same method described in the purification of compound **14**. Fractions containing fluorescently labelled tetra-amide **17** (N_5L_4[NBD]) were identified by TLC (1:1 diethyl ether:ethyl acetate Rf=0.71), combined, and concentrated by rotary evaporation. The resultant orange film was purified by HPLC (85:15 methanol:THF) by the same method described in the purification of compound **16**.

Penta-amide **9** (N_5L_5), t_R=9.4 min, was collected over the time range 9.0-12.0 minutes (44 mg, 14% yield based on penta-amine **4** as the limiting reagent). Labelled tetra-amide **17** (N_5L_4[NBD]), t_R=4.6 min, was collected over the time range 4.2-7.1 minutes. The solvent was removed by rotary

evaporation and the resultant orange film was recrystallized from 1.5 ml CH_3CN at 0°C to give 22 mg of orange solid (6.9% yield based on penta-amine **4** as the limiting reagent).

FTIR data are presented in Table 2-5. ^1H NMR data are presented in Table 2-6. Melting point 66-68°C. λ_{max} (DMF) 484.5 nm. Mass spectrum m/e expected 1106.8811(M^+), 942.8715 (M^+- NBD), found 942.8860 (M^+-NBD).

Labelled Penta-amide **18** (N_6L_5[NBD])

Hexa-amine **5** (31.5 mg, 0.122 mmol) and 78 mg (0.366 mmol) of proton sponge (**12**) were dissolved in 10 mL of THF at 60°C. A solution containing 140 mg (0.366 mmol) of lauric anhydride and 73 mg (0.366 mmol) of NBD-Cl (**13**) dissolved in 2 mL of THF was added to the solution of free base. The reaction mixture was stirred at 60°C for 3 min, then lauroyl chloride was added to the solution dropwise by the same method as described in the preparation of compound **15**. A total of 61 mg (0.278 mmol) of lauroyl chloride was added to the reaction mixture.

Upon completion of the reaction (based on TLC analysis), the crude mixture was filtered, loaded onto silica gel and partially purified using a dry silica gel column by the same method described in the purification of

compound **14**, decreasing the ratio of diethyl ether:ethyl acetate as required to elute all fluorescently labelled material from the column. Fractions containing fluorescently labelled penta-amide **18** (N_6L_5[NBD]) were identified by TLC (ethyl acetate Rf= 0.53), combined, and concentrated by rotary evaporation. The resultant orange film was purified by HPLC (75:25 methanol:THF) by the same method described in the purification of compound **16**.

Hexa-amide **10** (N_6L_6), t_R=7.4 min, was collected over the time range 6.5-11.5 minutes (15 mg, 13% yield based on hexa-amine **5** as the limiting reagent). Labelled penta-amide **18** (N_6L_5[NBD]), t_R=4.5 min, was collected over the time range 3.7-5.8 minutes. The solvent was removed by rotary evaporation and the resultant orange film was recrystallized from 1.5 ml CH_3CN at 0°C to give 7.0 mg of orange solid (6.5% yield based on hexa-amine **5** as the limiting reagent).

FTIR data are presented in Table 2-5. ^{1}H NMR data are presented in Table 2-6. Melting point 65-66°C. λ_{max} (DMF) 489.0 nm. Mass spectrum m/e expected 1332.0903 (M^+), 1168.0807 (M^+- NBD), found 1168.0763 (M^+- NBD).

2.6 References

1. Vaz, W.L., Goodsaid-Zalduonda, F., and Jacobson, K., Lateral Diffusion of Lipids and proteins in Bilayer Membranes, *FEBS Lett.*,**1984** *174*, 199-207.
2. Hancock, R.D., and Martell, A.E., Ligand Design for Selective Complexation of Metal Ions in Aqueous Solution. *Chem. Rev.* **1989**, *89*, 1875-1914.
3. Kodama, M., and Kimura, E., Complexation of the Macrocyclic Hexa-amine Ligand 1,4,7,10,13,16, Hexa-azacyclo-octadecane, *J. Chem. Soc. Dalton Trans.*, **1980**, 2536-2538.
4. Studer, M., and Kaden T.A., Metal Complexes with Macrocyclic Ligands, Part XXV, *Helv. Chim. Acta.*, **1986**, *69*, 2081-2086.
5. Akkaya, E.U., Huston, M.E., and Czarnik, A.W., Chelation-Enhanced Fluorescence of Anthrylazamacrocycle Conjugate Probes in Aqueous Solutions, *J. Am. Chem. Soc.*, **1990**, *112*, 3590-3593.
6. Bernhard, P.V., and Lawrance, G.A., Complexes of Polyaza Macrocycles Bearing Pendent Coordinating Groups, *Coord. Chem. Rev.*, **1990**, *104*, 297-343.
7. Gatto, V.J., and Gokel, G.W., Synthesis of Calcium-Selective, Substituted Diaza-Crown Ethers, *J. Am. Chem. Soc.*, **1984**, *106*, 8240-8244.

8. Kodama, M. and Kimura, E., Effects of Cyclization and Ring Size on Complex Formation Between Penta-amine Ligands and Copper (II), *J. Chem. Soc., Dalton Trans.*, **1978**, 104-110.

9. Van Westrenen, J., and Sherry, A.D., Sufomethylation of Di-, Tri- and Polyazamacrocycles: A New Route to Entry of Mixed-Side Chain Macrocyclic Chelates, *Bioconj. Chem.*, **1992**, *3*, 524-532.

10. Buøen, S., Dale, J., and Krane, J., Hydroxyethylation of Macrocyclic Polyamines; Inhibition by Partial Protonation, *Acta. Chem. Scand. B.*, **1984**, *38*, 773-778.

11. Umezawa, Y., Kataoka, M., and Takami, W., Potentiometric Adenosine Triphosphate Polyanion Sensor Using a Lipophilic Macrocyclic Polyamine Liquid Membrane, *Anal. Chem.*, **1988**, *50*, 2392-2396.

12. Malthête, J., Poupinet, D., Vilanove, R, and Lehn, J.M., Monolayers of Macrocyclic Polyamides at the Air-Water Interface, *J. Chem. Soc. Chem.Comm.*, **1989**, 1016.

13. Mertesdorf., C., Plesnivy, T., Ringsdorf, H., and Suci, P.A., Monolayers of Amphiphilic Azacrowns: Characterization of Monolayer Behaviour and Specific Interaction with Nucleotides, *Langmuir*, **1992**, *8*, 2531-2537.

14. Lehn, J.M., Malthête, J., and Levelut, A., Tubular Mesophases: Liquid Crystals Consisting of Macrocyclic Polyamides *J. Chem. Soc. Chem. Comm.*, **1985**, 1794-1796.

15. Idziak, S.H.J., Maliszewskyj, N.C., Heiney, P.A., McCauley, J.P., Sengeler, P.A., and Smith, A.B., Structure and Mesophases of Hexacyclen Derivatives, *J. Am. Chem. Soc.*, **1991**, *113*, 7666-7672.

16. March, J., *Advanced Organic Chemistry*, John Wiley and Sons Inc., Toronto, **1985**, pg. 315.

17. Perrin, D.D., *Dissociation Constants of Organic Bases in Aqueous Solution*, Page Bros. Inc., London, U.K., **1965**, pg 156.

18. Gordon, A.J. and Ford, R.A., *The Chemist's Companion*, John Wiley and Sons Inc., Toronto, **1972**, pg 59.

19. Paprica, P.A., Baird, N.C., and Petersen, N.O., Theoretical and Experimental Analyses of Optical Transitions of Nitrobenzoxadiazole (NBD) Derivatives, *J. Photochem. Photobiol. A: Chemistry*, **1993**, *70*, 51-57. Appendix 1.

20. Chattopadhyay, A., Chemistry and Biology of N-(7-nitro-benz-oxa-1,3-diazol-4-yl)-Labelled Lipids: Fluorescent Probes of Biological and Model Membranes, *Chemistry and Physics of Lipids*, **1990**, *53*, 1-15.

21. Petersen, N.O., Intramolecular Fluorescence Energy Transfer in Nitrobenzoxadiazole Derivatives of Polyene Antibiotics. *Can. J. Chem.*, **1985**, *63*, 1, 77.

22. Balcolm, B.J., and Petersen, N.O., Solvent Dependence of Carboxylic Acid Condensations with Dicyclohexylcarbodiimide, *J. Org. Chem.*, **1989**, *54*, 1922.

23. ^{1}H NMR (D_2O + HCl) δ (200 MHz) 8.08, 6.28 (C<u>H</u>=C<u>H</u>, AB Pattern 2H, 8Hz), 3.79 (C<u>H</u>$_2$N(NBD)C<u>H</u>$_2$, t, 4H), 2.74 (C<u>H</u>$_2$N(H)C<u>H</u>$_2$, t, 4H). Mass spectrum m/e expected 249.0862, found 249.0856 (M^+).

Chapter 3

DETERMINATION OF MOLECULAR STRUCTURE: VARIABLE TEMPERATURE NMR AND MOLECULAR MODELLING ANALYSES

3.1 Introduction

The organic syntheses in this project were undertaken with a single goal: to prepare molecules which have properties and dimensions such that they will provide insight into the relationship between the lateral diffusion coefficients and surface areas of intermediately sized molecules in model membrane systems. Interpretation of our diffusion results depends on the ability to link macroscopic properties to molecular structure. With this in mind we put considerable effort into looking at techniques which would provide us with information about the molecular structure and the dimensions of our probe molecules.

3.2 Variable Temperature NMR Studies

3.2.1 Theory

In science it is generally the case that the tool used to study any property must have characteristic dimensions similar in distance or time units to the property which is being studied. Thus X-rays with wavelengths on the order of 10^{-10} m are used to determine molecular structure, and ^{14}C, which has

a half-life of 57300 years, is used to determine the age of organic matter on a geological time scale.

NMR spectroscopy is often the tool of choice for the study of dynamic molecular processes because there is a number of timescales available. Consider two species, A and B, which each have distinct NMR signals, but are in equilibrium;

$$A \underset{k_b}{\overset{k_a}{\rightleftharpoons}} B$$

The NMR time scale for exchange of the two magnetically nonequivalent sites is inversely proportional to the separation of the signals in Hz. If the rate of interconversion of A and B is slow compared to the NMR time scale for the process, the observed NMR spectrum will consist of two different signals, and the system is said to be at the slow-exchange limit. At the other extreme, the fast-exchange limit, equilibrium between A and B is very fast compared to the NMR time scale, and the observed NMR spectrum exhibits one average signal for the two, magnetically non-equivalent, species.

It is a well known fact that rotation of the (O)C-N bond of amides is restricted, and this phenomenon is attributed to the fact that the (O)C-N bond of amides has some double bond character due to the contribution of resonance structure 3-1b (Figure 3-1).[2] The sp^3 carbons bound to the nitrogen of the

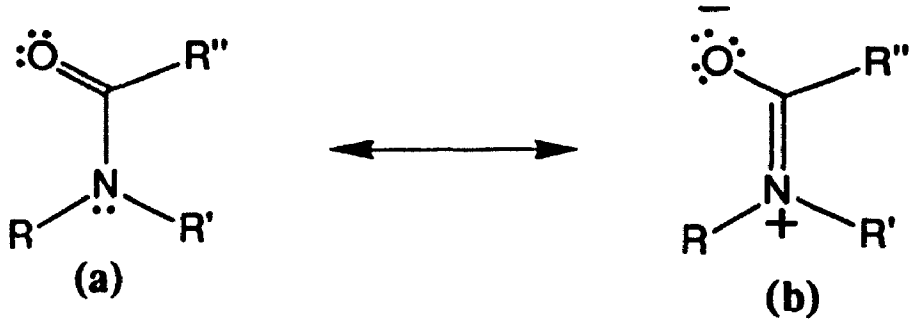

Figure 3-1: Resonance Structures of Amides

amide group are classified as cis or trans to the amide carbonyl because of the partial double bond character of the (O)C-N bond. Magnetically, the cis and trans sp^3 carbons are not equivalent because of the shielding and deshielding effects of the amide group as illustrated in Figure 3-2.[1] Therefore, at room temperature, the ^1H NMR spectrum of most amides exhibits two different signals for the sp^3 carbons bound to nitrogen. As amides in solution are heated, the rate of rotation about the (O)C-N bond increases, and eventually the two signals may coalesce to a single observed peak which has a frequency mid-way between the two signals observed at low temperature. The rate of amide rotation about the (O)C-N bond is usually slow enough that both the fast exchange and slow exchange limits are accessible between -20° C to 200° C. Therefore, variable temperature ^1H NMR is a suitable method for determining the rate of rotation of (O)C-N bonds in amides, and numerous amide systems have been studied by this method.[2]

The experimental objective was to use variable temperature NMR to determine the extent of sp^2 character exhibited by nitrogen atoms in our macrocyclic polyamide probe molecules. Initially, NMR spectra were analyzed and cis and trans methylene groups of the amides were identified. Once exchange sites had been determined, the rates and activation energies of rotation of (O)C-N bonds and (NBD)-N bonds were calculated using dynamic ^1H NMR analysis.

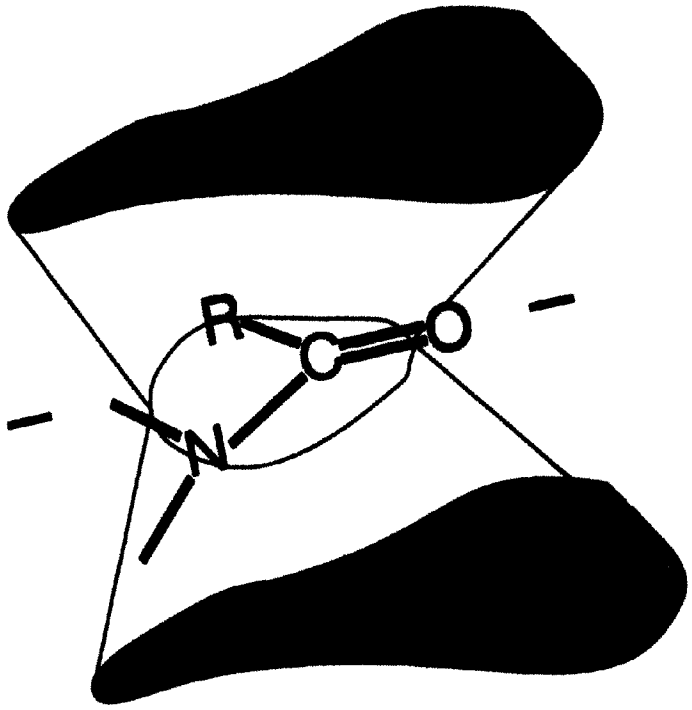

Figure 3-2: Diagram Showing Sheilded (+) and Desheilded (-) regions around the amide bond.

3.2.2 Variable Temperature NMR Analysis of Di-Amide 6 (N_2L_2)

In the ^1H NMR spectrum of di-amide **6** (N_2L_2), splitting due to the non-equivalence of axial and equatorial protons of the methylene groups in the six membered ring cannot be resolved (Figure 3-3). Instead, the signals corresponding to the methylene groups of the six membered ring consist of overlapping multiplets with a combined bandwidth at half maximum intensity greater than 18 Hz (300 MHz spectrum). Other regions of the ^1H NMR spectrum corresponding to the alkyl chain protons are well resolved, with bandwidths at half maximum intensity less than 4 Hz. It is probable that each broad multiplet observed for the methylene groups of the six membered ring corresponds to an AA'BB' pattern which contains eight absorptions within each 18 Hz bandwidth; however, the multiplets may also be broadened as a result of restricted conformational motion within the six membered ring.

There are several techniques which can be used to determine rate constants and thermodynamic data from variable temperature NMR analysis. In general, methods based on correlating decreases in signal bandwidth with increases in exchange rates have been shown to be accurate over the entire range of exchange broadening temperatures.[3] However, because of the inherent coupling and other factors which cause broadening of the methylene signals of the six membered ring of di-amide **6** (N_2L_2), NMR techniques based on band-width broadening are not appropriate for analysis of this molecule.

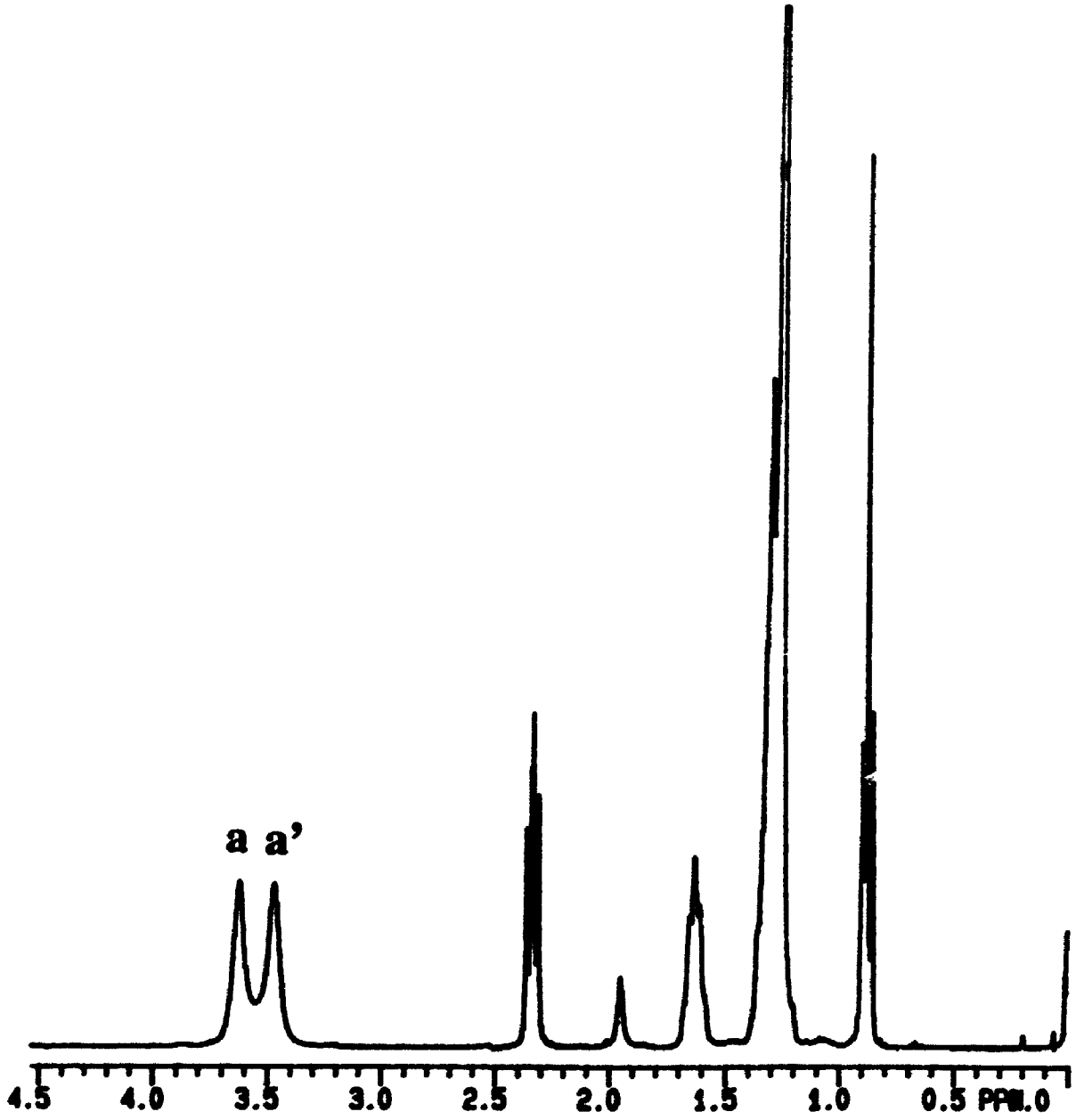

Figure 3-3: ^{1}H NMR Spectrum of Di-amide 6 (N_2L_2) at 21°C. Signals a and a' are the observed signals for the protons of the six-membered ring

If the difference (in Hz) between two signals in an exchange system is large enough for two separate signals to be resolved at low temperature, rate constants for dynamic processes can also be calculated from NMR spectra using methods based on observed peak separation as a function of temperature.[3] The difference in frequency ($\delta\upsilon$) between two sites in an exchanging system when no exchange is detectable is defined as:[3]

Equation 3-1 $$\delta\nu = \nu_a - \nu_b$$

where υ_a and υ_b are the observed frequencies corresponding to the two different NMR signals of species A and B, respectively. Likewise, the observed difference in frequency between two signals which are undergoing exchange is defined as:[3]

Equation 3-2 $$\delta\nu_e = \nu_{a(e)} - \nu_{b(e)}$$

At any temperature, the rate of exchange (k) can be calculated as;[3]

Equation 3-3 $$k = \frac{\pi}{\sqrt{2}}\sqrt{(\delta\nu^2 - \delta\nu_e^2)}$$

At the coalescence temperature, when an average signal for A and B is observed in the NMR spectrum, Equation 3-3 simplifies to;

Equation 3-4 $$k = \frac{\pi \delta \nu}{\sqrt{2}}$$

In some cases it has been shown that $\delta\upsilon$ exhibits a temperature dependence. This fact, combined with the fact that rate constants from peak separation methods can only be determined at or below the coalescence temperature, are the main reasons why bandwidth methods are generally preferred for dynamic NMR analyses. Nevertheless, the peak separation method was the only method suitable for analysis of our experimental data, therefore dynamic NMR analysis based on peak separation was used to calculate the rate of (O)C-N bond rotation in di-amide **6** (N_2L_2).

^{1}H NMR spectra of di-amide **6** (N_2L_2) were recorded at several temperatures; some representative spectra are shown in Figure 3-4. These experiments indicate that the coalescence temperature for amide bond rotation in di-amide **6** (N_2L_2) is 49°C. The rates of rotation of the (O)C-N bond at various temperatures were calculated using equations 3-3 and 3-4, and are presented in Table 3-1. A $\delta\upsilon$ value of 45.2 Hz was calculated as the difference between the ring methylene signals at 21°C. The peaks corresponding to the methylene groups adjacent to the carbonyl were asymmetric on ^{1}H NMR spectra below this temperature.

According to transition state theory, the rate constant (k) for two species in equilibrium with no intermediates is related to the activation energy (E_a)

Temperature (°C)	Rate Constant k (sec^{-1}) for (O)C-N bond rotation
25	12
30	30
33	45
36	54
42	65
48	96
49	100

Table 3-1: Rate Constants for Rotation of the (O)C-N bond in Di-amide **6** (N_2L_2)

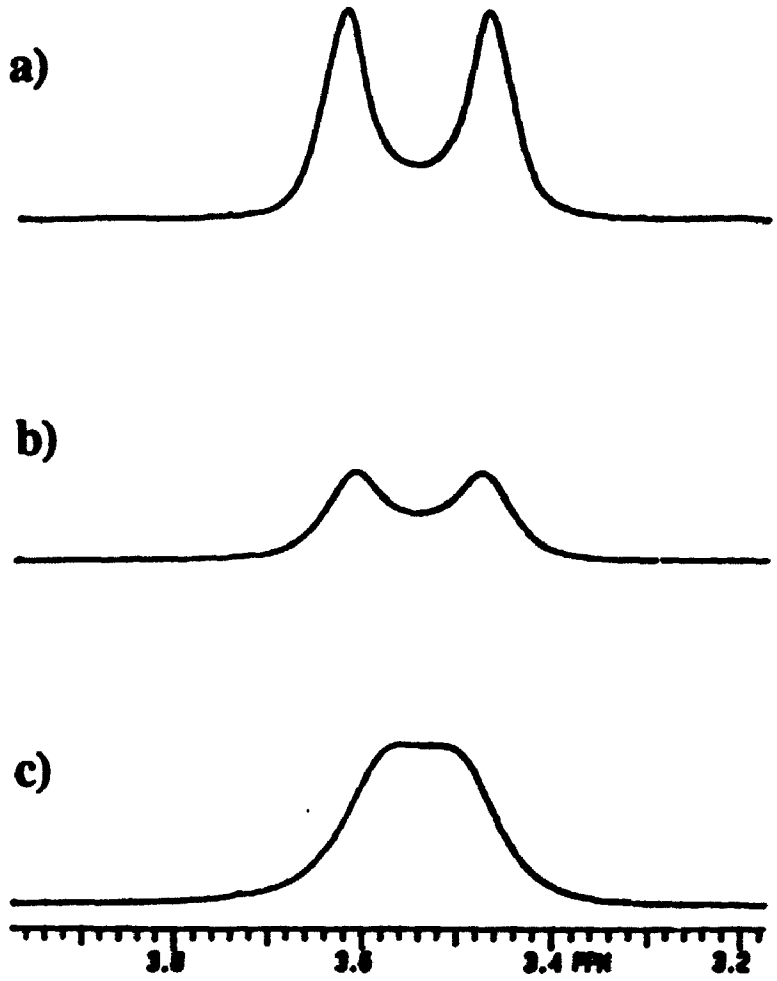

Figure 3-4: ^{1}H NMR Spectra of Di-Amide **6** (N_2L_2) at (a) 21°C, (b) 33°C, and (c) 49°C.

and the Arrhenius constant A for the process;

Equation 3-5 $$\ln k = \ln A - \frac{E_a}{RT}$$

Therefore an Arrhenius plot of ln k vs $1/T$ should produce a straight line with a slope equal to $-E_a/R$. A plot of ln k vs 1/T for rotation of the (O)C-N bond is shown in Figure 3-5. The rates calculated at 25° and 30°C were not included in the line of best fit, since $\delta\upsilon_e$ is known to be insensitive to changes in k at low temperatures.[3] When these low temperature points are excluded, the Arrhenius plot for (O)C-N bond rotation is a straight line (r=0.992) with a slope corresponding to E_a=40 kJ/mol. Based on the parameters from the line of best fit, the rate constant at 25°C was calculated to be 30 sec^{-1} which corresponds to a lifetime ($1/2k$) of 17 msec for each amide conformer.

It is possible that the measured $\delta\upsilon$ value of 45.19 Hz is slightly smaller than the actual $\delta\upsilon$ value because the peaks in the ^{1}H NMR spectrum of di-amide **6** (N_2L_2) at 21°C which were used to calculated $\delta\upsilon$ are broadened (Figure 3-4). The spectrum recorded at this temperature may therefore represent a system which is undergoing some exchange. If a $\delta\upsilon$ value of 46.69 Hz (1.5 Hz greater than the measured value) is used to calculate k, then all of the data points fall on a straight line and the Arrhenius plot based on these calculations yields a line of best fit with r=0.994 and a slope corresponding to an activation energy of 40.5 kJ/mol (Figure 3-5). Therefore, the estimated

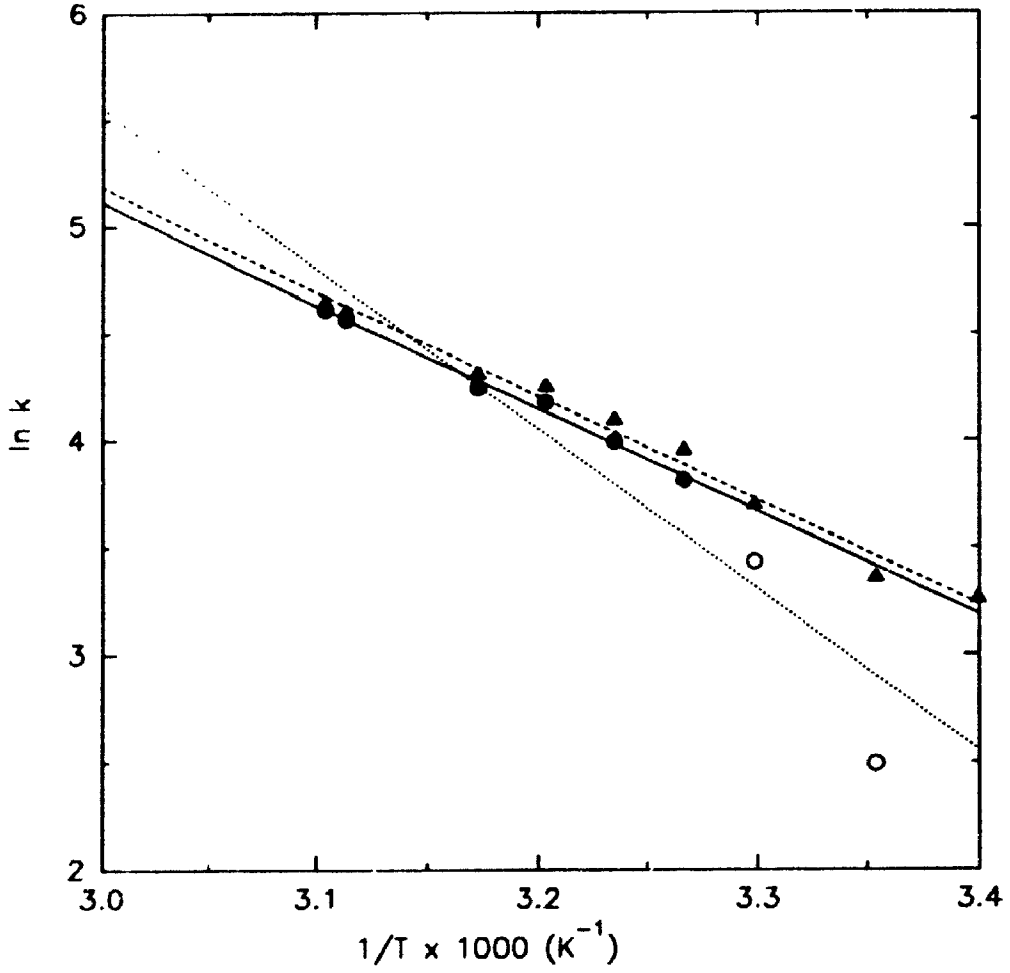

Figure 3-5: Arrhenius Plots for the Rate of Rotation of the (O)C-N bond in Di-amide 6 (N_2L_2)

The dotted line (o) includes all experimental data, the solid line (●) is based on k values for temperature above 33°C. The dashed line (▲) is the calculated line of best fit for δυ=46.69 Hz (1.5Hz larger than the measured value).

for the activation energy obtained by this method is equivalent to the value obtained if low temperature points are excluded from the line of best fit within experimental uncertainty.

The calculated activation energy of 40 kJ/mol is considerably smaller than the 83 kJ/mol activation energy barrier to (O)C-N bond rotation in N,N-dimethylacetamide.[4] NMR experiments on N,N'-dimethyl-α,α,α-trimethylacetamide indicate that the activation energy for this aliphatic tertiary amide is 48 kJ/mol.[5] This relatively low activation energy is attributed to an increase in ground state energy due to unfavourable steric interactions of the t-butyl group with the methyl groups bonded to the nitrogen of the amide in the planar configuration. It is probable that the low activation energy for (O)C-N bond rotation in di-amide **6** (N_2L_2) also results from an increased energy of the ground state due to the tendency of nitrogens in unsaturated six-membered rings to exist in sp^3 instead of sp^2 hybridized states due to ring strain.

The fact that the Arrhenius plot for (O)C-N bond rotation in di-amide **6** (N_2L_2) is straight line with a correlation coefficient close to unity indicates that variation of $\delta\upsilon$ over the temperature range (33-49°C) does not have a significant effect on calculations of the rate of (O)C-N bond rotation based on NMR peak separation.

3.2.3 Variable Temperature NMR Analysis of Labelled Mono-Amide 14

Labelled mono-amide **14** (N_2L[NBD]) (Figure 3-6) contains one (O)C-N bond which is expected to exhibit restricted rotation due to the contribution of resonance structure 3-6b. It is also possible that restricted rotation of the bond linking the NBD group to the cyclic ring, i.e., the (NBD)-N bond, will occur due to contribution of resonance structure 3-6c. The ^{1}H NMR spectrum of labelled mono-amide **14** (N_2L[NBD]) at 22°C is shown in Figure 3-7. The region corresponding to the methylene groups of the six membered ring of labelled mono-amide **14** (N_2L[NBD]) consists of four broadened multiplets. As was the case for di-amide **6** (N_2L_2), coupling of axial and equatorial protons of the six-membered ring cannot be resolved. Therefore, we used the peak separation method to calculated the rates of rotation of the (O)C-N and (NBD)-N bonds in labelled mono-amide **14** (N_2L[NBD]).

Several representative ^{1}H NMR spectra of labelled mono-amide **14** (N_2L[NBD]) at different temperatures are shown in Figure 3-8. The signals labelled a and a' coalesce at 49°C, the same temperature at which coalescence was observed in the ^{1}H NMR spectrum of di-amide **6** (N_2L_2). We therefore assign signals a and a' to the methylene groups adjacent to the amide group. Coalescence of signals b and b' occurs at a higher temperature (59°C). These signals are therefore assigned to the methylene groups adjacent to the NBD group.

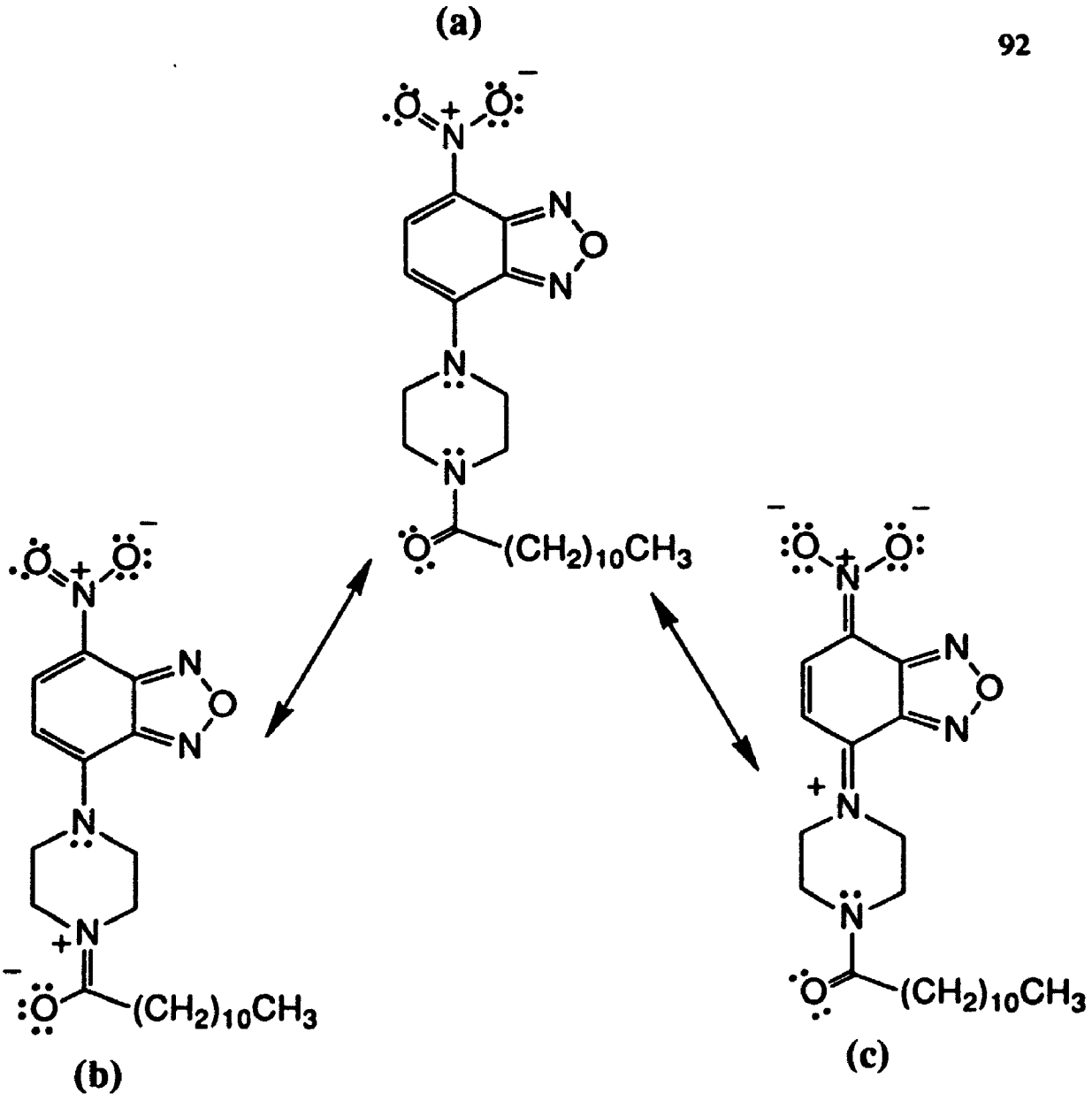

Figure 3-6: Resonance Structures of Labelled Mono-Amide 14 ($N_2L[NBD]$)

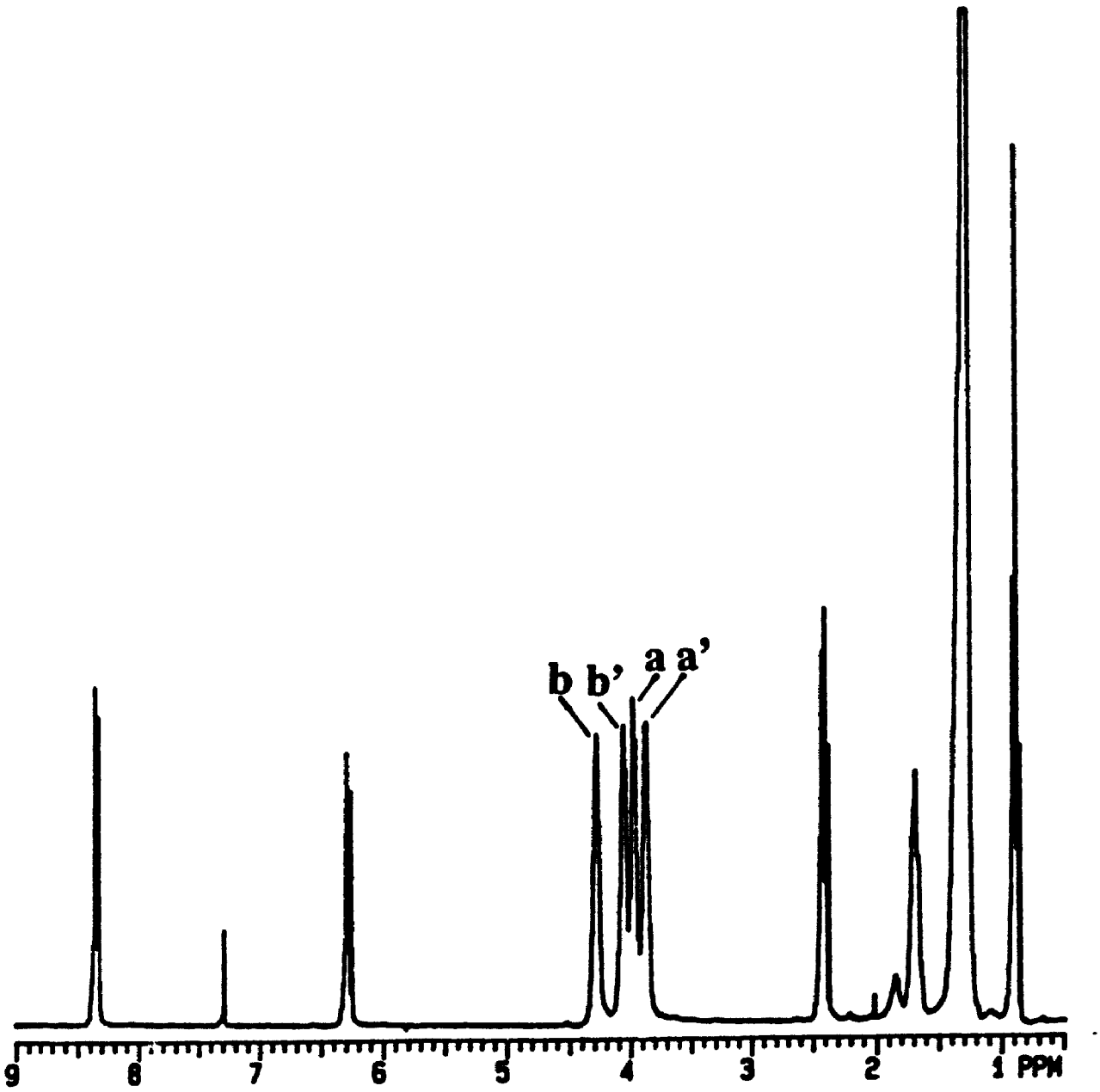

Figure 3-7: ^{1}H NMR Spectrum of Labelled Mono-Amide 14 (N_2L[NBD]) at 22°C.

Signals observed for the methylene groups adjacent to the amide group (a and a') and the NBD group (b and b') are labelled.

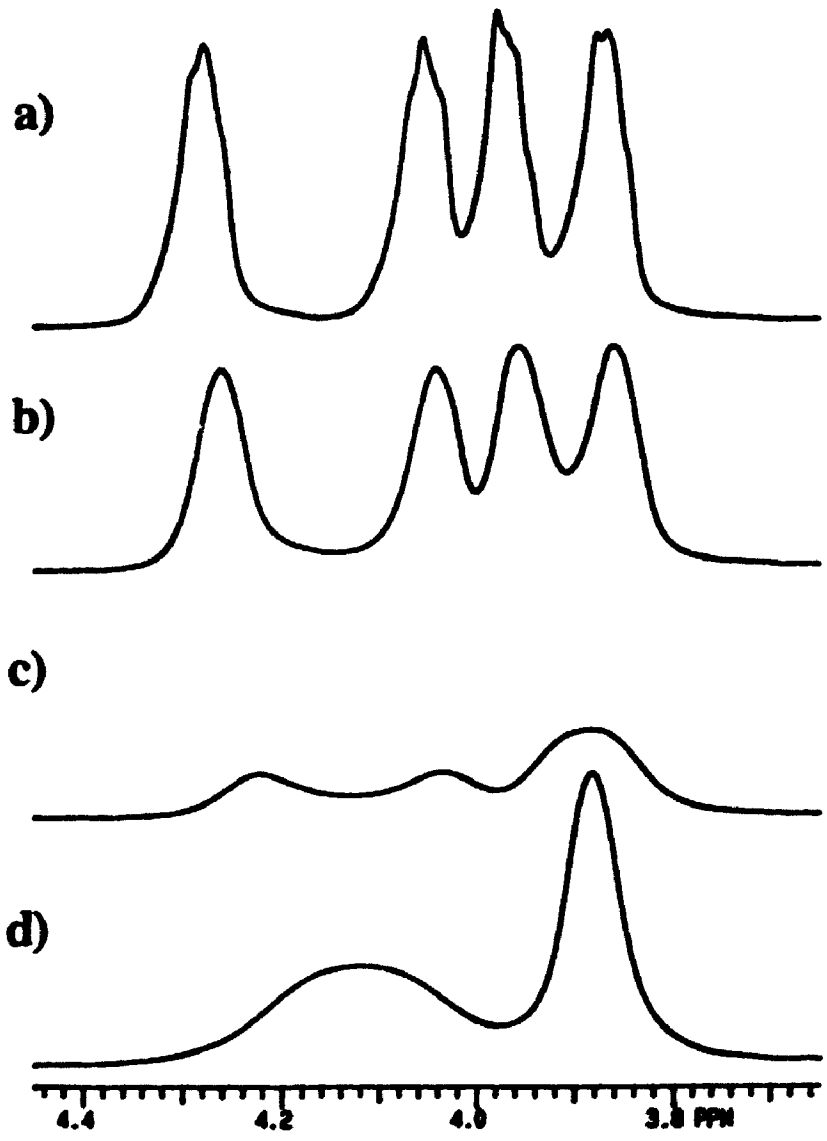

Figure 3-8: ^{1}H NMR Spectra of Labelled Mono-Amide **14** (N_2L[NBD]) at (a) 22°C, (b) 35°C, (c) 49°C, and (d) 59°C.

The rates of (O)C-N and (NBD)-N bond rotation at various temperatures were calculated using equations 3-3 and 3-4 and are presented in Table 3-2. The $\delta\upsilon$ values which we used for all calculations was the difference between the ring methylene signals at 22°C (34.8 Hz for (O)C-N bond rotation, 67.3 Hz for (NBD)-N bond rotation), which was the lowest temperature at which a ^{1}H spectrum was recorded.

The Arrhenius plot for rotation of the (O)C-N bond in labelled mono-amide **14** (N_2L[NBD]) is a straight line (r=0.994) with a slope corresponding to E_a= 41 kJ/mol (Figure 3-9). This value is approximately equal to the value calculated for (O)C-N bond rotation in di-amide **6** (N_2L_2), which confirms the assignment of these signals as the methylene groups adjacent to the amide group. Based on the parameters from the line of best fit, the rate constant at 25°C was calculated to be 22 sec^{-1}, which corresponds to a lifetime of 23 msec for each amide isomer. These values for the lifetimes of amide isomers at 25°C indicate that rotation of the (O)C-N bond in solution is fast enough at room temperature to allow for rapid interconversion of cis and trans isomers of amides.

The Arrhenius plot for rotation of the (NBD)-N bond is also a straight line (r=0.998) with a slope corresponding to E_a= 59 kJ/mol (Figure 3-9). As was the case for di-amide **6** (N_2L_2), the fact that the Arrhenius plots for labelled mono-amide **14** (N_2L[NBD]) produce straight lines with correlation

Temperature (°C)	Rate Constant k (sec^{-1})	
	(O)C-N bond rotation	(NBD)-N bond rotation
35	39	30
40	47	41
42	53	48
43	56	52
44	60	56
45	62	62
46	66	65
47	70	71
48	75	78
49	75	84
56		124
58		148
59		150

Table 3-2: Rate Constants for Rotation of the (O)C-N bond and the (NBD)-N bond in Labelled Mono-Amide **14** (N_2L[NBD])

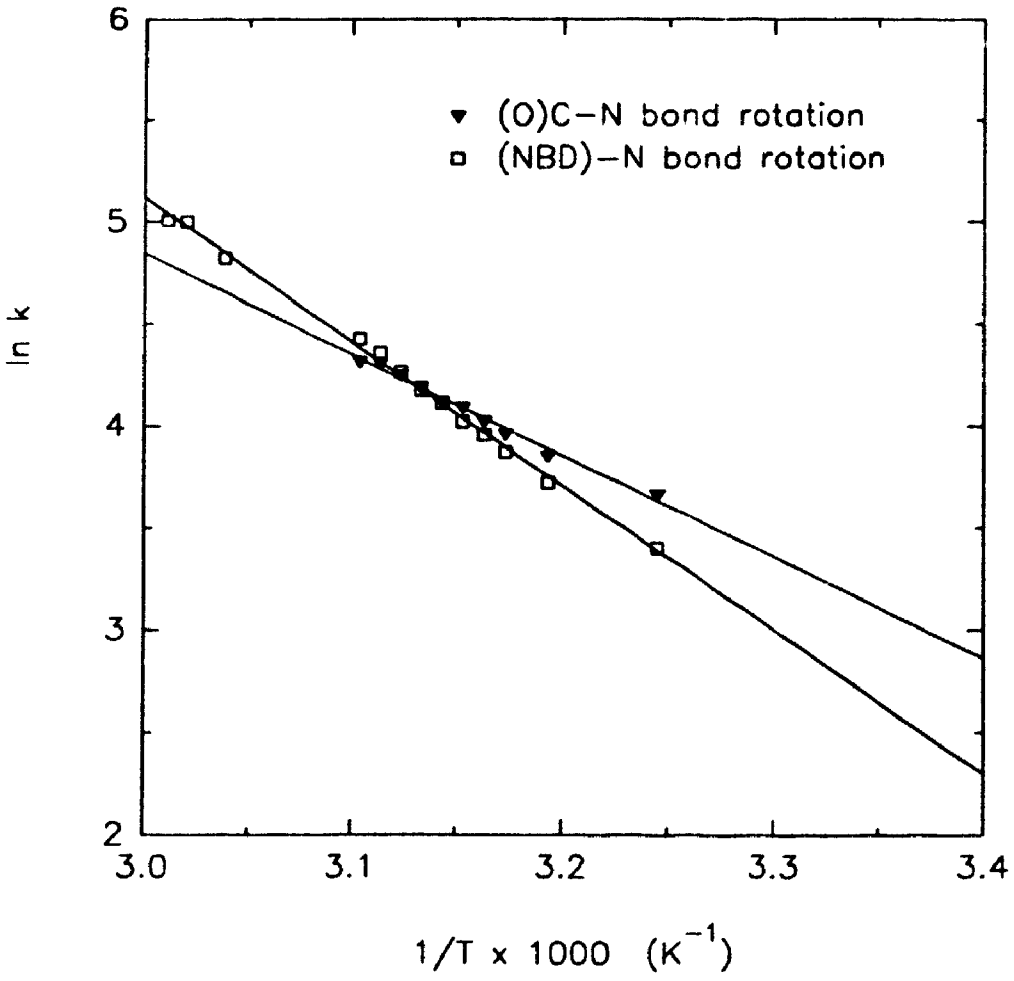

Figure 3-9: Arrhenius Plot for the Rate of Rotation of the (O)C-N Bond and the (NBD)-N bond in Labelled Monoamide 14 (N_2L[NBD]).

coefficients close to unity indicates that variation of $\delta\upsilon$ over the temperature range (35-59°C) does not have a significant effect on calculation of the rate of C-N bond rotation based on NMR peak separation. Based on the parameters from the line of best fit, the rate constant for (NBD)-N bond rotation at 25°C was calculated to be 14 sec^{-1}, which corresponds to a lifetime of 36 msec for each NBD isomer.

The fact that rotation of the (NBD)-N bond is more restricted than rotation of the (O)C-N bond is probably related to the fact that electrons from the nitrogen atom can delocalize over the entire aromatic ring system of the NBD group. Therefore resonance structure 3-6c may contribute more to the structure of labelled mono-amide than resonance structure 3-6b.

3.2.4 NMR Analyses of Larger Macrocyclic Polyamides

The ^{1}H NMR spectra of macrocyclic polyamides **7,8,9,10** (N_3L_3, N_4L_4, N_5L_5, N_6L_6) (Table 2-2) were more complex than those of di-amide **6** (N_2L_2) and labelled mono-amide **14** (N_2L[NBD]). The ^{1}H NMR spectrum of macrocyclic polyamides (**7,8,9,10**) were recorded at several temperatures and each spectrum had some general characteristics which were similar to those of the ^{1}H NMR spectrum of di-amide **6** (N_2L_2). For each macrocyclic polyamide, the signals observed for the methylene groups of the macrocyclic ring consisted of two or more broad multiplets centred at approximately 3.5 ppm. However,

none of these multiplets had the same coalescence temperature as was observed for N_2L_2.

The ^1H NMR spectra of labelled macrocyclic polyamides **15**, **16**, **17**, **18** (N_3L_2[NBD], N_4L_3[NBD], N_5L_4[NBD], N_6L_5[NBD]) were recorded at room temperature (Table 2-6, pg 49). In general these spectra were similar to the ^1H NMR spectra of the analogous unlabelled macrocyclic polyamides, with the important distinction that the multiplets observed for the ring methylene groups of each labelled macrocyclic polyamide contained peaks at ~4.5-4.0 ppm, which correspond to methylene groups adjacent to nitrogen bound to NBD.

A detailed dynamic NMR analysis of labelled and unlabelled macrocyclic polyamides (**7**, **8**, **9**, **10**, **15**, **16**, **17**, **18**) was considered beyond the primary objective of this thesis. However, based on the ^1H NMR spectra of these compounds, it is reasonable to conclude that the amide groups and NBD-N groups in each macrocyclic polyamide are planar.

3.2.5 Summary of Variable Temperature NMR Studies

Our variable temperature NMR analysis of di-amide **6** (N_2L_2) and labelled mono-amide **14** (N_2L[NBD]) has indicated that the amide groups of the cyclic ring are planar structures which are expected to have lifetimes of 17-23 msec at 25°C.

Rotation of the (NBD)-N bond was also shown to be restricted, and cis/trans isomers of NBD nitrogen derivatives of macrocyclic polyamines are predicted to have lifetimes of ~36 msec at 25° C. The energy barrier to inversion for (NBD)-N bond rotation was actually greater than that for (O)C-N bond rotation (59 kJ/mol vs 40-41 kJ/mol). Therefore, since the amide bond is generally considered to be planar, it is reasonable to conclude that the (NBD)-N group will likewise exhibit planar geometry.

A detailed NMR analysis of larger macrocyclic polyamides was not performed. However, the ^{1}H NMR spectral data for all of our probe molecules is consistent with the hypothesis that the nitrogens in the macrocyclic rings are planar (i.e., exhibit sp^2 character).

3.3 Molecular Modelling Analysis

3.3.1 Alchemy II and the Alchemy Minimizer

Based on our variable temperature NMR experiments, we concluded that all of the nitrogens in our macrocyclic polyamides were best represented as sp^2 nitrogens. Therefore, the nitrogens of macrocyclic polyamides can be treated as planar atoms in molecular modelling analyses. All molecular modelling and energy minimization calculations were performed using Alchemy II (TRIPOS) on a 486 DX personal computer. Dr. D.H. Hunter generously provided access to the Alchemy II software for these analyses. The Alchemy minimizer performs a conjugate gradient minimization on a force field equation which is dependent on the positions of atoms. The Alchemy minimizer calculates the potential energy of a molecule as the sum of the following terms;[6]

Equation 3-6 $$E = E_{str} + E_{ang} + E_{tor} + E_{vdw} + E_{oop}$$

E_{str} = bond stretching energy term
E_{ang} = angle bending energy term
E_{tor} = torsional energy term
E_{vdw} = van der Waals energy term
E_{oop} = out-of-plane bending energy term

The minimizer automatically makes small adjustments in the position of atoms, then evaluates the change in potential energy as a function of molecular geometry. If the automatic adjustment results in an increase in energy, the adjustment is reversed and another small adjustment on the geometry of the

molecules is performed. Bond, angle, torsional, and out of plane bending energy terms are calculated by comparing the geometry of a molecule with equilibrium values which are stored in Alchemy data files. The van der Waals energy is calculated as the sum of the van der Waals interactions of each atom based on its van der Waals radii and the van der Waals radii of proximate atoms. In our calculations, minimizations for each molecule were performed until the difference between potential energy from successive iterations varied less than 1 cal/mol.

The Alchemy equilibrium parameters were used without modification in all cases except the torsional energy term for planar nitrogen bound to aromatic carbon. Our variable temperature NMR experiments indicated that the C(aromatic)-N bond of NBD-nitrogen derivatives exhibited at least as much double bond character as the C(carbonyl)-N bond of amides. Accordingly, the torsional energy term for planar nitrogen bound to aromatic carbon was set equal to that of planar nitrogen bound to carbonyl carbon.

3.3.2 Molecular Modelling of Di-amide 6 (N_2L_2)

Our primary reason for undertaking molecular modelling analysis was to obtain information about the surface areas of the unlabelled and NBD-labelled macrocyclic polyamides described in Chapter 2 (Figure 2-2, and 2-3 respectively). Figure 3-10 shows two di-amide piperazine derivatives. The

molecular structure of di-acetamide **22** was determined by minimizing the structure obtained by covalently linking two, planar, N,N-dimethylacetamide groups. Because both the carbonyl carbons and nitrogens of the piperazine ring are treated as sp^2 hybridized atoms, the geometry of di-acetamide **22** is rigid except for the possibility of rotation about the CH_2-CH_2 bonds in the six-membered ring. After minimization, the geometry of the six membered ring was established to be a chair-like conformation with both amide groups in the plane of the six-membered ring.

By analogy with phospholipids (Figure 1-1) and other amphiphiles, we expect that di-amide **6** (N_2L_2) in monolayer or lipid bilayer systems will exist in a conformation which maximizes the interactions between alkyl chains on the molecule. We are interested in the surface area at the hydrophilic surface of each molecule, since this is the value which corresponds to the surface area of the diffusant in lipid bilayer membranes. A computer molecular model of di-amide **6** (N_2L_2) was obtained by covalently linking minimized, 10-carbon alkyl chains to the methylene groups α to the carbonyl groups in di-acetamide **22**. Since we are using these molecular mechanics calculations to determine the surface areas of the macrocyclic polyamides in monolayer or lipid bilayer systems, the dihedral angle of attachment of the alkyl chain to the methylene group α to the carbonyl was set to 90° in order to maximize the interaction between alkyl chains on the molecule (Figure 3-10a, compound **6**).

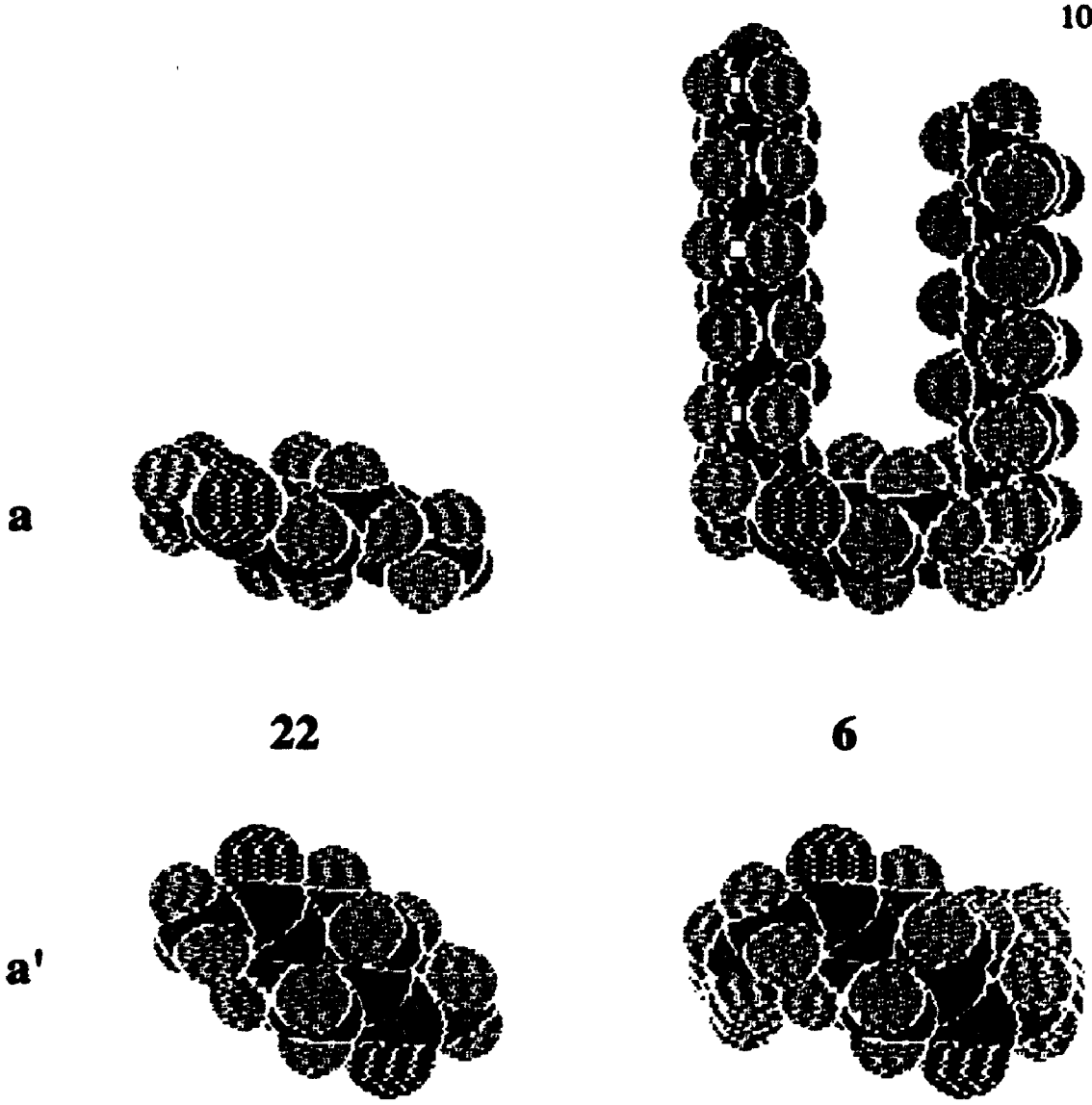

Figure 3-10: Computer Models of Di-Amides

Space-filled projections of Diacetamide 22 are shown; (a) with the hydrophilic surface normal to the plane of the page (a') with the hydrophilic surface in the plane of the page. Space-filled projections of di-amide 6 in a conformation which maximizes the interaction between alkyl chains are shown in the same orientations. According to these projections, the surface area of the hydrophilic surface of di-amide 6 is approximately equal to the surface area of the hydrophilic surface of diacetamide 22.

Our computer models indicated that if the alkyl chains of each lauroyl amide are in the all-trans conformation, then the surface area of di-lauroyl di-amide **6** (N_2L_2) should be approximately equal to the surface area of the di-acetamide **22**, since the diacetamide ring occupies a greater two dimensional space at the hydrophilic surface of the molecule than the alkyl chains of di-amide **6** (N_2L_2). Accordingly, all subsequent surface area measurements for larger polylauroyl macrocyclic polyamides were calculated based on the minimum surface areas of macrocyclic polyacetamides. To emphasize the relationship between these macrocyclic polyacetamides and the polylauroyl macrocyclic polyamides described in Chapter 2, the computer models are labelled using the same numbers and abbreviations.

3.3.3 Molecular Modelling of Macrocyclic Polyacetamides

The minimized structures of macrocyclic polyacetamides based on our unlabelled probe molecules are presented in Figure 3-11. All molecules were constructed by covalently linking planar, N,N-dimethyl acetamide units and then minimized using the Alchemy minimizer.

One interesting aspect of the geometry of our probe molecules which was immediately apparent was the fact that all of the macrocyclic polyacetamides have rigid, planar structures. In all of the macrocyclic polyacetamides, the only bonds free to rotate in the macrocyclic ring region

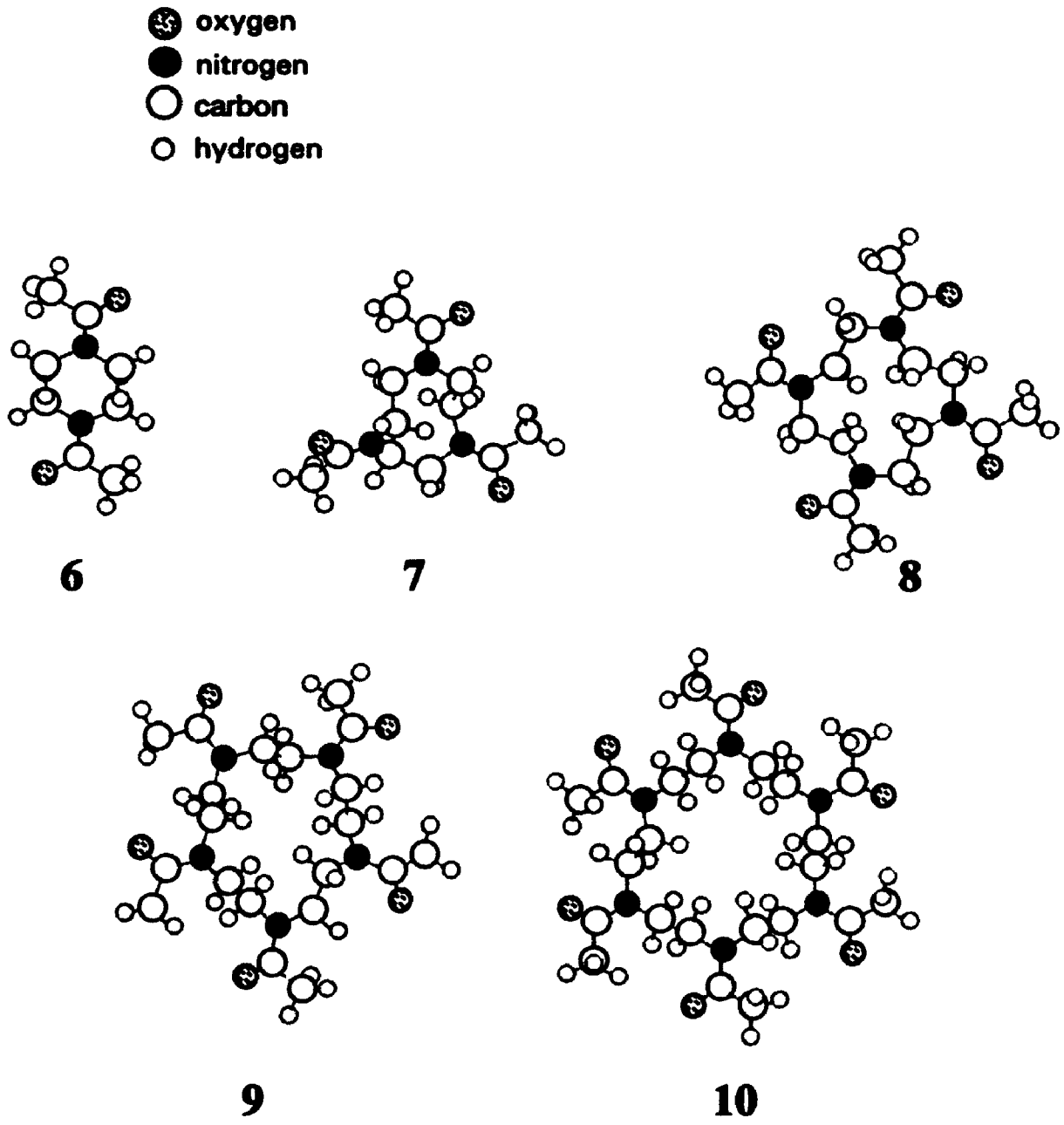

Figure 3-11: Ball and Stick Representations of Macrocyclic Polyamides

Each molecule is shown in the orientation which corresponds to its maximum possible hydrophilic surface in the plane of the page.

of the molecule are the bonds between adjacent methylene groups of the macrocyclic ring. For example, tetra-amide 8 (N_4L_4) contains only four bonds in its polar region which can undergo rotation, and this rotation is constrained by ring strain. Three views of one conformation of macrocyclic tetra-acetamide are illustrated in Figure 3-12. The bonds in the macrocyclic ring which can undergo rotation are labelled with arrows.

The space-filling display option of Alchemy II was used to obtain two dimensional space-filled projections of polyacetyl derivatives of macrocyclic polyamides (Figure 3-13). The Alchemy space-filling function produces a two-dimensional image of a molecule in which each atom is represented by a sphere of radius equal to its van der Waals radius. Using Alchemy II it is possible to determine the distance between non-bonded atoms in computer molecular models, therefore Alchemy II was utilized to determine some reference distances within our molecules, and these distances were used to construct the scalar bar shown in Figure 3-13. The surface areas of macrocyclic polyamides were calculated by photocopying the two-dimensional projections shown in Figure 3-13 onto 20 lb weight paper, cutting out the molecular projections and weighing the projection of each molecule. Surface areas were calculated relative to a 100Å^2 square which was prepared in the same manner. The results from these calculations are presented in Table 3-3.

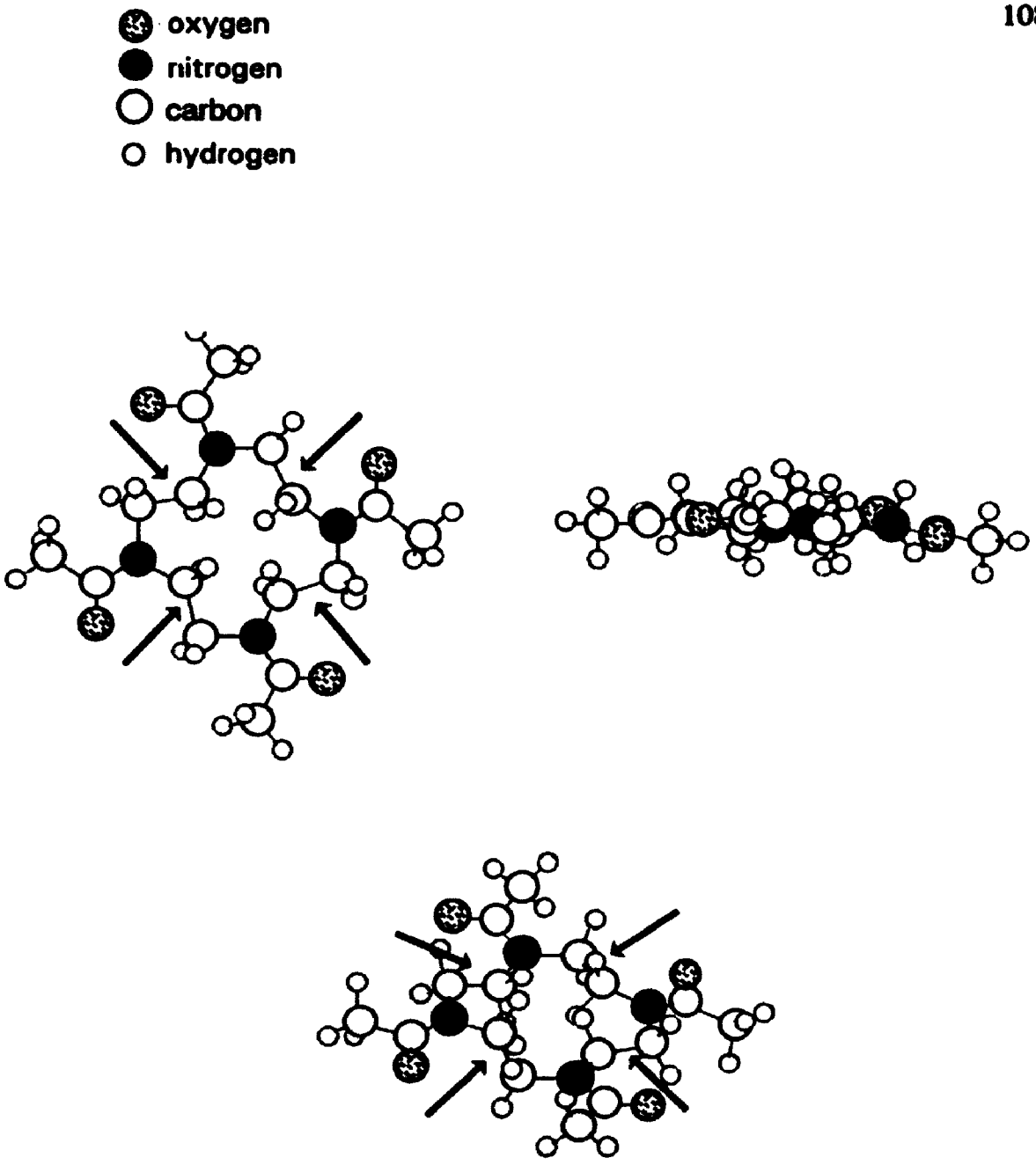

Figure 3-12: Restricted Rotation in Macrocyclic Tetra-amides

Macrocyclic tetra-acetamide is shown from three different perspectives. The arrows indicate the only bonds in the hydrophilic portion of the molecule which can undergo rotation.

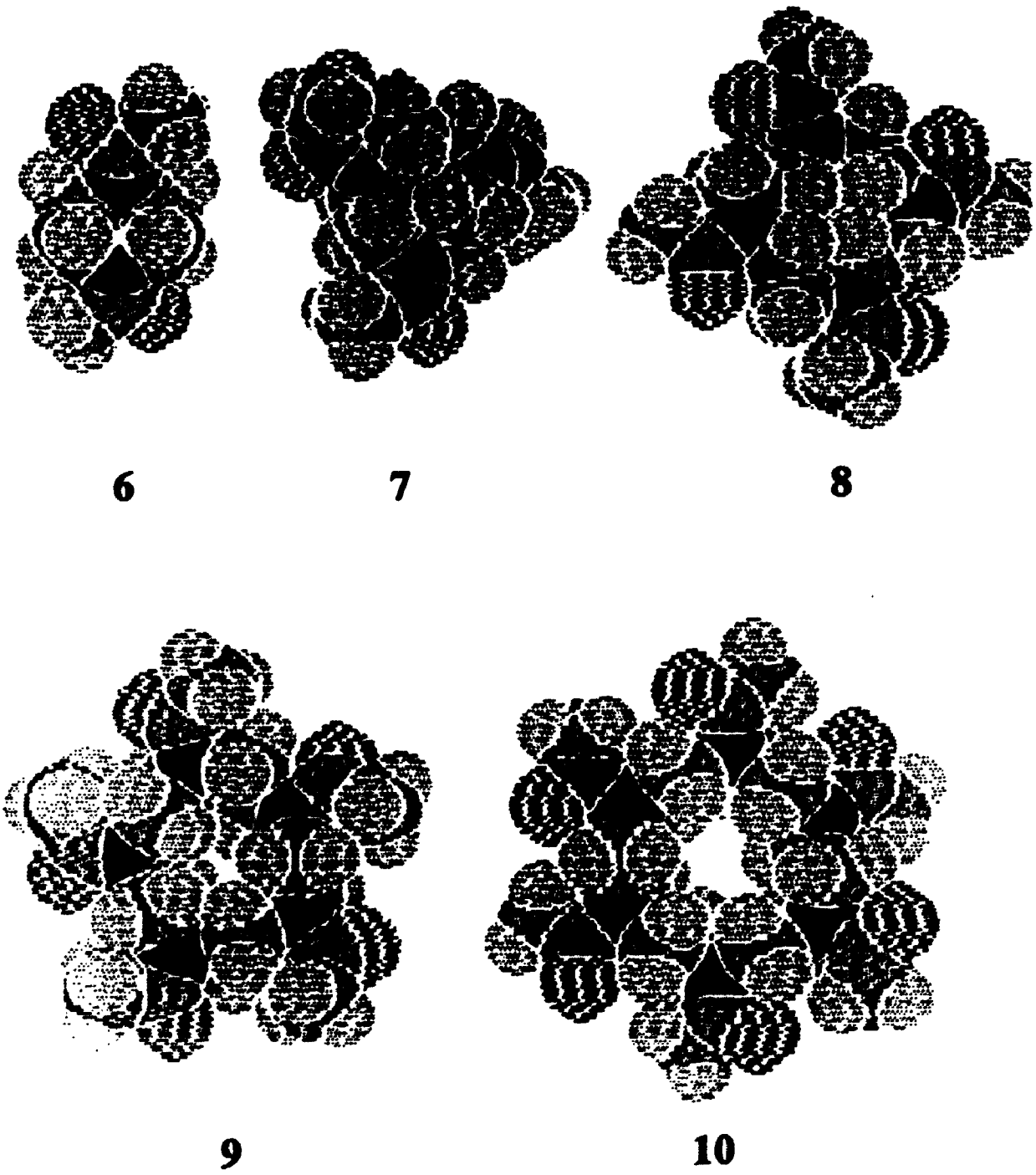

Figure 3-13: Space-filled Representations of Macrocyclic Polyamides

number of nitrogen atoms in macrocyclic ring	Surface Area of Hydrophilic Group (Å^2)			
	unlabelled macrocyclic polyamide	surface area‡	NBD-labelled macrocyclic polyamide	surface area‡
2	**6**, N_2L_2	55	**14**, N_2L[NBD]	62
3	**7**, N_3L_3	75	**15**, N_3L_2[NBD]	67
4	**8**, N_4L_4	106	**16**, N_4L_3[NBD]	108
5	**9**, N_5L_5	130	**17**, N_5L_4[NBD]	128
6	**10**, N_6L_6	154	**18**, N_6L_5[NBD]	144

Table 3-3: Surface Areas of Labelled and Unlabelled Macrocyclic Polyamides Calculated Using Alchemy II Computer Models

‡ Each surface area corresponds to the surface area of the hydrophilic surface of macrocyclic polyacetamides.

3.3.4 Molecular Modelling of Labelled Macrocyclic Polyamides

The minimized structures of NBD-labelled macrocyclic polyacetamides based on our labelled probe molecules are presented in Figure 3-14. Molecules were constructed by deleting one acetamide group from the minimized macrocyclic polyacetamides, and adding one (previously minimized) NBD group. The entire NBD-labelled structure was then minimized. Because the nitrogen bound to the NBD group was treated as a sp^2 hybridized atom, the nitrogen atoms of labelled macrocyclic polyamides exhibited the same planarity as those in unlabelled macrocyclic polyamides. The surface areas of NBD-labelled macrocyclic polyacetamides were calculated using the method described for unlabelled macrocyclic polyamides (Table 3-3). The results from our molecular modelling analyses predict that the absolute surface area of the NBD group is slightly larger than the surface area of one acetamide group (or the minimum planar surface area of one lauroyl amide group at the hydrophilic surface). (Figure 3-15, Figure 3-16)

Because the NBD group is slightly larger than an acetamide group, there are more unfavourable van der Waals interactions between the NBD aromatic ring and the hydrogens of the macrocyclic ring. From our molecular modelling analyses it appears that these unfavourable van der Waals interactions give rise to a minimum energy conformation of

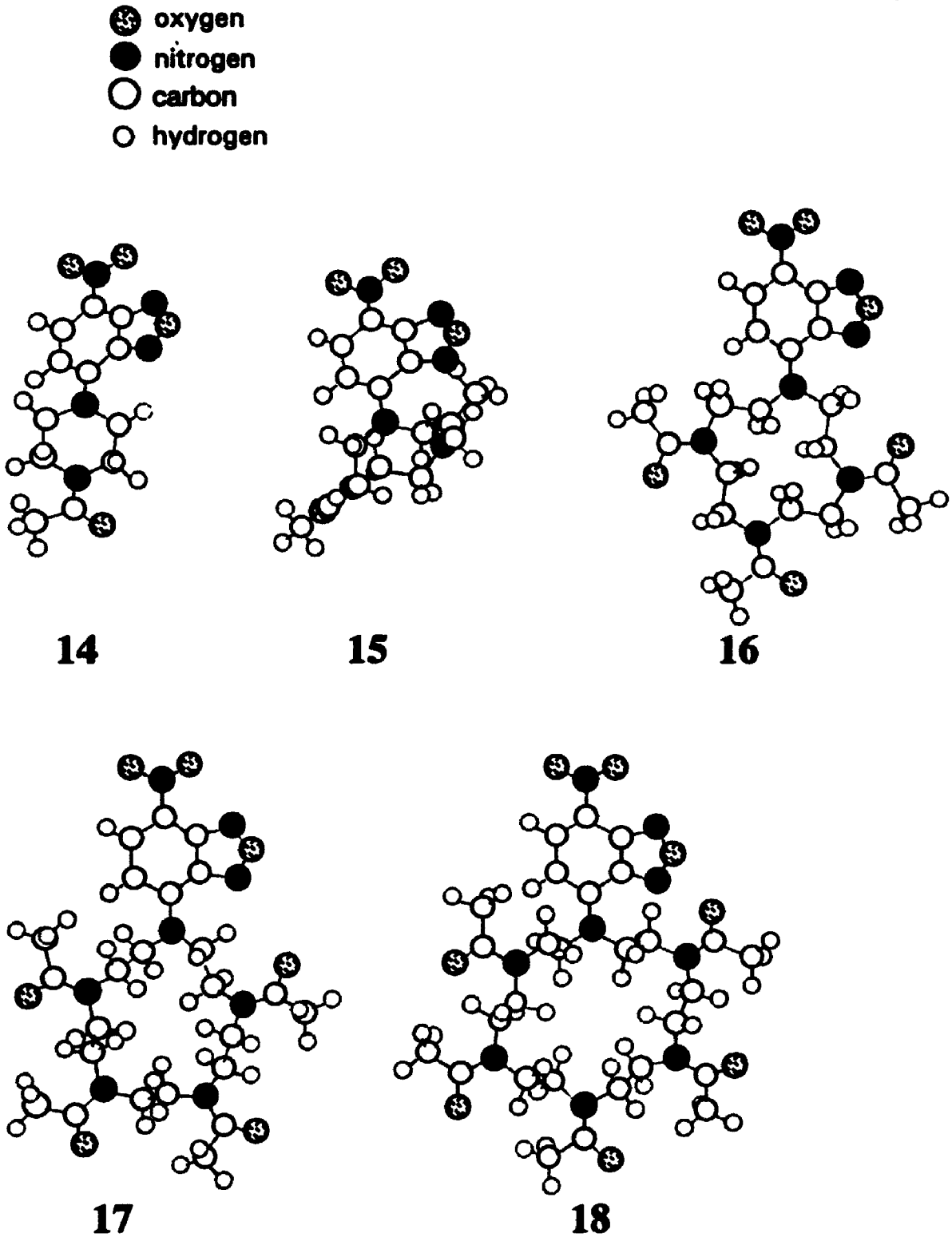

igure 3-14: Ball and Stick Representations of Labelled Macrocyclic Polyamides

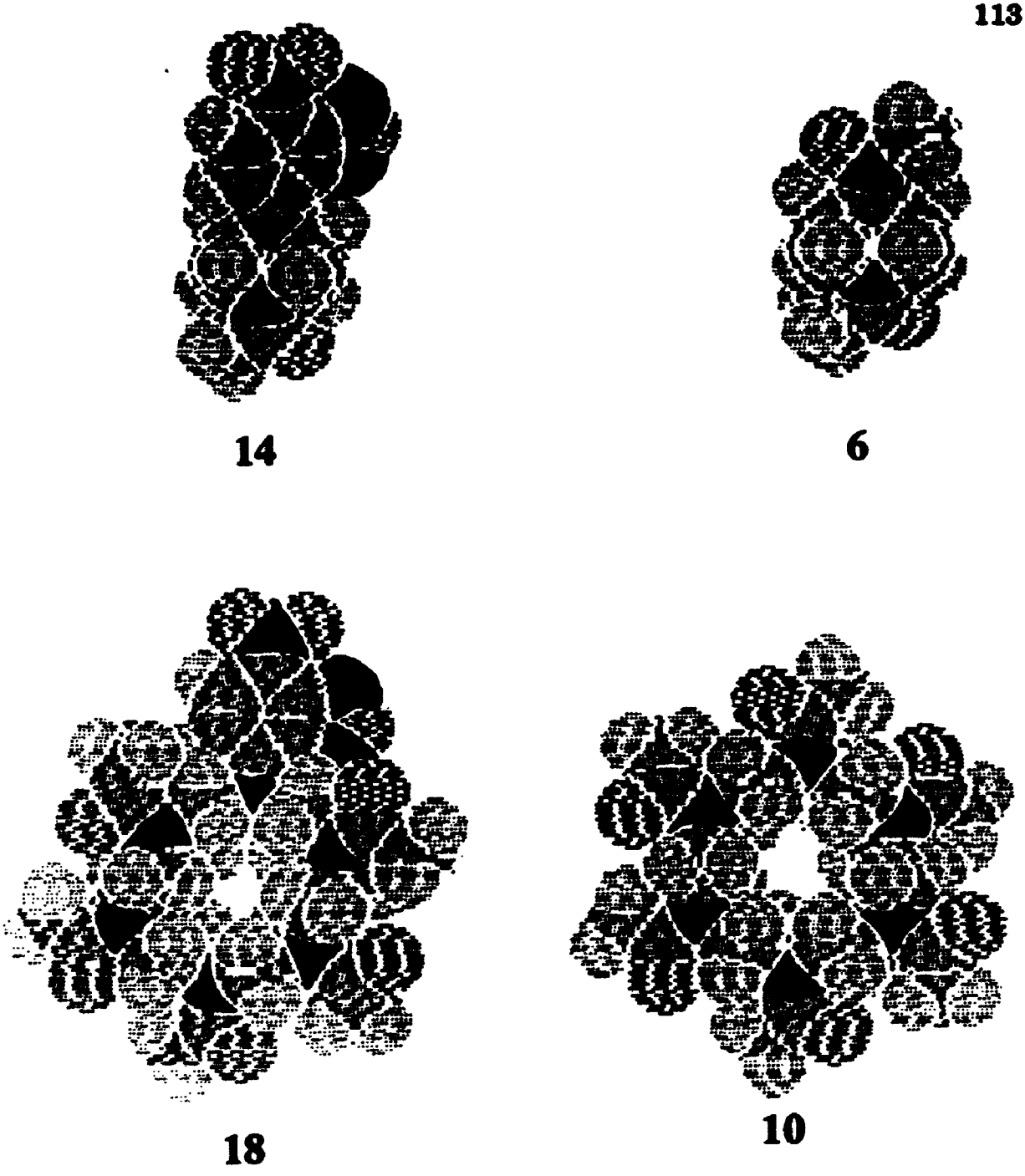

Figure 3-15:Space-filled Representations of Labelled and Unlabelled Polyacetamide Analogues of The Smallest {14, (N_2L[NBD]), 6, (N_2L_2)} and Largest {18, (N_6L_5[NBD], 10, (N_6L_6)} Probe Molecules.

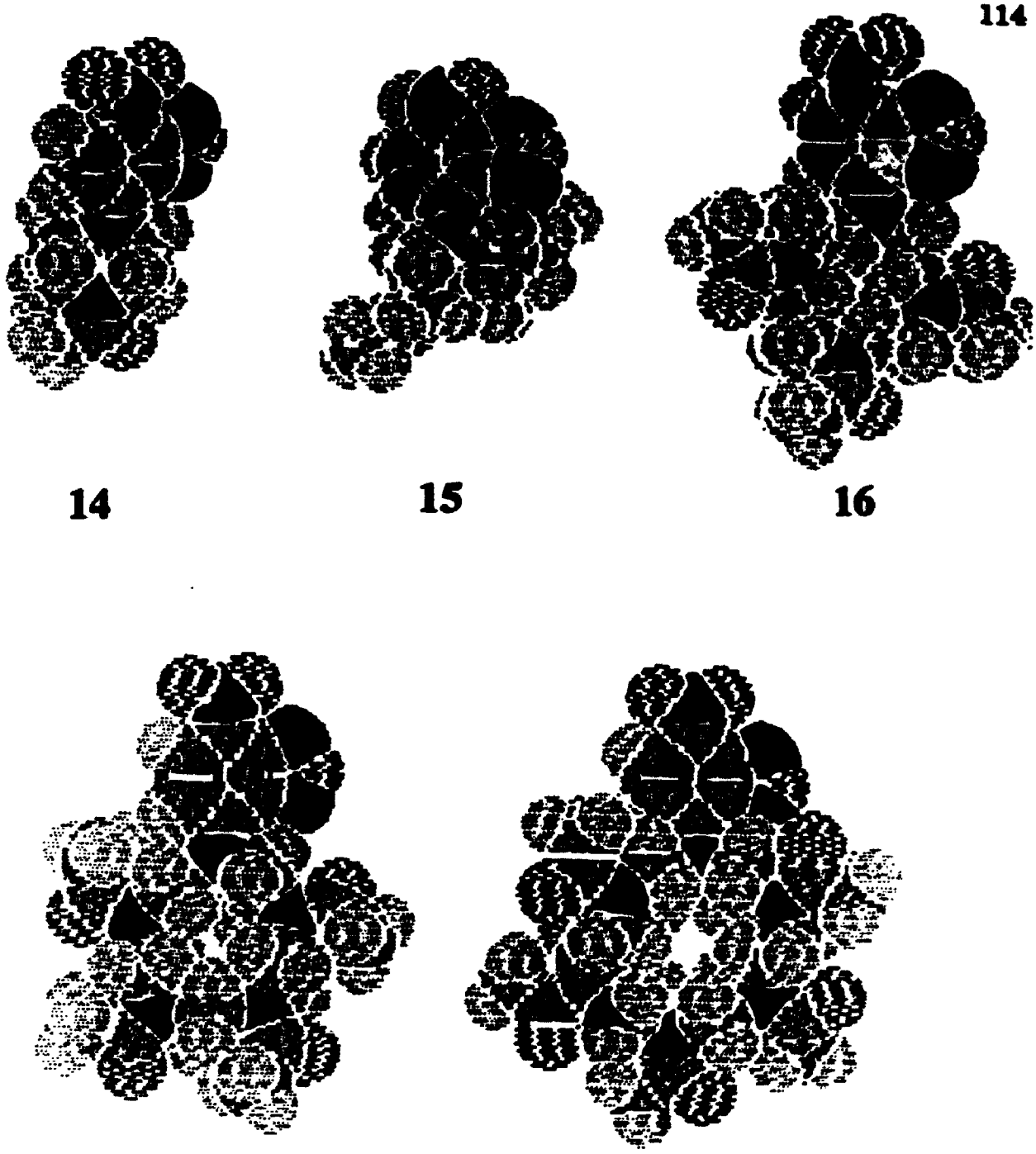

Figure 3-16: Space-Filled Representations of Labelled Macrocyclic Polyamides

N_3L_2[NBD] where all nitrogens of the cyclononane ring are planar, but the two amide groups lie in a plane which is 90° to the plane of the NBD group. Similarly, in labelled tri-amide **16** (N_4L_3[NBD]) and larger labelled macrocyclic polyamides, the NBD group is tilted slightly relative to the plane of the amide groups, and this tilt decreases the projected surface area of the hydrophilic surface of each molecule. Therefore, based on our molecular modelling analysis, we predict that each NBD-labelled macrocyclic polyamide (except labelled di-amide **15** N_3L_2[NBD]), will have approximately the same surface area as the corresponding unlabelled macrocyclic polyamide. Labelled di-amide (N_3L_2[NBD]) is predicted to be slightly smaller than the corresponding unlabelled tri-amide (N_3L_3) because the NBD group is oriented at a 90° angle relative to the plane defined by the amide groups on the macrocyclic ring.

3.4 Conclusions

Our variable temperature NMR experiments have indicated that the amide bonds in macrocyclic polyamides are planar and have appreciable double bond character. Likewise, variable temperature NMR has shown that the nitrogen-carbon bond which covalently links the NBD group to piperazine in labelled mono-amide **14** (N_2L[NBD]) has double bond character. The ^{1}H spectra of larger macrocyclic polyamides are also consistent with the presence of planar nitrogen atoms within each macrocyclic ring.

Our conclusion that macrocyclic polyamides should exist in conformations which are rigid and planar due to the contribution of sp^2 derivatized nitrogen is novel. Previous researchers have commented on the fixed geometry of the macrocyclic ring in macrocyclic polyamides[7,8,9] but have not correlated this rigidity to any specific property, or distinguished it from the geometry of analogous macrocyclic polyamines. The planarity of amide bonds is well known, and it is therefore surprising that the amide groups of macrocyclic polyamides had not been previously treated as planar moieties.

The conclusion that rotation of the (NBD)-N bond of nitrogen derivatives of NBD is more restricted than rotation of (O)C-N bonds in amides will have far-reaching implications for biochemical research. Previous molecular orbital calculations have indicated that the permanent and transition state dipole moments of NBD-nitrogen derivatives are aligned along the axis of

the (NBD)-N bond.[10] Other researchers have reported that nitrogen derivatives of NBD are likely to undergo charge transfer type transitions, with electron density moving from the nitrogen to the nitrobenzoxadiazole ring.[11] These findings suggest that the nitrogen atom and the NBD group in nitrogen derivatives of NBD are linked through a π orbital system.

Our NMR analysis indicates that rotation of the (NBD)-N bond is restricted. The fact that there is a 59 kJ/mol energy barrier to rotation suggests π bonding via contribution of resonance structure 3-6c is significant. The concept that the NBD-N bond has double bond character will allow for simplification of the models used in fluorescence depolarization and energy transfer experiments and allow for a more precise interpretation of experimental results for nitrogen derivatives of NBD obtained by these methods.

Based on the variable temperature NMR results, all nitrogens in the macrocyclic ring section of macrocyclic polyamides have been assigned planar (sp^2) geometry. Molecular modelling analysis of our labelled and unlabelled macrocyclic polyamides has provided insight into the geometry of our probe molecules. Specifically, our Alchemy II calculations predict that labelled and unlabelled macrocyclic polyamides should have hydrophilic groups with rigid planar geometry. According to these calculations, the minimum possible surface areas of the hydrophilic surfaces of polylauroyl macrocyclic

polyamides should be approximately equal to the surface areas of analogous polyacetyl macrocyclic polyamides.

Our calculations of surface areas based on macrocyclic polyacetamides suggest that there should be a systematic increasing trend in surface area of macrocyclic polyamides as one increases the number of nitrogen atoms in the macrocyclic ring. Finally, our computer calculations suggest that NBD-labelled macrocyclic polyamides (except labelled di-amide 7 (N_3L_2[NBD]) should have surface areas which are very similar to the surface areas of analogous unlabelled macrocyclic polyamides.

3.5 Experimental (Dynamic NMR)

Samples for dynamic NMR experiments were prepared by dissolving ~30 mg of solid material in ~1 mL of $CDCl_3$. The solutions were transferred to 5mm o.d. NMR tubes, evacuated under vacuum and sealed with an acetylene torch. Samples were tested at high temperatures prior to NMR analysis to ensure the stability of the samples. All ^1H NMR spectra were acquired with a Varian XL-300 spectrometer operating at 300 MHz. The NMR spectrometer was equipped with a Gemini Variable Temperature Control unit which had been calibrated using ethylene glycol. Temperature was controlled within ±0.2°C.

In a typical experiment the sample was allowed to equilibrate for at least 20 minutes after the probe had reached the desired temperature. Once the sample had equilibrated, shimming was performed and 16 transients were collected. Fourier transforms on spectral data were performed without signal enhancement or line broadening functions. ^1H NMR chemical shifts are reported in ppm relative to TMS as an internal standard.

3.6 References

1. Akitt, J.W., *NMR and Chemistry, Second Edition*, Chapman and Hall, New York, **1983**, pg. 20.
2. Stewart, W.E., and Siddall III, T.H., Nuclear Magnetic Resonance Studies of Amides, *Chem. Rev.*, *70*, **1970**, 517-551.
3. Sandström, J., *Dynamic NMR Spectroscopy*, Academic Press, Toronto, **1982**
4. Csizmadia, I.G., Peterson, M.R., Kozmutza, C., and Robb, M.A., Recent Advances in the Theoretical Treatment of Acid Derivatives, *The Chemistry of Acid Derivatives Part 1*, Saul Patai ed., John Wiley and Sons, Toronto, **1979**, pg 26.
5. Graham, L.L., and Diel, R.E., Nuclear Magnetic Resonance Studies of Internal Rotation in Aliphatic Tertiary Amides, *J. Phys. Chem.*, *75*, *8*, **1969**, 2698-2699.
6. *Alchemy II Manual*, Tripos Associates Inc., St. Louis Missouri, **1988**
7. Malthête, J., Poupinet, D., Vilanove, R, and Lehn, J.M., Monolayers of Macrocyclic Polyamides at the Air-Water Interface, *J.Chem.Soc. Chem.Comm.*, **1989**, 1016.
8. Lehn, J.M., Malthête, J., and Levelut, A., Tubular Mesophases: Liquid Crystals Consisting of Macrocyclic Polyamides *J.Chem.Soc. Chem.Comm.*, **1985**, 1794-1796.

9. Mertesdorf, C., and Ringsdorf, H., Self-Organization of Substituted Azacrowns Based on their Discoid and Amphiphilic Nature, *Liquid Crystals*, *5*, **1989**, 1757-1772.

10. Paprica, P.A., Baird, N.C., and Petersen, N.O., Theoretical and Experimental Analyses of Optical Transitions of Nitrobenzoxadiazole (NBD) Derivatives, *J.Photochem. Photobiol. A: Chemistry*, **1993**, *70*, 51-57. **Appendix I.**

11. Suzuki, H., and Hiratsuka, H., Photophysical and Structural Study on Nonlinear Optical Properties of Benzoxadiazole Derivatives, *SPIE, Vol 936, Nonlinear Optical Properties of Organic Materials*, **1988**, 97-106.

Chapter 4

SURFACE AREA DETERMINATION OF MACROCYCLIC POLYAMIDES AT THE AIR-WATER INTERFACE

4.1 Experimental Objective

The goal of this research project is to correlate the surface areas of our labelled macrocyclic polyamide molecules with their diffusion coefficients in model membrane systems. Clearly, the success of this project depends on our ability to determine the surface areas of our labelled macrocyclic polyamides in lipid bilayer systems. Measurements of amphiphilic head groups in monolayer systems can be used to approximate surface areas in lipid bilayers, since amphiphiles in monolayers and lipid bilayers generally exhibit similar conformations. Therefore we chose to measure the surface areas of macrocyclic polyamides in monolayer systems.

Because the correlation of the surface areas of large amphiphiles with molecular structure at the air-water interface is not necessarily straightforward, the first step was the determination of surface areas of unlabelled macrocyclic polyamides (**6, 7, 8, 9, 10**) at the air water interface. Subsequent analysis of labelled macrocyclic polyamides (**14, 15, 16, 17, 18**), combined with our knowledge that the NBD-N group is planar, should allow us to determine the surface areas of our NBD labelled probe molecules in monolayer systems.

Recently, the pressure of DMPC lipid bilayers at 36°C has been estimated to be approximately 30 mN/m.[1] Therefore, our experimental approach was to determine the surface areas of our macrocyclic polyamides in monolayers at 30 mN/m, in the hope that these values would correspond to the surface areas which macrocyclic polyamides exhibit in lipid bilayer membranes.

4.2 The Study of Monomolecular Films[2,3]

When a small amount of water insoluble, non-volatile, organic material is carefully deposited on the surface of water, the material will either:

(i) form a compact drop;

or (ii) spread out over the entire aqueous surface and form a two-dimensional film.

A stable monolayer will form if the cohesive forces between water and the organic molecule are stronger than the cohesive forces between different molecules of the organic material. When a monomolecular film forms, the surface tension of the system is decreased; therefore, it is possible to measure the surface pressure (Π) of the monolayer relative to the surface pressure of pure water.

The state of monomolecular films can be classified as solid, liquid, or gaseous depending on the strength of the forces between the film-forming

molecules. Representations of film-forming molecules in various monolayer states are shown in Figure 4-1. If the forces between film-forming molecules are weak, molecules move independently of each other on the aqueous surface and the film is classified as gaseous. At the other extreme, when van der Waals interactions between film-forming molecules are strong, the molecules of the film adhere to each other and the monolayer is classified as solid. Films with intermediate properties are classified as liquid monolayers.

Most studies of monomolecular films at the air-water interface are performed using a Langmuir Film Balance (Figure 4-2). The major components of a typical Langmuir film balance are:

(a) A hollow trough, constructed of water repellant material (usually Teflon) which contains the aqueous phase;

(b) A movable bar (usually constructed of Teflon), which is used to compress the monomolecular film;

(c) A free-floating barrier (usually constructed of Teflon) which is connected to a pressure transducer (d); this 'float' is used to measure the surface pressure (Π) of a monomolecular film as a function of the area it occupies.

In a typical monolayer experiment, the subphase (usually water) is poured into the trough until a positive meniscus forms, then a small amount of material is deposited on the subphase using a volatile organic solvent. The

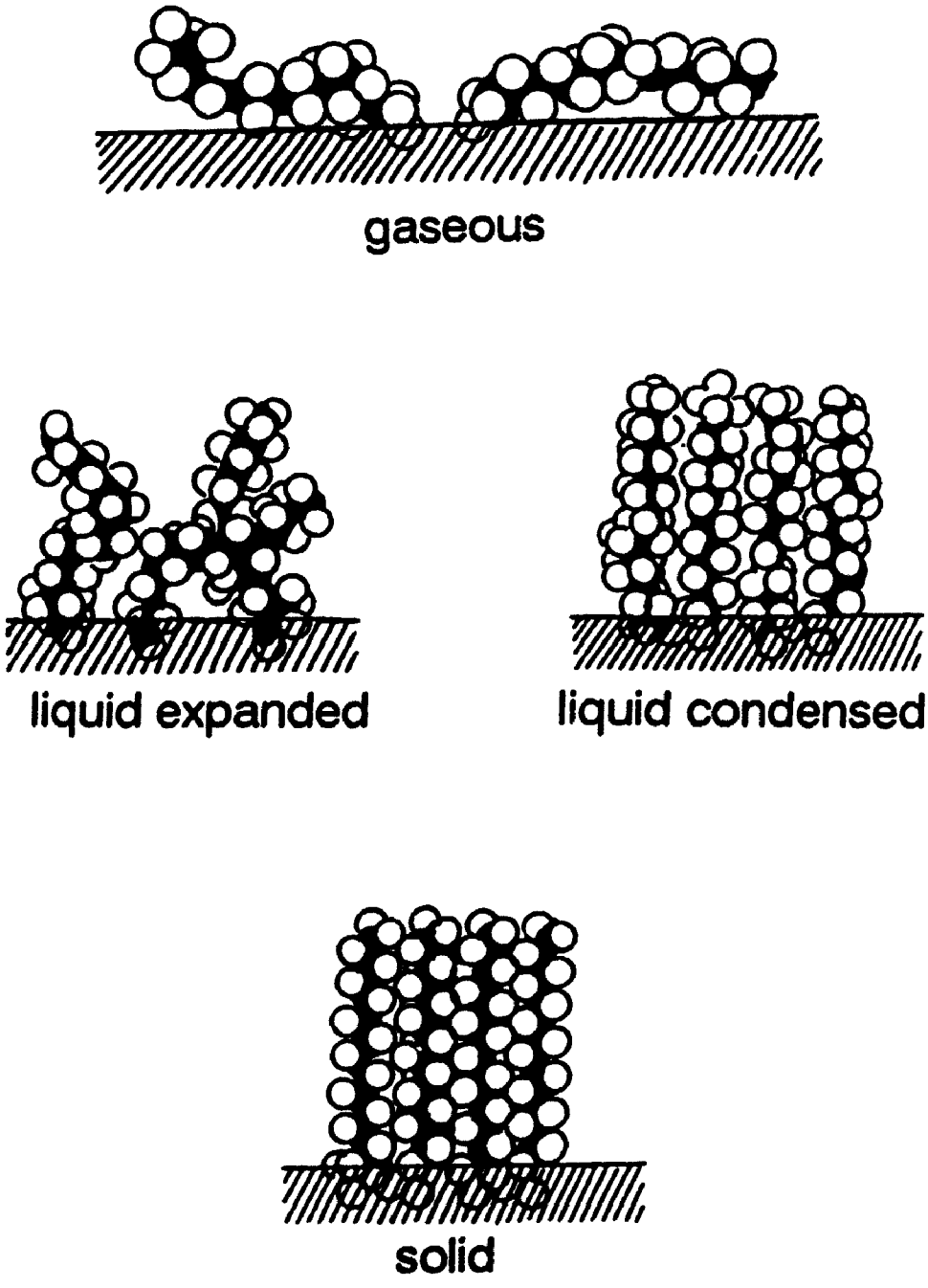

Figure 4-1: **Schematic Representation of Different States of Amphiphiles in Monomolecular Films.**[4]

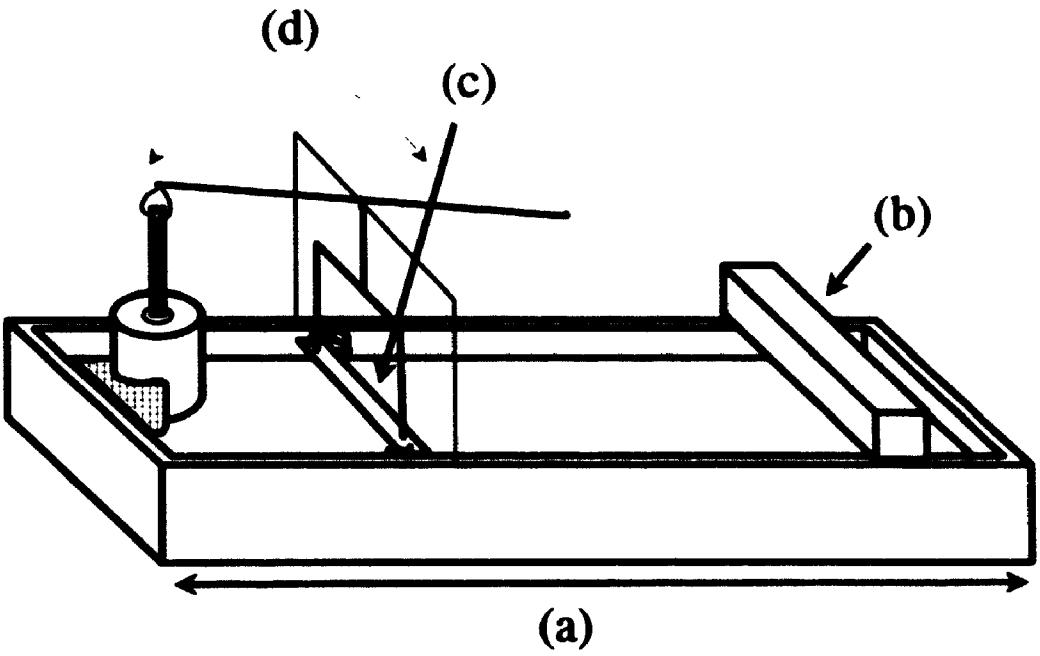

Figure 4-2: Schematic Representation of a Langmuir Film Balance

Several components are labelled: the trough (a), the movable bar (b) and the float (c) which is connected to a pressure transducer (d). Water is poured into the trough until a positive meniscus forms, the film-forming molecules are deposited on the aqueous surface on the area between (b) anc (c).

volatile solvent is allowed to evaporate, then the surface pressure is monitored as the movable barrier is advanced towards the pressure transducer at a rate slower than the amount of time required for the molecules in the monolayer to achieve conformational equilibrium. If the number of moles of the organic material and the surface area between the movable bar and the Teflon barrier are known, then one can plot the surface pressure (Π) as a function of the surface area per molecule in the monolayer film (Figure 4-3). It follows that the surface area of a film-forming molecule at a given surface pressure and temperature can be calculated by interpolation. Alternatively, one can extend the line corresponding the steepest part of the curve for a monolayer transition, and determine the surface area at zero pressure by extrapolation.

As the area available for spreading decreases during a monolayer experiment, monomolecular films may undergo changes of state. Graphically, the state of a monolayer can be determined by the rate at which surface pressure (Π) varies with the surface area per molecule. Two theoretical monolayer curves are illustrated in Figure 4-3. In the gaseous state monolayers are very compressible. The surface pressure (Π) of monolayers in the gaseous state varies with surface area per mole (SA/n) according to Equation 4-1, which is the two-dimensional analogue of the ideal gas law:

Equation 4-1 $$\Pi = (RT) \times \frac{n}{SA}$$

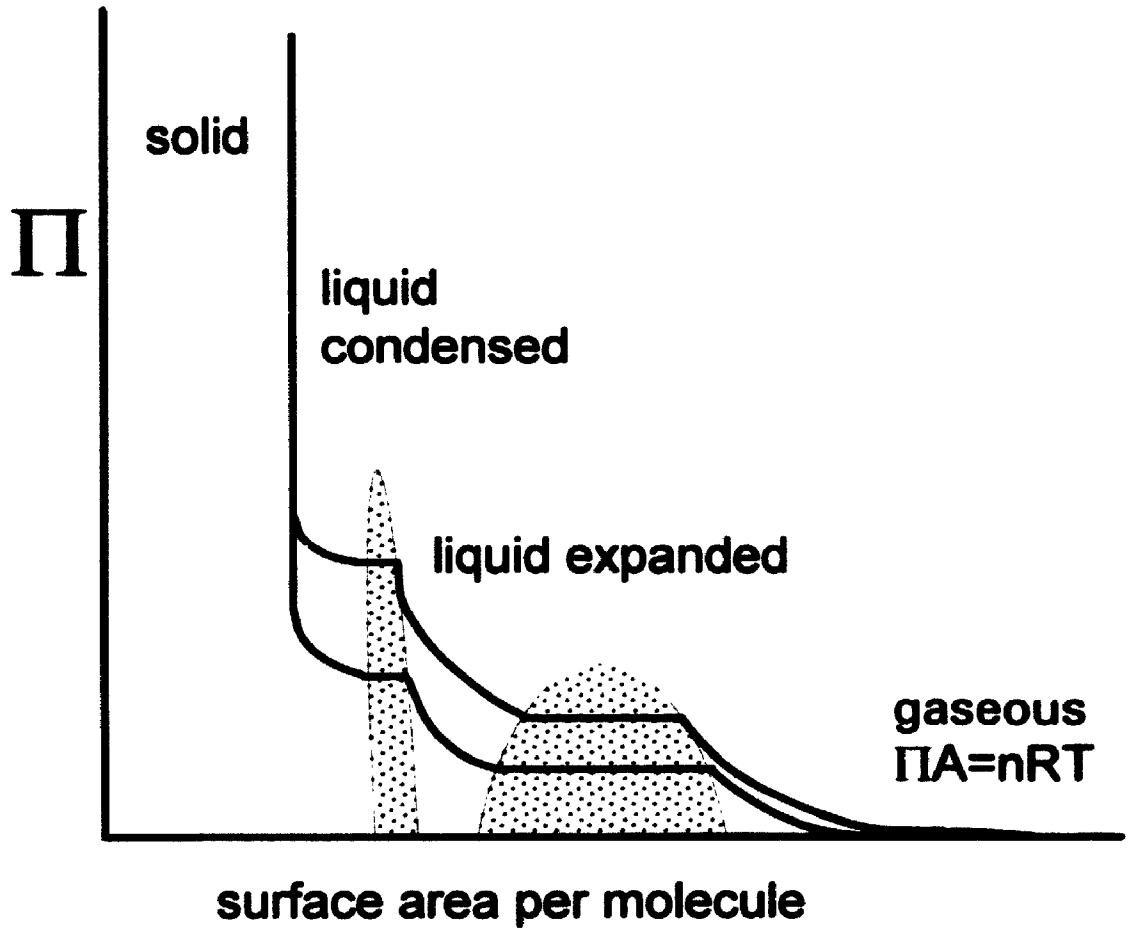

Figure 4-3: Theoretical Surface Pressure (Π) vs Surface Area Curves

Curves for two different temperatures are shown for a theoretical amphiphile. The lower line represents the curve obtained at the lower temperature. The shaded areas represent regions where two phases co-exist, however, if the monolayer is compressed at high temperatures, plateaus corresponding to these regions may not be present. Regions of the curve corresponding to gaseous, liquid expanded, liquid condensed and solid phases are labelled.

It follows that a plot of Π vs. surface area per molecule for film-forming molecules in the gaseous state will give a hyperbolic curve (Figure 4-3).

In the solid state, monolayers have very low compressibility (as do three dimensional solids), and there is a rapid increase in surface pressure over a narrow range of surface areas. Liquid monolayers, with properties intermediate between those of gaseous and solid films, can exist in either the liquid expanded or liquid condensed state. As indicated in figure 4-3, monolayer curves are temperature dependent. This phenomenon reflects the 'melting' and 'boiling' properties of monomolecular films.

4.3 Surface Areas of Phospholipids

Phospholipids (Figure 1-1) in monolayer or bilayer systems can exist in either the gel (solid) state, in which the hydrocarbon chains are rigid and close packed, or the liquid crystalline (liquid condensed) state, in which the hydrocarbon chains can undergo rotation and local conformational motion. The temperature at which a phospholipid undergoes a change of state varies depending on the hydrophilic head group of the phospholipid, the length, extent of unsaturation and branching of the hydrocarbon chains attached to it, and whether the phospholipid is in a monolayer or bilayer assembly.

Dimyristoylphosphatidylcholine (DMPC, Figure 1-1) which contains two linear, saturated, fourteen carbon acyl chains and a choline head group, has a transition temperature of 23°C in bilayer membranes.[5] DMPC bilayers are often used to measure lateral diffusion coefficients, since both the liquid crystalline and gel states are close enough to room temperature that they are readily accessible with standard heating and cooling equipment. DMPC was chosen for our diffusion measurement experiments for this reason (Chapter 5). However, because of the low transition temperature of DMPC, the shape of Π vs. Surface Area isotherms for the phospholipid are extremely temperature dependent[6] over the ranges of 19−25°C and 0-20 mN/m, and it is therefore difficult to obtain reproducible monolayer curves for DMPC without a Langmuir film balance which is equipped with a temperature control unit.

Dipalmitoylphosphatidylcholine (DPPC) contains two linear, saturated, 16 carbon acyl chains and a choline head group. DPPC has a higher transition temperature than DMPC (41°C) in bilayer membranes.[5] Both DMPC and DPPC exhibit the same surface area in monolayer and lipid bilayer systems, because both phospholipids contain the the choline headgroup, which is the factor that determines the surface area of phosphatidylcholines with linear, saturated alkyl chains. We did not have access to a temperature controlled Langmuir film balance, therefore we performed monolayer experiments using DPPC with the expectation that the surface area measurements we obtained

from these experiments would reflect the surface areas of DMPC in lipid bilayer membranes.

A study of the surface area of DPPC as a function of surface pressure was performed at 21±2°C. Results from different experiments were reproducible within ±2% of the mean, and are shown in Figure 4-4 and 4-5. These results are in close agreement with previously published data[2] for DPPC which report a surface area of ~50Å^2 at Π~30 mN/m; however it should be noted that these values can only be used to approximate the surface area of phosphatidylcholine in membranes because they are obtained from monolayers in the solid state.

4.4 Surface Areas of Macrocyclic Polyamides

The surface areas of macrocyclic polyamides **6**, **7**, **8**, **9**, **10** (N_2L_2, N_3L_3, N_4L_4, N_5L_5, N_6L_6) were determined as a function of surface pressure using a Langmuir film balance. Despite the fact that macrocyclic polyamides were stored in a vacuum dessicator, NMR analysis indicated that all of the macrocyclic polyamides which we prepared contained up to 10% water. Attempts to dry the macrocyclic polyamides under vacuum, or to dry solutions of macrocyclic polyamides using molecular sieves or anhydrous $MgSO_4$, were unsuccessful. Therefore, it was necessary to calculate the number of waters of hydration for each macrocyclic polyamide. This was accomplished by

comparing integration of the water peak in the ^1H NMR spectrum of a 30 mg sample of macrocyclic polyamide to integration of the signals observed for the methylene groups of the macrocyclic ring. The corrected molar mass (including waters of hydration) for each macrocyclic polyamide was then used to calculate the concentrations of solutions which were prepared for monolayer experiments.

Three or more monolayer curves were obtained for each macrocyclic polyamide from at least two different solutions. The surface areas obtained from the curves for monolayers prepared from the same solution were reproducible within a range $\pm 2\%$ of the mean; surface areas obtained from curves prepared from different solutions were reproducible within a range of $\pm 10\%$ of the mean.

From the slopes of the compression curves, one can conclude that each macrocyclic polyamide forms a stable monolayer which undergoes a gas-liquid transition at low pressure, and exhibits a liquid compression curve in the pressure range 0-40 mN/m. The results from these experiments are shown graphically in Figure 4-4 and in Table 4-1. The transitions for di-amide **6** (N_2L_2) and penta-amide **9** (N_5L_5) level off below 30 mN/m, therefore the surface areas at 30 mN/m were calculated by extrapolation from the line defined by the steepest part of each curve.

Each macrocyclic polyamide in the series exhibits a distinct surface area

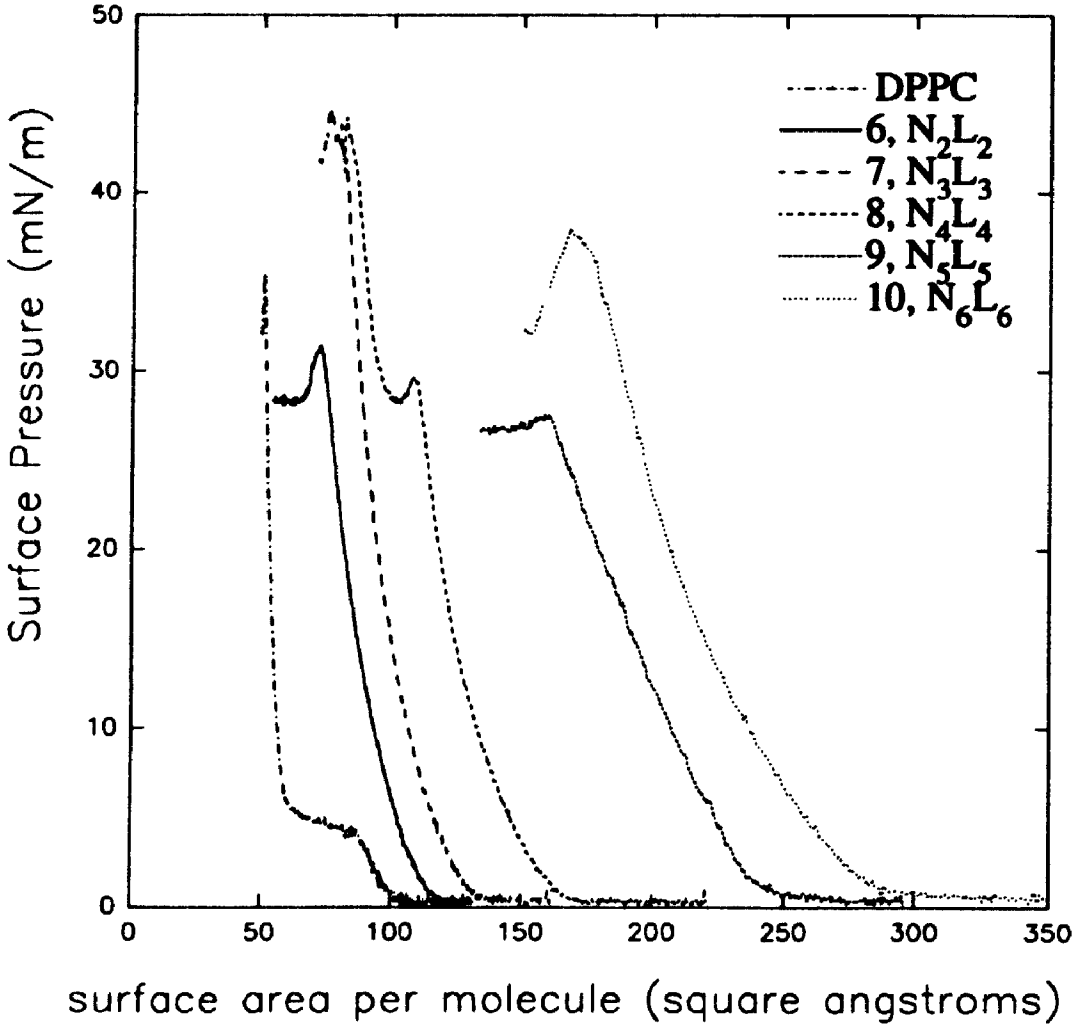

Figure 4-4: Surface Pressure vs Surface Area Curves for Unlabelled Macrocyclic Polyamides

Amphiphile	Surface Area (Å^2)				
	0 mN/m	10 mN/m	20 mN/m	23 mN/m	30 mN/m
DPPC	59‡	57	53	53	51
6, N_2L_2	99‡	90	82	79	74
14, N_2L[NBD]	65‡	52	42‡	38‡	30‡
7, N_3L_3	107‡	107	96	93	88
15, N_3L_2[NBD]	116‡	103	90	86	77‡
8, N_4L_4	139‡	134	119	116	110
16, N_4L_3[NBD]	129‡	122	109	105	100
9, N_5L_5	230‡	193	181	172	153‡
17, N_5L_4[NBD]	230‡	204	180	172	156‡
10, N_6L_6	245‡	238	207	200	189
18, N_6L_5[NBD]	291‡	272	246	239	224

Table 4-1: Surface Areas of Macrocyclic Polyamides Calculated from Monolayer Experiments

‡ calculated by extrapolation of line defined by the steepest part of the curve

at all pressures less than or equal to 30 mN/m, and all of these surface areas were larger than the surface area of DPPC. Based on these results, we have calculated the surface area per lauroyl amide group, by dividing the surface area per macrocyclic polyamide at a given pressure by the number of amide groups in that molecule. The results from these calculations are presented graphically in Figure 4-5. These calculations indicate that there is approximately 31 ± 4 Å^2 per amide group at 30 mN/m.

Lehn[7] has measured the surface pressure of hexa-amide **10** (N_6L_6) up to 5 mN/m and calculated a surface area of $235 \pm 5\%$ Å^2 for hexa-amide **10** (N_6L_6) in a monolayer at zero pressure by extrapolating the line defined by the steepest part of the curve at pressures ≤ 5 mN/m. The value which we obtain using this method (i.e., extrapolation of the steepest line of the curve below 30 mN/m) gave $245 \pm 10\%$ Å^2. This value is slightly larger than the value calculated by Lehn; however, the values can be considered equal within experimental error. Ringsdorf et al. have also reported values for the surface area of hexa-myristoyl hexa-amide which are more than 30% smaller than the values obtained for hexa-amide **10** (N_6L_6) in our experiments.[8] It is probable that our average value for the surface area of hexa-amide **10** (N_6L_6) is larger than values reported elsewhere because our values properly take into account the fact that the macrocyclic polyamides which were used to prepare solutions for monolayer experiments contained water.

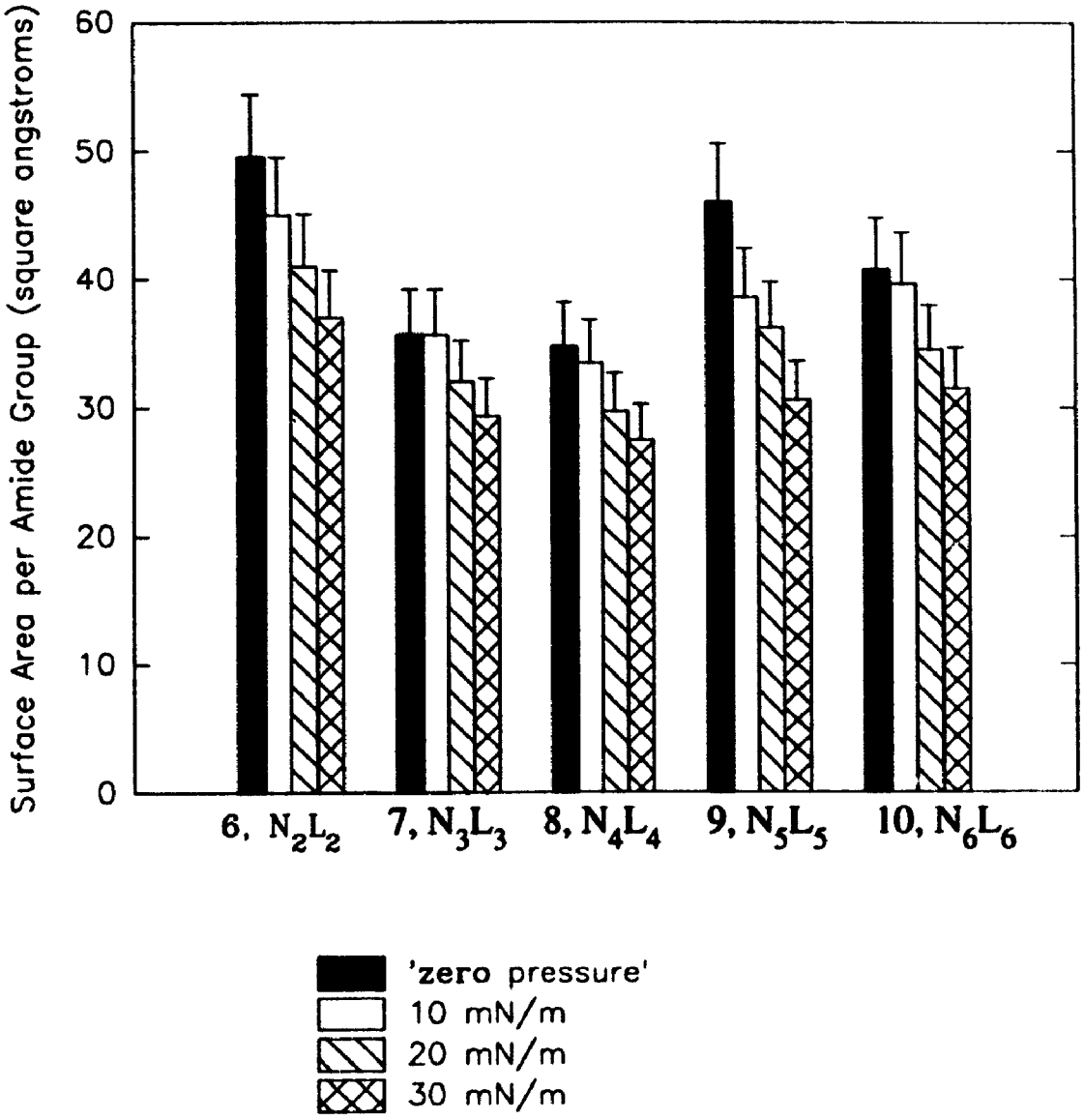

Figure 4-5: Variation of Surface Area in Macrocyclic Polyamides as a Function of Number of Amide Groups per Macrocyclic Ring.

4.5 Surface Areas of Labelled Macrocyclic Polyamides

The surface areas of NBD-labelled macrocyclic polyamides **14**, **15**, **16**, **17**, **18** (N_2L[NBD], N_3L_2[NBD], N_4L_3[NBD], N_5L_4[NBD], N_6L_5[NBD]) were determined as a function of surface pressure using a Langmuir film balance. Like their unlabelled analogues, labelled macrocyclic polyamides contained up to 10% water per sample, which could not be removed by standard techniques. The number of waters of hydration for labelled macrocyclic polyamides could not be calculated accurately based on integration of the water peak in the ^{1}H NMR spectra, because the ^{1}H NMR of NBD-labelled macrocyclic polyamides contained signals which were broadened relative to those observed in unlabelled macrocyclic polyamides due to the asymmetry of the molecules associated with the NBD substituent. Instead, the extinction coefficients for NBD-labelled macrocyclic polyamides at $\lambda \simeq 490$ nm were calculated from weighed samples which had been dried under vacuum at 60°C for one half hour, then the concentrations of other solutions prepared for monolayer experiments were calculated based on their absorbance using Beer's law.

Three or more monolayer curves were obtained for each labelled macrocyclic polyamide from a minimum of two different solutions. Surface areas obtained from the curves for monolayers prepared from the same solution were reproducible within a range $\pm 2\%$. Surface areas obtained from curves prepared from different solutions were reproducible within a range of

±10%. All of the labelled macrocyclic polyamides form stable monolayers which undergo gas-liquid transitions at low pressures, and exhibit liquid compression curves in the pressure range 0-40 mN/m. The results from these experiments are shown graphically in Figure 4-6, and in Table 4-1. Labelled macrocyclic polyamides **15**, **16**, **17**, **18** (N_3L_2[NBD], N_4L_3[NBD], N_5L_4[NBD], N_6L_5[NBD]) have surface areas which are approximately equal to those exhibited by the analogous unlabelled macrocyclic polyamides (within experimental error).

Labelled mono-amide **14** (N_2L[NBD]) exhibited a much smaller surface area than the corresponding unlabelled di-amide **6** (N_2L_2). The surface area of di-amide **6** (N_2L_2) is consistent with the amphiphile assuming a conformation with both amide groups in a plane parallel to the aqueous surface (illustrated in Figure 3-15). In contrast, the surface area of labelled mono-amide **14** (N_2L[NBD]) is consistent with the amphiphile assuming an orientation where the plane of the NBD group is normal to the surface of the air-water interface (Figure 4-7a).

If labelled mono-amide **14** (N_2L[NBD]) exhibits this orientation in DMPC bilayers, then both the amide group and the NBD group will reside within the region of the bilayer defined by the hydrophilic choline headgroup (Figure 4-7). Experiments performed on other NBD-labelled amphiphiles in lipid bilayer membranes have indicated that the NBD fluorophore is not too

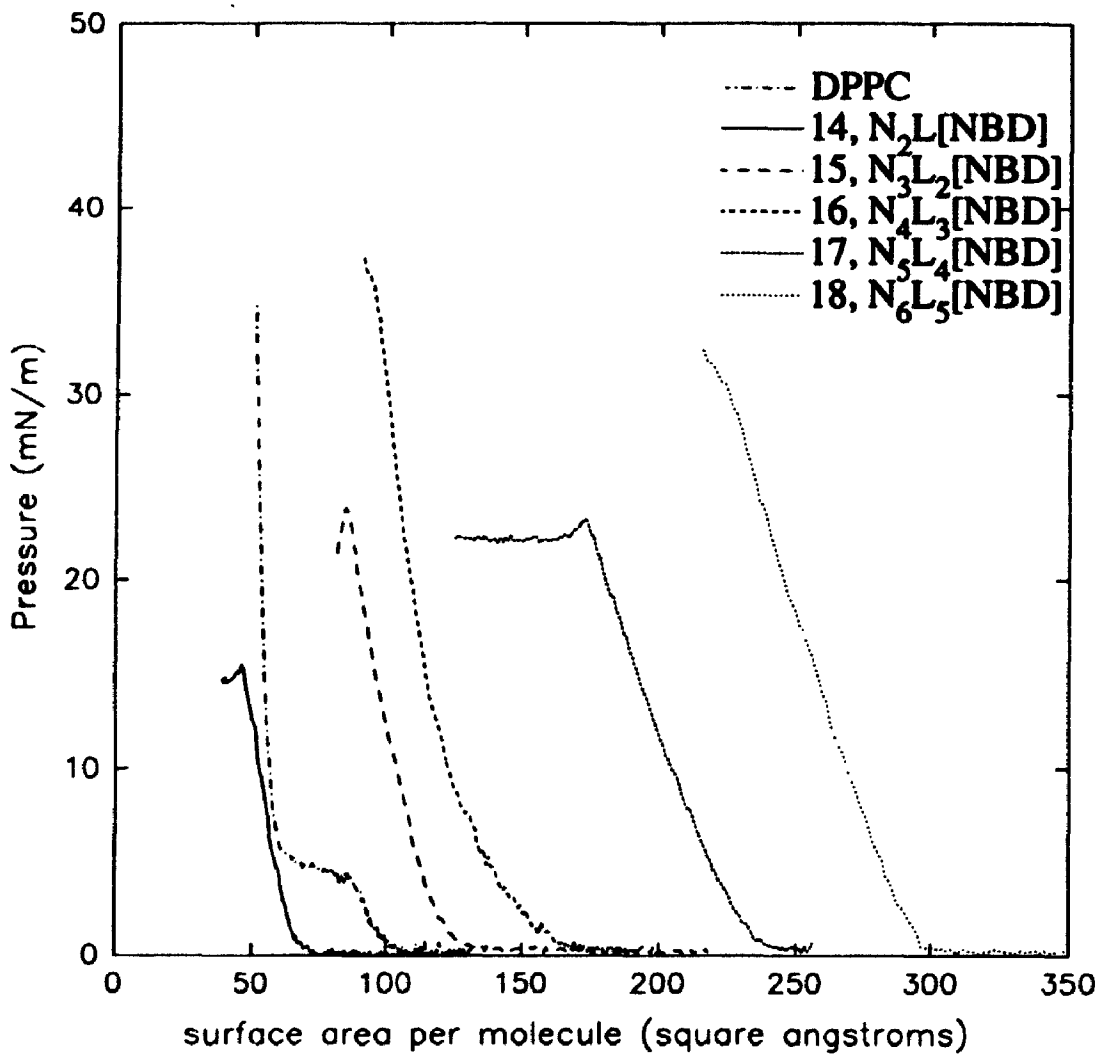

Figure 4-6: Surface Pressure vs. Surface Area Curves for NBD-Labelled Macrocyclic Polyamides

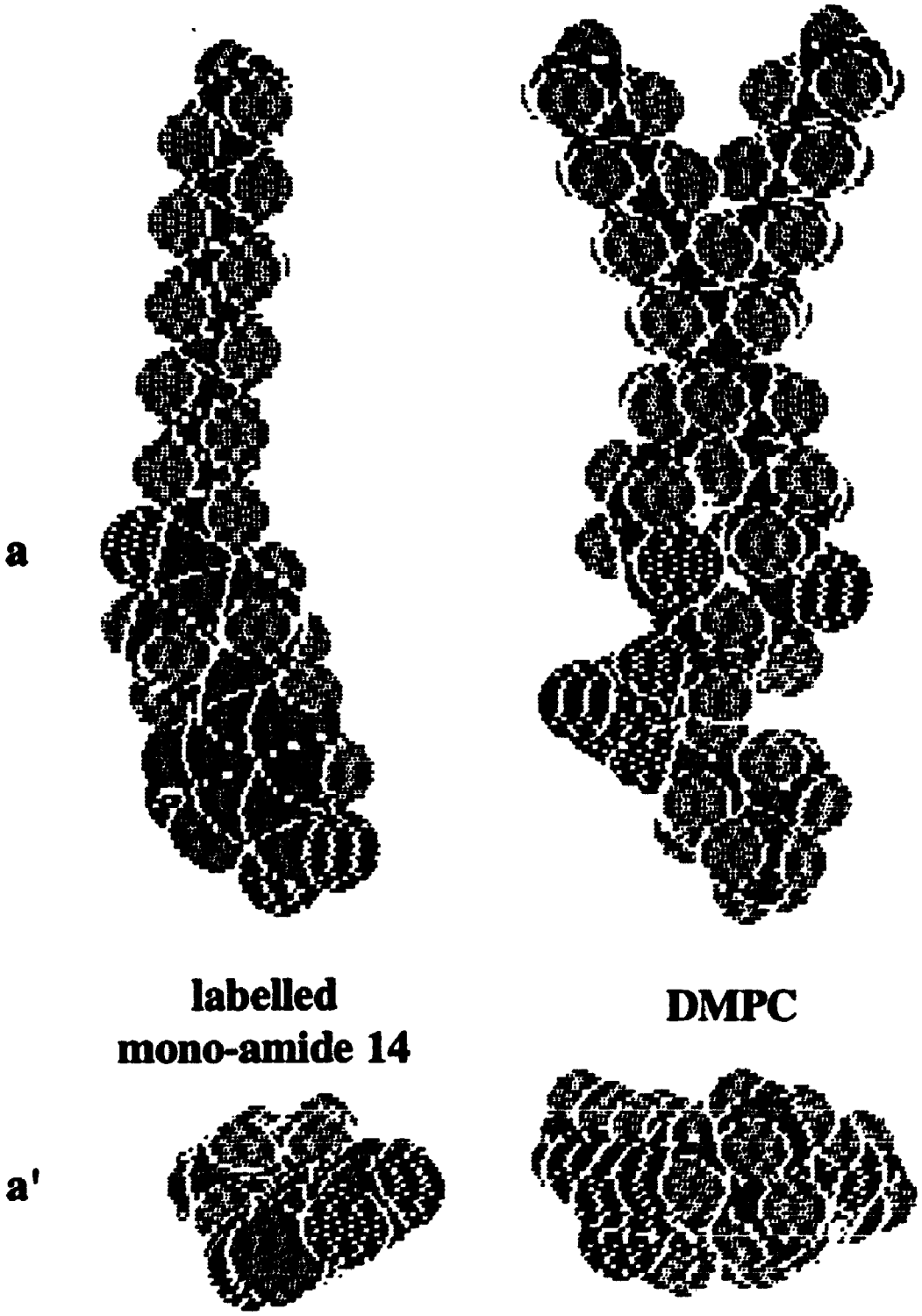

Figure 4-7: Space-Filled Representations of Labelled Mono-amide 14 and DMPC

Labelled mono-amide 14 and DMPC are shown from two different perspectives; (a) the hydrophilic surface is in a horizontal plane normal to the plane of the page, (a') the hydrophilic surface is in the plane of the page.

polar to be buried within the hydrophobic region of lipid bilayer membranes.[9] Therefore there is experimental evidence in support of the conformation shown in Figure 4-7 in lipid bilayer systems. It is also interesting to note that if the planes of the NBD and amide groups in labelled mono-amide **14** (N_2L[NBD]) are perpendicular to the air-water interface, then the minimum surface area of labelled mono-amide **14** (N_2L[NBD]) is predicted to be smaller than the surface area of DMPC (Figure 4-7). This prediction is consistent with the results obtained from our monolayer experiments.

4.6 Surface Areas in Mixed Monolayer Systems

4.6.1 Theory

One of the goals of this research was to determine the surface areas of our labelled macrocyclic probe molecules in phospholipid bilayer membranes at 30 mN/m. The results from our experiments on monolayers comprised of pure macrocyclic polyamides indicate that all of the macrocyclic polyamides exhibit distinct surface areas at any monolayer pressure. In order to increase our knowledge of the surface areas of macrocyclic polyamides in bilayer phospholipid membranes, several experiments were also performed on mixed monolayers containing DPPC and macrocyclic polyamide.

Two different amphiphiles, 'A' and 'B', in a single monolayer may undergo ideal mixing or form domains. In situations where the components are ideally mixed, a plot of the surface area vs. the mole fraction of one component should give a straight line which passes through the points corresponding to the surface area of pure 'A' ($X_A = 1.00$) and the surface area of pure 'B' ($X_A = 0.00$, $X_B = 1.00$).[2]

4.6.2 Mixed Monolayers of Penta-amide 9 (N_5L_5) and DPPC

The surface area per molecule as a function of surface pressure for mixed monolayers containing penta-amide **9** (N_5L_5) and DPPC was determined using a Langmuir film Balance. Π vs. surface area isotherms are shown in

Figure 4-8. Each curve was obtained for one solution consisting of mixed penta-amide **9** (N_5L_5) and DPPC. From these monolayer curves it is apparent that the transition of penta-amide **9** (N_5L_5) is preserved in all of the mixed monolayer films.

The variation of surface area as a function of the mole fraction of penta-amide **9** (N_5L_5) is indicated in Figure 4-9. These calculations indicate that at low pressure penta-amide **9** (N_5L_5) and DPPC appear to be completely (ideally) mixed. The results at high pressures are not as easily interpreted. Here, deviation from the line representing ideal mixing is more extreme; however, the trend of increasing surface area is still similar to the line corresponding to a two component system with homogeneous phase mixing.

4.6.3 Mixed Monolayers of Labelled Tetra-amide 16 (N_4L_3[NBD]) and DPPC

The surface area per molecule as a function of the surface pressure for mixed monolayers containing labelled tetra-amide **16** (N_4L_3[NBD]) and DPPC was determined using a Langmuir Film Balance. Π vs. surface area isotherms are shown in Figure 4-10. Each curve was obtained for one solution consisting of mixed labelled tetra-amide **16** (N_4L_3[NBD]) and DPPC. One important result is the fact that the Π vs. surface area curve for the mixed monolayer with $X(N_4L_3[NBD]) = 0.008$ is equal to the curve

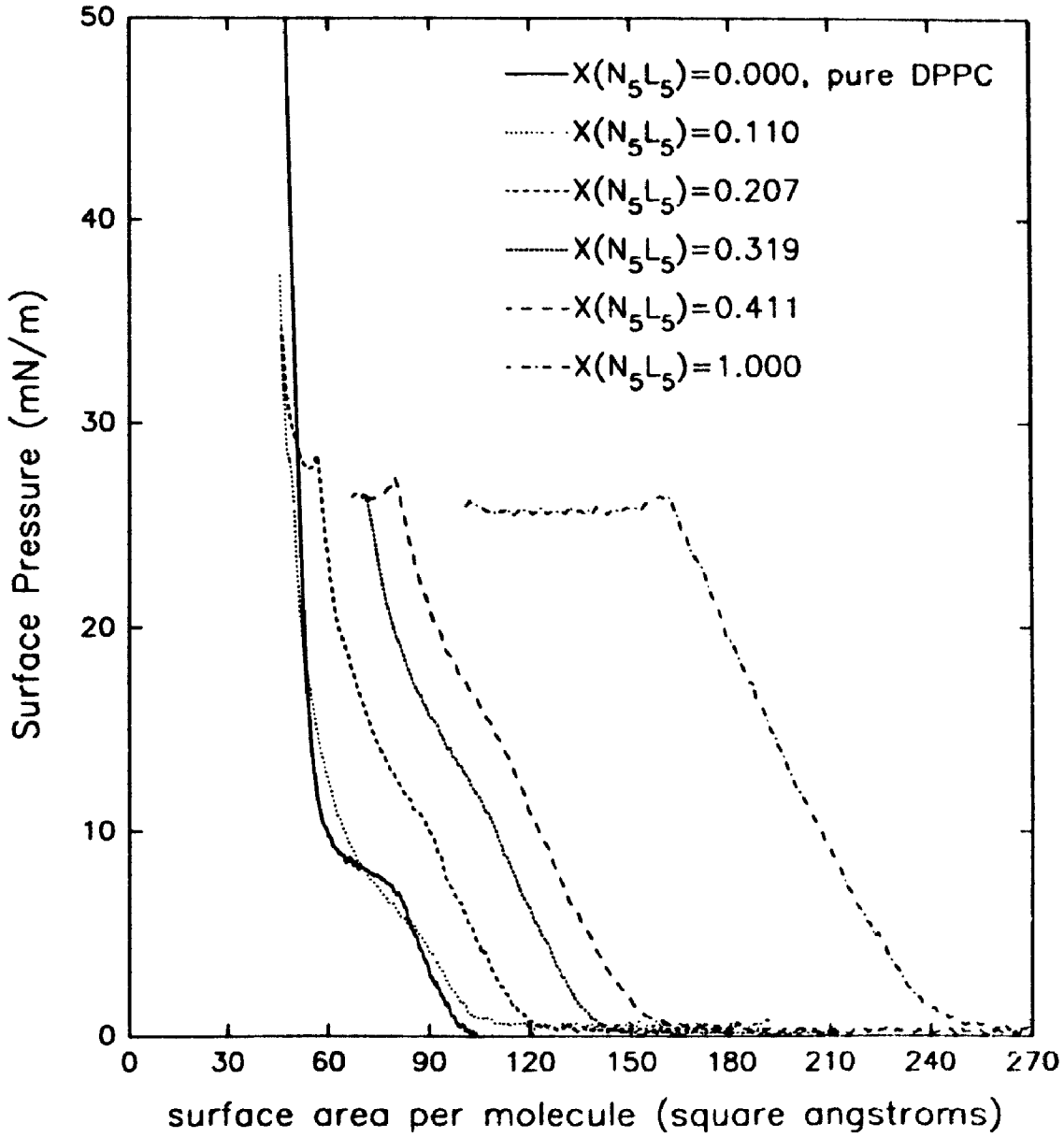

Figure 4-8: Surface Pressure vs. Surface Area Curves for Mixed Monolayers Containing Penta-amide 9 (N_5L_5) and DPPC.

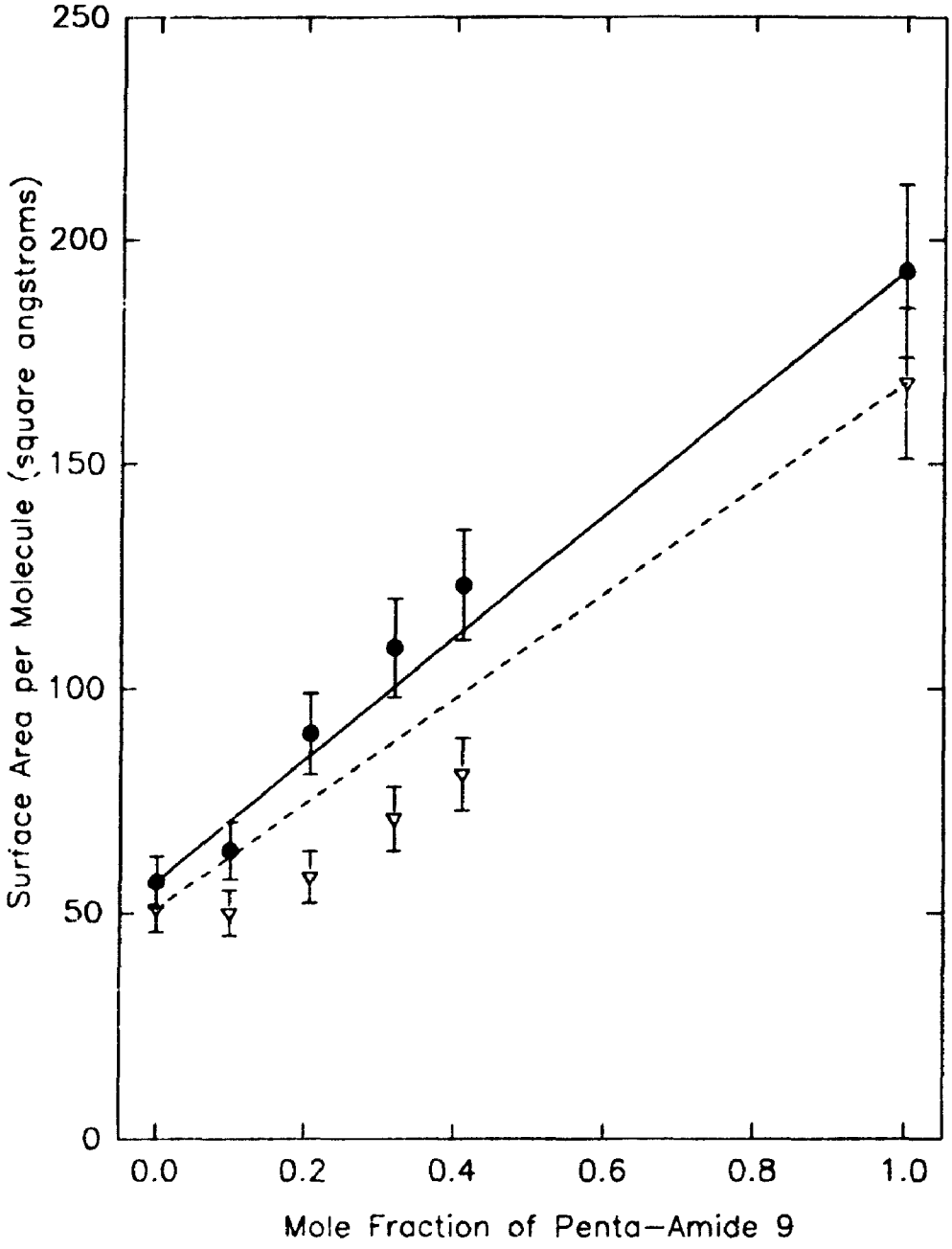

Figure 4-9: Surface Area per Molecule vs. Mole Fraction of Penta-amide 9 (N_5L_5) in Mixed Monolayers with DPPC.

Data points and the line of ideal mixing at 10 mN/m (● ,——) and 26.5 mN/m (▽ ,- - - -) are shown.

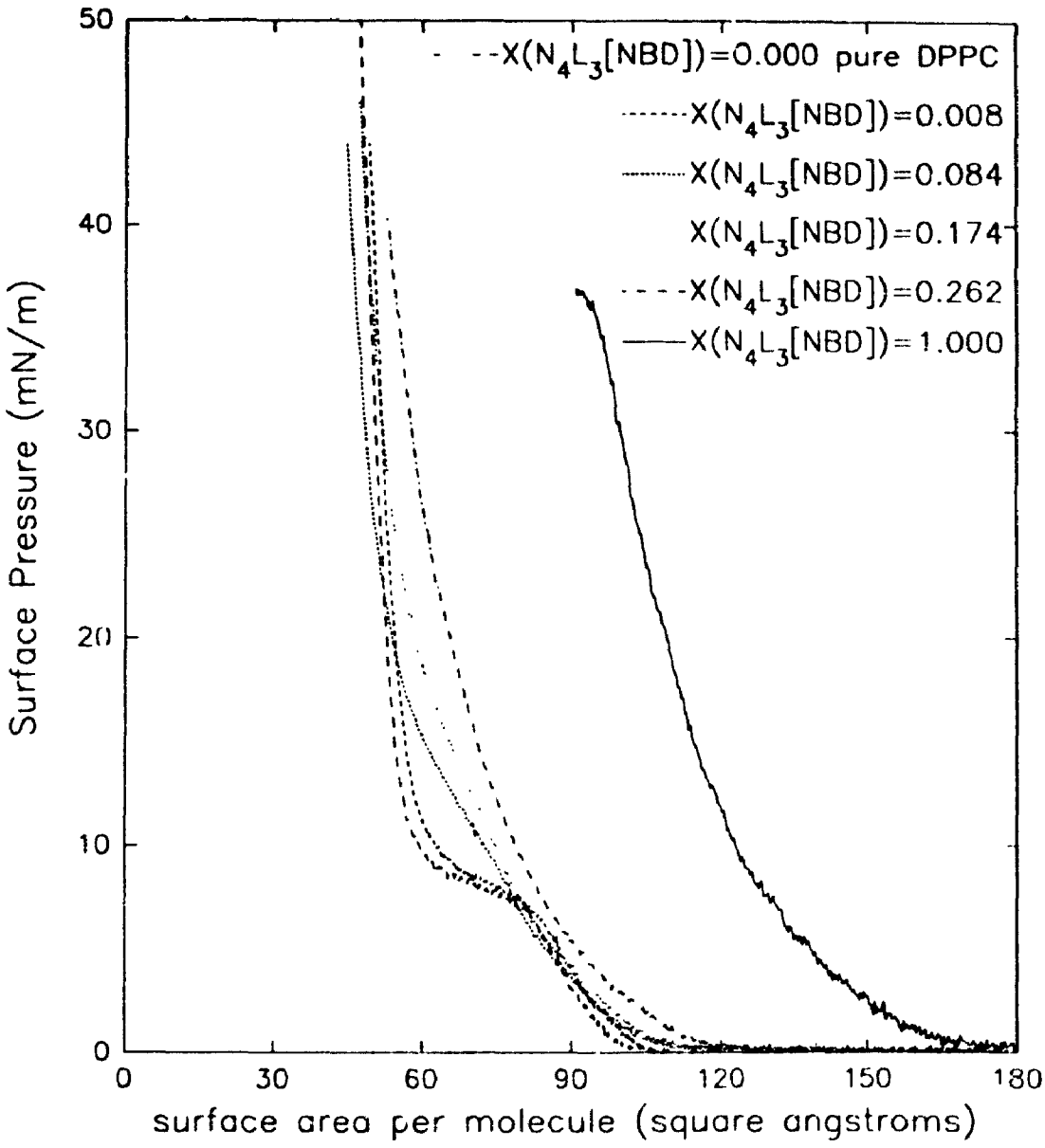

Figure 4-10: Surface Pressure vs. Surface Area Curves for Mixed Monolayers Containing Labelled Tetra-amide 16 (N_4L_3{NBD}) and DPPC.

corresponding to pure DPPC (within experimental error). Recently, Bredlow et al. have reported that mixed phospholipid monolayers containing 1% NBD-labelled phospholipid exhibit large increases in surface area relative to the surface areas of pure phospholipid monolayers.[10] Our results for labelled tetra-amide **16** (N_4L_3[NBD]) suggest that 0.8% (mol/mol) of this amphiphile does not significantly alter the surface area of DPPC phospholipids in mixed monomolecular films. Since diffusion measurements are performed using lipid bilayer membranes which contain 0.1% labelled amphiphile, it is probable that the surface areas of phospholipids in these lipid bilayer systems will likewise be unaffected by the presence of labelled macrocyclic polyamide amphiphiles.

The variation of surface area as a function of the mole fraction of labelled tetra-amide **16** (N_4L_3[NBD]) is indicated in Figure 4-11. As was the case with penta-amide **9** (N_5L_5), at low pressure tetra-amide **16** (N_4L_3[NBD]) and DPPC appear to be completely (ideally) mixed. The results at 20 and 30 mN/m are not as easily interpreted; however, the trend of increasing surface area is still similar to the line corresponding to two component system with homogeneous phase mixing.

4.6.4 Summary of Results from Mixed Monolayer Systems

Mixed monolayers of macrocyclic polyamides and DPPC at low surface pressures undergo ideal mixing. Results for mixed monolayers at

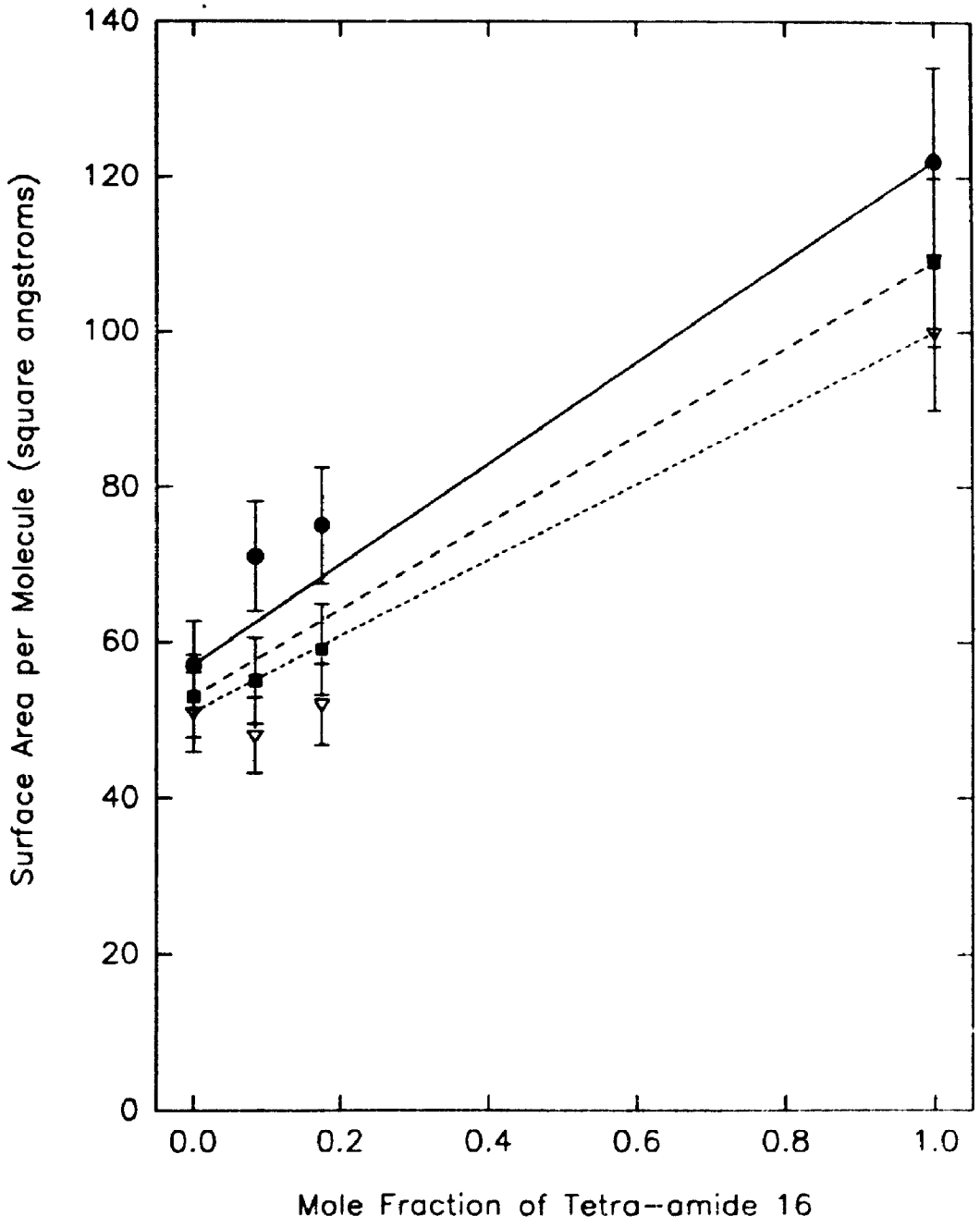

Figure 4-11: Surface Area per Molecule vs. Mole Fraction of Labelled Tetra-amide 16 (N_4L_3[NBD]) in Mixed Monolayers with DPPC.

Data points and the line of ideal mixing at 10 mN/m (● ,——), 20 mN/m (■ ,- - - -), and 30 mN/m (▽ ,·····) are shown.

surface pressures greater than 20 mN/m are less conclusive, but not inconsistent with ideal mixing (within experimental error). Based on these results, the best approximation of surface area of amphiphiles in lipid bilayer membranes is obtained from measurements made on monolayers consisting of pure macrocyclic polyamide.

4.7 Comparison of Results from Monolayer Experiments and Molecular Modelling Analyses

In general, the surface areas obtained from monolayer experiments are larger than those obtained from molecular modelling calculations (Tables 4-1 and 3-3 respectively). These results are anticipated because molecular modelling calculations provide information about the minimum van der Waals surface areas of individual molecules, whereas the surface area values obtained from monolayer experiments represent the average surface area occupied per molecule when the molecules are arranged in a two-dimensional lattice. Since the compressibility of the monolayer curves for macrocyclic polyamides indicates that these amphiphiles are in a liquid-like state below 40 mN/m, one would expect the observed surface area per molecule at 0-40 mN/m to be considerably larger than the surface area of an individual molecule, or the surface area per molecule of a two-dimensional lattice of amphiphiles in the solid state.

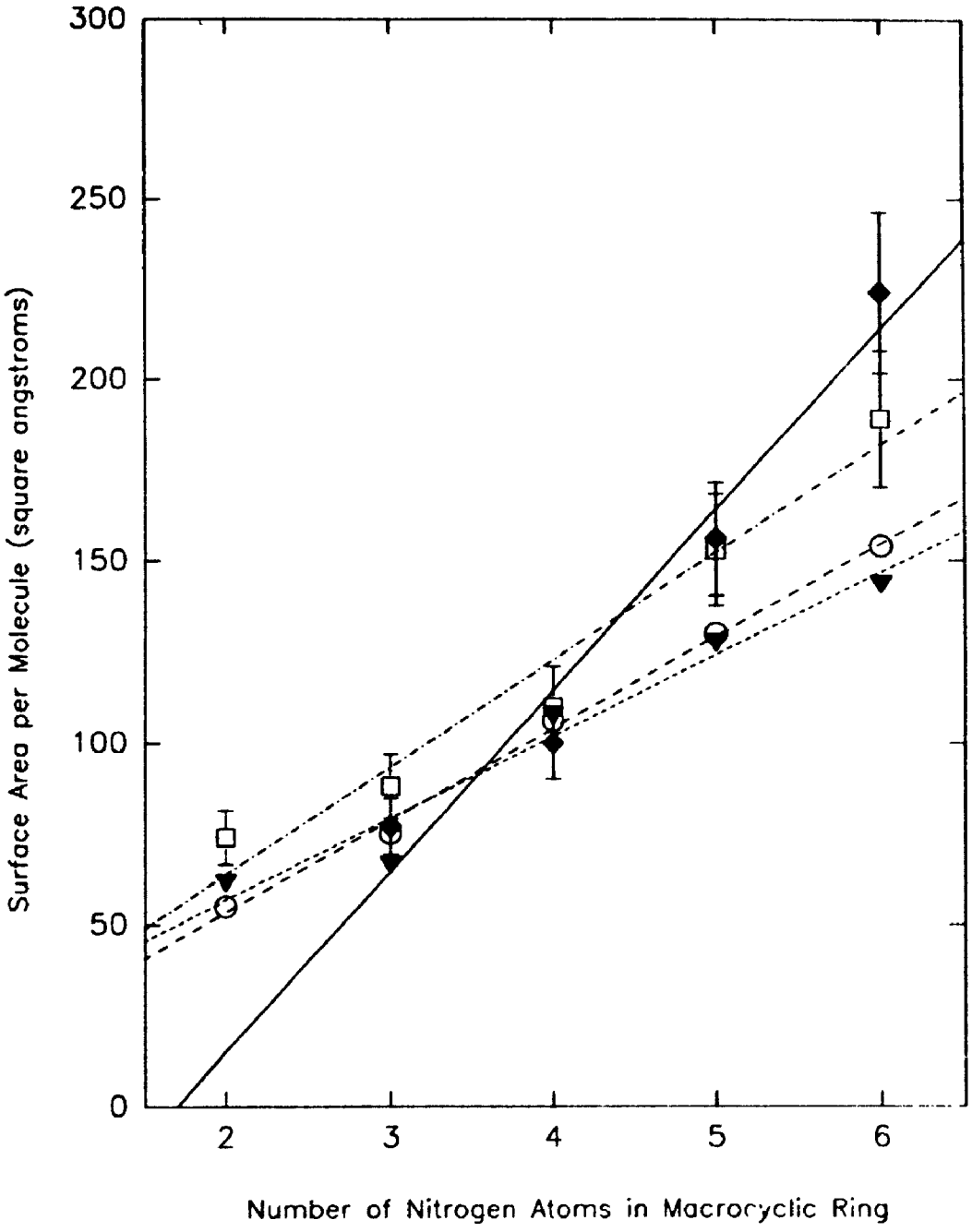

Figure 4-12: Trend of Increasing Surface Area for Macrocyclic Polyamides

Plots for calculations based on computer models of unlabelled compounds (○), computer models of NBD-labelled compounds (▼), monolayer measurements of unlabelled compounds (□) and monolayer measurements of NBD-labelled compounds (◆) are shown.

Figure 4-12 shows the variation of the predicted surface areas for macrocyclic polyamides as a function of the number of nitrogen atoms per macrocycle. Though the surface area values obtained from molecular modelling analysis are smaller than those obtained from monolayer experiments performed on unlabelled macrocyclic polyamides, the trends of increasing surface area are similar.

This trend of increasing surface as a function of the number of nitrogens in the macrocyclic ring is more pronounced for NBD-labelled macrocyclic polyamides. The surface area of labelled mono-amide **14** (N_2L[NBD]) was not included in the line of best fit because there is reason to believe that it exhibits an orientation in monolayers which is different from the other labelled macrocyclic polyamides (see section 4-5). This increase in the rate of change of surface area over the series of labelled macrocyclic polyamides may arise because the NBD group in smaller labelled cyclic polyamides is more tilted relative to the plane of the cyclic ring than in larger labelled macrocyclic polyamides.

Based on these results, one can conclude that our computer molecular models were reasonably accurate in their prediction of rigid planar geometry of macrocyclic polyamides, but did not accurately predict the distance between molecules in a liquid-like monomolecular film.

4.8 Conclusions

The surface areas of labelled and unlabelled macrocyclic polyamides were determined at 30 mN/m in pure monolayer systems. The surface areas of two macrocyclic polyamides were also determined in mixed monolayers with DPPC; however, the results from these experiments were less conclusive than the values obtained from monolayers composed of pure macrocyclic polyamide. The results for labelled mono-amide **14** (N_2L[NBD]) suggest that a minimum of two amide groups per cyclic ring are required to keep the plane of the macrocyclic ring parallel to the air-water interface in monomolecular films.

Most importantly, because each labelled macrocyclic polyamide exhibits a unique surface area in monomolecular films at pressures less than or equal to 30 mN/m, it is reasonable to conclude that each of our labelled probe molecules will exhibit distinct surface areas in lipid bilayer membranes. Our research objective was to determine the diffusion coefficients of molecules which have surface areas in the theoretical range of 50-300 $Å^2$, since this region lies between the domains which have been experimentally correlated to Free Area and Continuum theory respectively (Figure 1-7). The surface areas of labelled macrocyclic polyamides determined from monolayer experiments suggest that these molecules will be excellent probes to investigate the relationship between diffusion coefficients and surface areas of intermediately sized amphiphiles.

4.9 Experimental

Π vs. surface area isotherms for macrocyclic polyamides were measured at 21±2°C. Professor J.R. Bolton generously provided access to a Langmuir Film Balance (Figure 4-2). The water reservoir of the balance was a 13 cm x 60 cm trough, machined from a solid block of teflon, which was mounted on a vibration isolated table. The surface area available for monolayer spreading was regulated using a computer controlled, teflon-wrapped iron bar which was moved along the sides of the trough. The surface pressure of monolayers was measured using a teflon float which was connected to the sides of the trough with teflon tape, and attached to a torsion balance and pressure transducer. The pressure transducer consisted of a metal bar suspended in a hole which was cut through a magnetic transducer (Figure 4-2). Lateral pressure on the teflon float causes the horizontal arm of the torsion balance, and the metal bar suspended from it, to tip away from the magnetic transducer. This alters the voltage of the transducer and thus provides a very sensitive measurement of surface pressure. The pressure transducer was calibrated regularly, and the pressure/voltage conversion factor was determined to be 38±2 mN/mV. The variation in surface pressure during a monolayer experiment was recorded using a Nicolet model 2090-IIIA oscilloscope. Details of the apparatus and computer interfacing have been described elsewhere.[11]

The subphase for all experiments was water, which was obtained from a Xenopure filtration system. The resistance of the water varied, but was consistently in the range of 13-16 MΩ. In a typical monolayer experiment, $\sim 30\mu g$ of macrocyclic polyamide was deposited on a clean aqueous surface from an ~ 1 mg/mL solution in glass distilled chloroform. The exact concentrations of the chloroform solutions were calculated based on the masses of hydrated macrocyclic polyamides. The waters of hydration per macrocyclic polyamide were determined using the methods discussed in section 4-3 and 4-4. At least 15 minutes was allowed for the chloroform to evaporate, then, the teflon bar was advanced towards the teflon float at a speed which corresponded to a rate of compression $\leq 10 Å^2$ per minute. Approximately 25 minutes was required for each compression curve. Π vs. surface area curves which were repeatedly obtained for the same monolayer (by allowing a monolayer film to expand and reach equilibrium between experiments) were reproducible within $\pm 1 Å^2$ per molecule. The surface areas obtained from curves for monolayers prepared from the same solution were reproducible within a range $\pm 2\%$, and surface areas obtained from curves prepared from different solutions were reproducible within a range of $\pm 10\%$.

Π vs. surface area curves for mixed monolayers were obtained from one solution. In a typical experiment, the appropriate volumes of chloroform solutions were mixed in a test tube to give ~ 50 nmol material with the desired

mole fraction. The solutions were allowed to mix for 30 minutes at room temperature and then the entire sample was deposited on the aqueous subphase in the monolayer trough. The test tube was rinsed with chloroform and the rinsings were also deposited on the aqueous subphase. Π vs. surface area curves which were repeatedly obtained for the same monolayer were reproducible within $\pm 1 Å^2$ per molecule.

4.10 References

1. Seelig, A., Local Anesthetics and Pressure: A Comparison of Dibucaine Binding to Lipid Monolayers and Bilayers, *Biochim. Biophys. Acta*, *899*, **1987** 196-205.
2. Birdi, K.S., *Lipid and Biopolymer Monolayers at Liquid Interfaces*, Plenum Press, New York, **1989**.
3. Adamson, A.W., *Physical Chemistry of Surfaces, Fifth Edition*, John Wiley and Sons, Inc., Toronto, **1990**.
4. Reproduced with Permission from; Cadenhead, D.A., in *Chemistry and Physics of Interfaces*, Ross, S., editor, American Chemical Society **1971**.
5. Yguerabide, J. and Foster, M.C., Fluorescence Spectroscopy of Biological Membranes , *Molecular Biology, Biochemistry and Biophysics*, **1981**, *33* (Membrane Spectroscopy), Grell, E., editor, Springer Verlag, pg 266.
6. Ries, H.E, Matsumoto, M., Uyeda, N, and Suito, E., Electron Microscope Studies of Monolayers of Lecithin, *Adv. Chem. Ser.* , *144*, (Monolayers, Mem. Symp. 1974), **1975**, 286-293.
7. Malthête, J., Poupinet, D., Vilanove, R, and Lehn, J.M., Monolayers of Macrocyclic Polyamides at the Air-Water Interface, *J. Chem. Soc. Chem.Comm.*, **1989**, 1016.

8. Mertesdorf, C., and Ringsdorf, H., Self-Organization of Substituted Azacrowns Based on their Discoid and Amphiphilic Nature, *Liquid Crystals*, *5*, **1989**, 1757-1772.

9. Chattopadhyay, A., Chemistry and Biology of N-(7-nitro-benz-oxa-1,3-diazo-4-yl)-Labelled Lipids: Fluorescent Probes of Biological and Model Membranes, *Chemistry and Physics of Lipids*, **1990**, *53*, 1-15.

10. Bredlow, A, Galla, H.J, and Bergelson, L.D., Influence of Fluorescent Lipid Probes on the Packing of Their Environment. A Monolayer Study, *Chemistry and Physics of Lipids*, **1992**, *62*, 293-301.

11. Dick, Harold A., Ph.D. Dissertation, *Photophysical and Photoelectrochemical Studies of a Langmuir-Blodgett Film of a Porphyrin Dye*, The University of Western Ontario, **1988**.

Chapter 5

DETERMINATION OF LATERAL DIFFUSION COEFFICIENTS

5.1 Experimental Objective

Diffusion coefficients can be determined using the Fluorescence Photobleaching Recovery method (FPR) which is also referred to as Fluorescence Recovery after Photobleaching (FRAP) and numerous review articles have been reported for the technique.[1,2,3] Frye and Edidin initiated the use of fluorescence to study lateral diffusion on cell surfaces in 1970.[4] Since that time, the diffusion coefficients of numerous fluorescently labelled species in cell and model membrane systems have been measured,[5,6] including the data points corresponding to the diffusion coefficients of proteins and lipids indicated in Figure 1-7.[7]

Our experimental objective was to correlate the lateral diffusion coefficients of intermediately sized amphiphiles (50-300 $Å^2$) with their surface areas in lipid bilayer membranes, and compare this data with existing theories for lateral diffusion in lipid bilayer membranes. To this end, we endeavoured to determine the lateral diffusion coefficients of labelled macrocyclic polyamides **14**, **15**, **16**, **17**, **18** (N_2L[NBD], N_3L_2[NBD], N_4L_3[NBD], N_5L_4[NBD], N_6L_5[NBD]) using FPR, and correlate these values with the surface areas of the amphiphiles which were determined using the monolayer

techniques (Chapter 4). In addition, the lateral diffusion coefficient of a fluorescently labelled phospholipid (NBD-PE) was measured as a control for our diffusion measurements.

5.2 Fluorescence Photobleaching Recovery and the Spot Photobleaching Technique[1,2,3]

FPR allows for the determination of the lateral diffusion coefficients (D) of fluorescently labelled species which have been incorporated into lipid vesicles (consisting of pure phospholipid) or cell membranes. It is necessary to incorporate extrinsic fluorescent labels into samples for FPR experiments because the phospholipids which comprise bilayer membranes are not inherently fluorescent.

Vesicles for FPR experiments are generally prepared by depositing ~500 nmol of lipid which contains ~0.1% (mol/mol) fluorescently labelled amphiphile in ~100 μL of chloroform on a glass slide or coverslip. The chloroform is removed under vacuum, then a drop of water or buffer is added to the lipid, and a coverslip is placed over the aqueous droplet. The sample is then sealed (usually with wax) and heated to at least 40°C to promote lipid hydration and swelling of vesicles. The vesicles which are formed by this method are usually multilamellar, and can be as large as 100 μm in diameter.

FPR is a microscopy-based technique which employs the sensitivity of

fluorescence based detection methods, combined with the spatial resolution of light microscopy. The apparatus for FPR experiments consists of a laser beam which is directed and focussed such that the beam of light forms a spot of known diameter (typically 1-2 μm) in the optical plane of a fluorescence microscope (Figure 5-1). In practice, a beam splitter is used to divide the laser beam into two separate beams of different intensity, which are coaxially realigned before they are directed into the microscope through its rear iris. The two beams are designated as the monitor beam and the bleach beam, respectively, and the bleach beam is usually 3-4 orders of magnitude more intense than the monitor beam.

The transverse intensity profile of the laser beam on the optical plane of the microscope is gaussian (Figure 5-2) and the intensity of the laser (I) varies with position in the optical plane according to Equation 5-1.

Equation 5-1

$$I(r) = I_o e^{\frac{-2r^2}{w^2}}$$

The radius of the beam (w) is defined as the r value at which the intensity falls to e^{-2} of its maximum value.

The fluorescent emission of the sample is measured normal to the surface of the sample with a photomultiplier tube (Figure 5-2). Though FPR experiments are based on the two-dimensional projection of the laser beam onto a vesicle or cell, in practice the laser beam traverses three dimensional

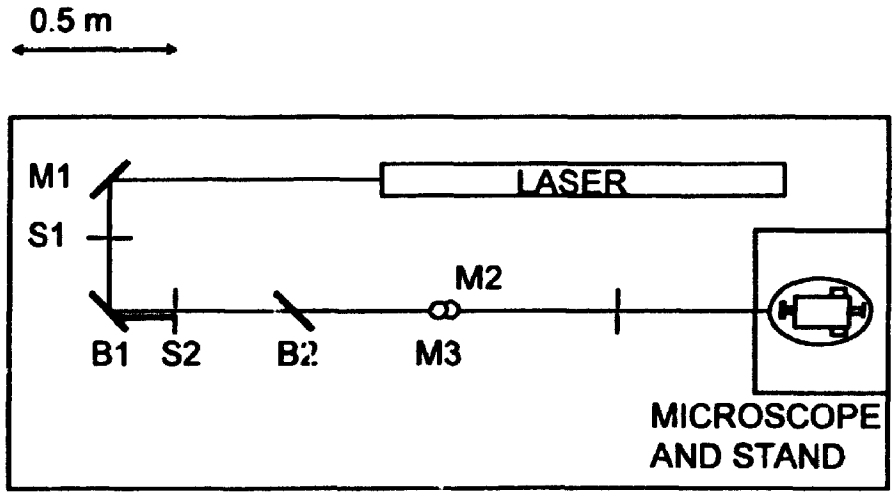

Figure 5-1: Schematic Representation of Microscope and Laser Setup

The beam splitters, B1 and B2 yield a pair of gaussian beams with intensities that differ by three or four orders of magnitude. The path of the stronger (bleach) beam is indicated by the thicker line. When shutter 2 (S2) is open the bleach beam is directed into the rear iris of the microscope. Mirrors, M1, M2 and M3 direct the beam, while shutter 1 (S1) limits the incident beam.

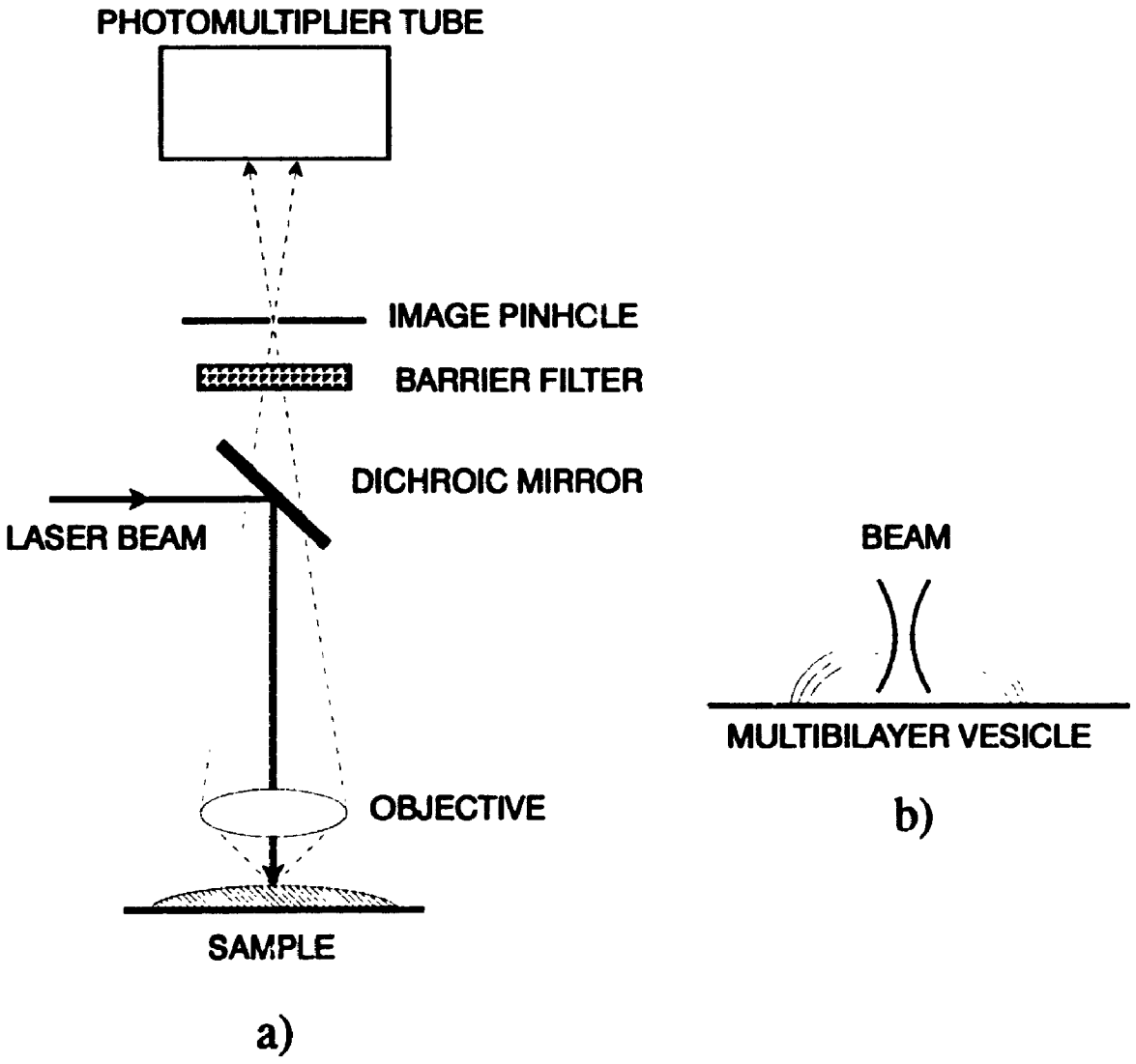

Figure 5-2: Schematic Representation of Image Plane Pinhole

(a) Flourescent emission is collected in the objective lens, passes through a dichroic mirror and barrier filter and is focussed on the aperture of an image plane pinhole. Only the fluorescence originating in the objective plane of focus (b) and small region surrounding it pass through the pinhole and are detected by the photomultiplier tube. Figures are not drawn to scale.

space before the desired spot is irradiated and fluorescence emission is detected. It is therefore possible that fluorescent molecules which are not inthe optical plane will contribute to the measured fluorescence signal.
A pinhole is utilized tc minimize the contribution which fluorescent species that are not in the optical plane make to the measured fluorescence. The pinhole is located at the image plane of the microscope. A 0.4 mm pinhole combined with a 1.2 μm beam spot yields a cylinder of detection which extends approximately 6 μm above and below the optical plane. Bilayer membranes are typically 4-6 nm thick, therefore several layers of the multilamellar vesicles are probed in each FPR experiment. However, since each bilayer in a multibilayer vesicle is discrete, each exhibits the same lateral diffusion behaviour. In fact, it is not only possible to obtain valid diffusion measurements using multilamellar vesicles, it is preferable since the fluorescence intensity observed for multilamellar vesicles is higher than that for single bilayers and the signal-to-noise ratio is therefore improved.

Before performing an FPR experiment, a single vesicle is brought into the centre of the optical plane of focus of the microscope. Visually, the vesicle appears to be in focus when the sides of the vesicle are in the focal plane of the microscope. The monitor beam is then activated to stimulate fluorescence emission, and the objective is moved away from the sample until a well defined fluorescent spot is visible. The position at which the

fluorescence spot is best resolved corresponds to the apex of curvature of a lipid vesicle. Once a vesicle has been positioned, an FPR experiment can begin.

In the first step of a typical FPR experiment, the fluorescence intensity of the spot defined by the monitor beam is measured. This fluorescence intensity, referred to as F(-), corresponds to the average measured fluorescence intensity as labelled amphiphiles diffuse in and out of the monitor beam spot. In the second step the sample is briefly irradiated with the bleach beam to effect irreversible photolysis (photobleaching) of 30-50% of the fluorescent species within the region defined by the beam spot. The fluorescence intensity immediately after the bleaching process is defined as F(0). After bleaching, lipid and incorporated amphiphile continue to diffuse in and out of the monitor beam spot. Over time, the concentration gradient between bleached amphiphile and labelled amphiphile is dissipated through the process of lateral diffusion, and the fluorescence intensity of the monitor beam spot returns to a constant level defined as F(∞). The steps in an FPR experiment are represented pictorially in Figure 5-3, and graphically in Figure 5-4.

The mobile fraction (X_m) of fluorescent molecules undergoing lateral diffusion is defined as;

Equation 5-2

$$X_m = \frac{F(\infty) - F(0)}{F(-) - F(0)}$$

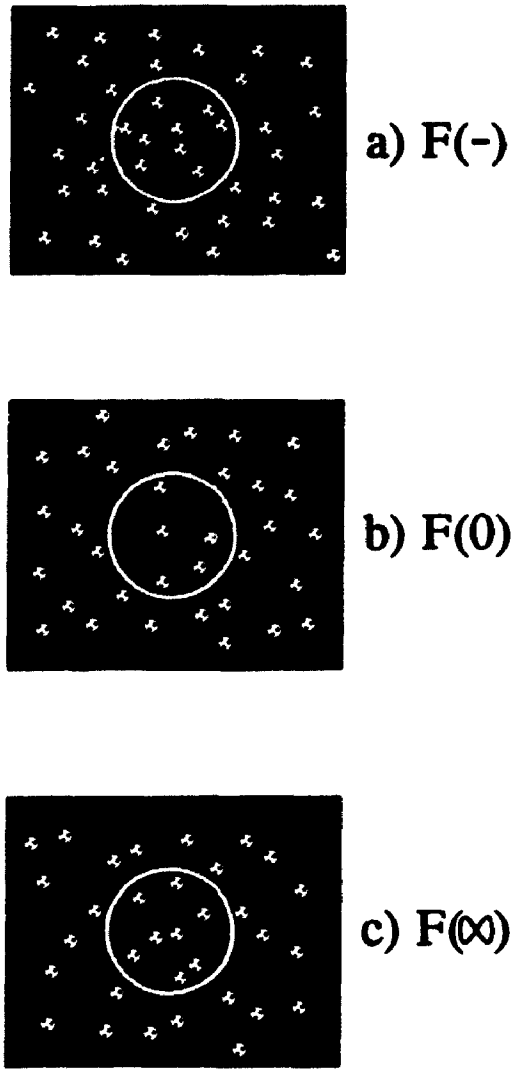

Figure 5-3: Illustrated Representation of an FPR Experiment

(⁘) flourescently labelled amphiphile (●) bleached amphiphile

(a) Flourescence from labelled diffusant molecules within the monitor beam spot (white circle) is monitored. (b) The sample is then irradiated with a brief pulse of light using the bleach beam to effect ~50% photolysis of the fluorescently labelled molecules within the monitor beam spot. The concentration gradient is dissipated through lateral diffusion, and eventually (c) the fluorescence returns to some constant level. Figures are not drawn to scale.

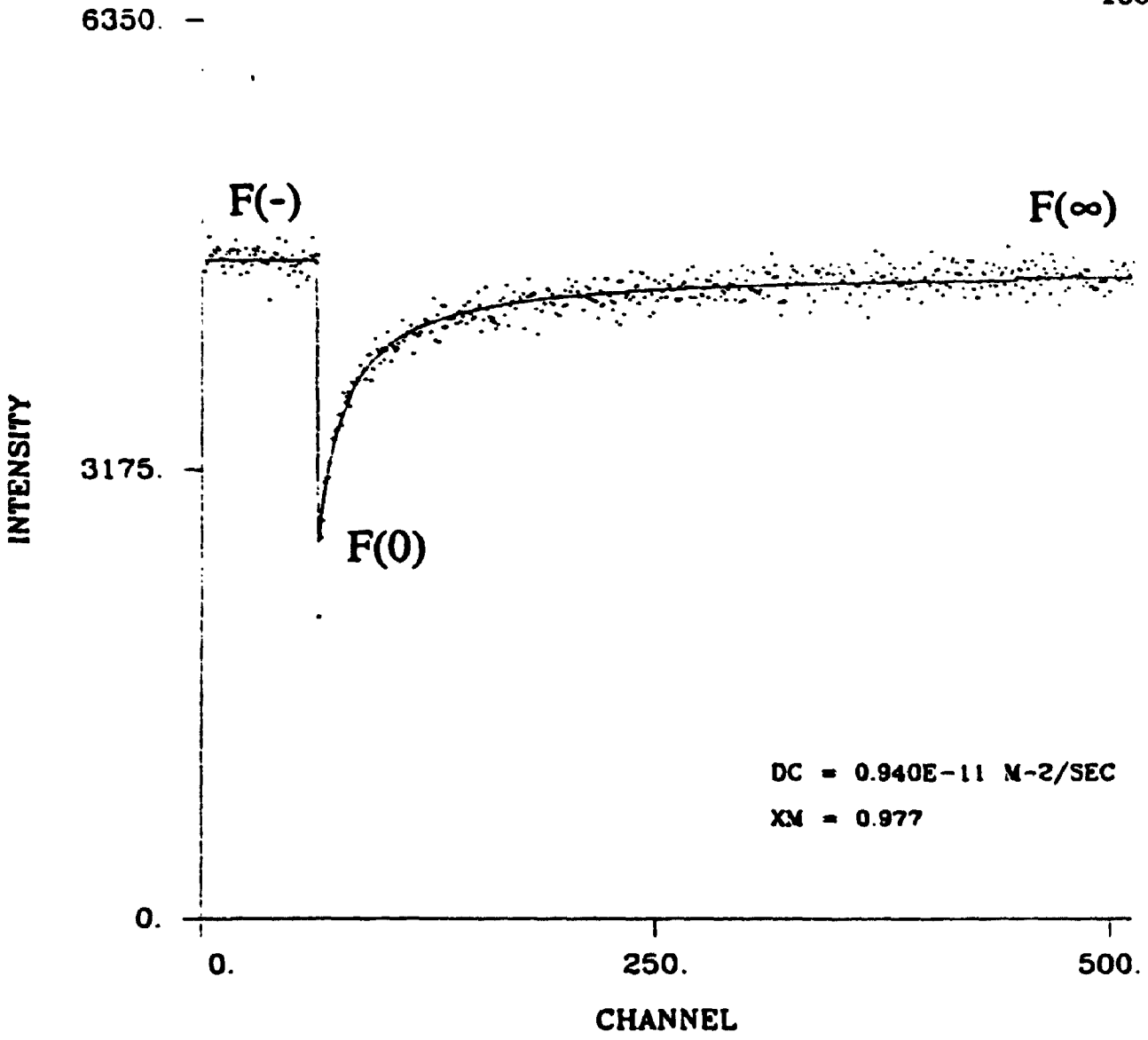

Figure 5-4: Sample Bleach Recovery Curve for Labelled Tri-amide 16, (N_4L_3[NBD]) Illustrating the Steps in an FPR Experiment

The pre-experiment fluorescence level, F(-), the fluorescence level immediately after amphiphiles have been bleached, F(0), and the constant level of fluorescence, F(∞), which is measured after the concentration gradient due to bleaching has dissipated, are indicated.

In model membrane systems, which do not contain macroscopic proteins that restrict lateral diffusion, the mobile fraction should be close to unity. Therefore, it is possible to perform multiple FPR experiments on the same spot of a single lipid vesicle, and this is generally done to improve the signal-to-noise ratio in FPR experiments.

If the concentration of fluorophore is low, then Beer's Law can be applied, and the measured fluorescence intensity is linearly related to the concentration of fluorescent amphiphile in the monitor beam spot. Experimentally, the rate of fluorescence recovery is fit to three parameters; the mobile fraction, X_m ; the bleach parameter K, and the characteristic recovery time, τ_D. The recovery time (τ_D) is also related to the lateral diffusion coefficient (D) according to Equation 5-3;

Equation 5-3

$$\tau_D = \frac{w^2}{4D}$$

Therefore, the lateral diffusion coefficient (D) can be extracted from the line of best fit on spot-photobleaching recovery curves.

5.3 Lateral Diffusion Coefficient Measurements

The diffusion coefficients for labelled macrocyclic polyamides **14**, **15**, **16**, **17**, **18** (N_2L[NBD], N_3L_2[NBD], N_4L_3[NBD], N_5L_4[NBD], N_6L_5[NBD]) and NBD-labelled phosphatidyl ethanolamine derived from egg lipid (NBD-PE) were determined in DMPC multilamellar vesicles at 36°C (Table 5-1). Data were acquired using the conditions described in the experimental section. For all amphiphiles the mobile fraction X_m was close to unity, which suggests that multiple experiments performed on the same vesicle will be valid.

The ratio of fluorescent probe:lipid for all FPR experiments was 1:1000. This concentration is often used when preparing samples for FPR experiments because it is low enough that the system approximates an ideal system but high enough to allow for good signal-to-noise ratios in experimental data.

Diffusion measurements were made at 36°C in DMPC lipid membranes in the liquid crystalline state. The experimental data which has been previously used to contrast the predictions of Free Area theory and Continuum theory was collected at 36°C.[7] Therefore we chose to perform FPR experiments at the same temperature in order to facilitate comparison of our results with those from previously published research. It is anticipated that the results obtained at 36°C will also have biological

NBD-Labelled Amphiphile	Diffusion Coefficient‡ (μm^2/sec)	Number of Measurements	X_m
NBD-PE	10.4 ± 0.4	47	0.981
14, N_2L[NBD]	9.8 ± 0.4	45	0.984
15, N_3L_2[NBD]	9.6 ± 0.5	35	0.997
16, N_4L_3[NBD]	8.3 ± 0.2	53	0.985
17, N_5L_4[NBD]	8.6 ± 0.3	42	0.972
18, N_6L_5[NBD]	5.4 ± 0.2	48	0.979

Table 5-1: Diffusion Coefficients of Labelled Macrocyclic Polyamides

‡ Mean diffusion coefficient ± standard error of the mean

significance because this temperature is close to body temperature.

Unfortunately, because of technical difficulties it was not possible to determine the exact diameter of the beam spot used in FPR experiments. This parameter is significant because it is required for the calculation of diffusion coefficients according to Equation 5-3. Our estimated value for the diameter of the beam spot was 1.2 μm, based on previous measured values on our FPR apparatus. Clearly, it is preferable to obtain the actual value of this parameter, and experiments to determine the diameter of the beam spot are forthcoming. If necessary, diffusion coefficients will be corrected using Equation 5-4;

Equation 5-4 $$D[corrected] = D[measured] \times \frac{w^2[measured]}{w^2[estimated]}$$

The rate of lateral diffusion of NBD-PE, is generally considered to be a measurement of the rate lipid self-diffusion since the amphiphile is a fluorescently derivatized phospholipid. Our value for the lateral diffusion coefficient of NBD−PE in DMPC lies within the range of values (8-14 μm^2/sec) which have been reported for the amphiphile,[2,6,8] but is larger than the value (8 μm^2/sec) reported by Vaz et al.[8] which was used to construct the graphical depiction of Free Area theory (Figure 1-7).[7] The range of values for the diffusion coefficient of NBD-PE in the literature has been attributed to small differences in instrument calibration in different laboratories.[2,6]

It should be noted that all experimental data for different labelled

amphiphiles was collected within one week, and the optics of the system were not adjusted during that time period. Therefore, if measured diffusion coefficients do require correction, the correction should be the same, constant factor ($w^2[measured]/w^2[estimated]$) for all experimental data. It follows that meaningful conclusions can be drawn from our FPR experiments based on the relative diffusion coefficient values, even when there is some uncertainty about the exact beam spot diameter.

For each labelled amphiphile, individual diffusion coefficients were reproducible within ~20% of the mean. However, because 35-53 independent measurements were made for each amphiphile, one can use statistics to obtain mean values for the diffusion coefficients which have smaller standard errors (3-7%), and 95% confidence limits (4-10%). The statistical spread of diffusion coefficient data for each labelled amphiphile is indicated in Figure 5-5.

These plots indicate that there is a larger spread of data for the labelled amphiphiles which diffuse most rapidly; NBD-PE, labelled mono−amide **14** (N_2L[NBD]) and labelled di-amide **15** (N_3L_2[NBD]). It is likely that this occurs because there is a larger experimental error associated with measuring the relatively short τ_D values for these experiments. Other researchers have utilized a larger beam spot (~4 μm) to determine the diffusion coefficient of NBD-PE under various conditions,[9] since increasing beam spot radius results in decreased τ_D values according to Equation 5-3. The disadvantage of using a

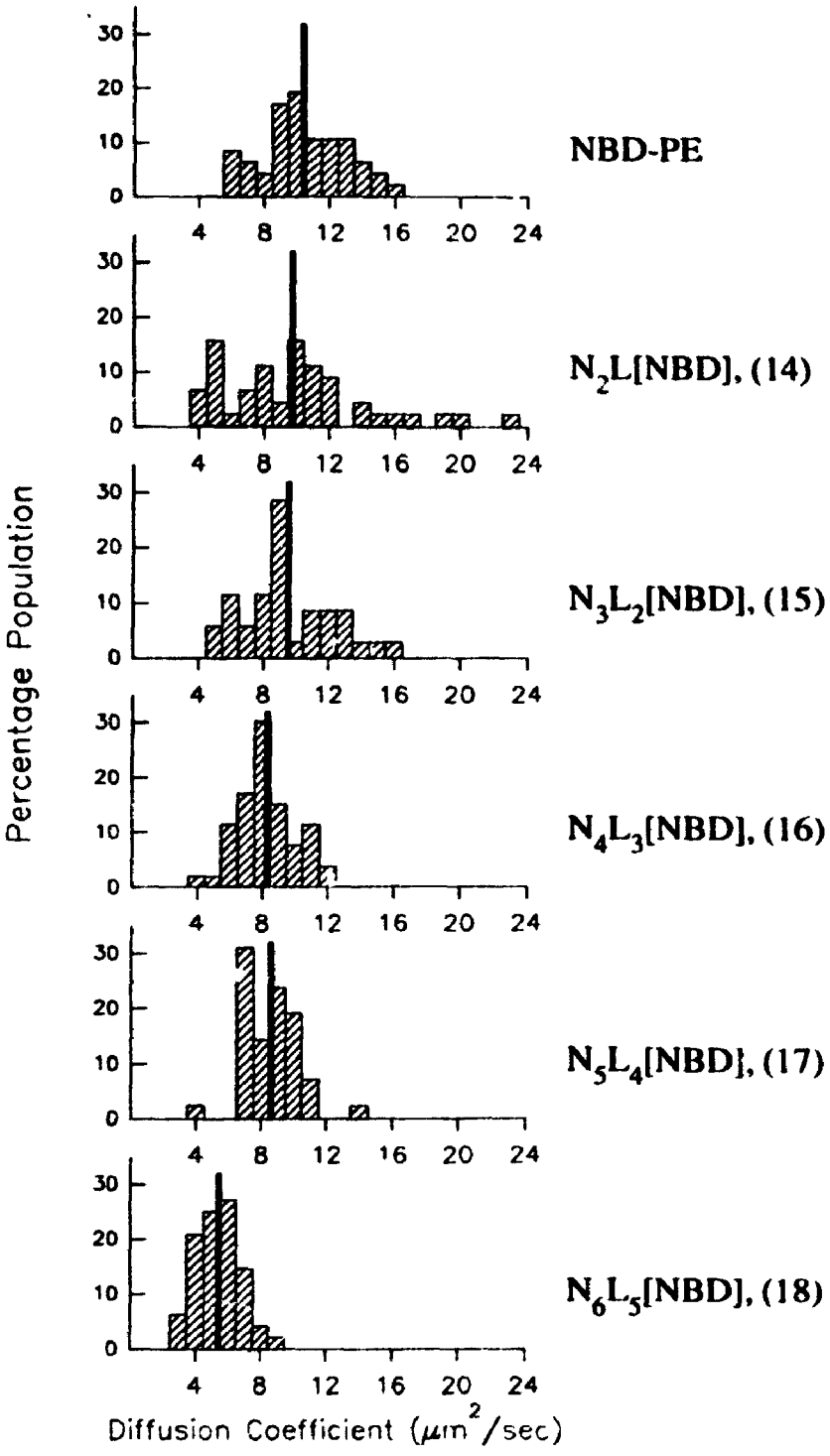

Figure 5-5: Statistical Distribution of Lateral Diffusion Coefficient Measurements

The dark line represents the mean value for each amphiphile

larger beam spot is that larger vesicles, which may be difficult to obtain, must be used in FPR experiments.

5.4 Correlation of Diffusion Coefficients with Surface Areas

The results from our FPR experiments (Table 5-1) were correlated with the surface areas of labelled macrocyclic polyamides at 30 mN/m determined using monolayer techniques (Table 5-2). The correlation between the results from the two separate sets of experiments clearly indicates that the rate of lateral diffusion exhibits a size dependence in the region of 30-250Å^2 (Figure 5-6). The (horizontal) error bars on the surface area measurements correspond to $\pm 10\%$ of the mean value. The (vertical) error bars on the diffusion measurements are the limits of 95% confidence based on the mean experimental diffusion coefficient for each labelled amphiphile. We consider the error bars to be true reflections of the certainty with which experimental results can be reported. Therefore, the true correlation between lateral diffusion coefficient and surface area for any given amphiphile is expected to fall within the region defined by the error bars, and is not necessarily the mean value represented by the ● symbol on Figure 5-6.

NBD-Labelled Amphiphile	Diffusion Coefficient‡ (μm^2/sec)	Surface Area§ at 30 mN/m ($Å^2$)
NBD-PE	10.4 ± 0.4	30 ± 3.0
14, N_2L[NBD]	9.8 ± 0.4	51 ± 5.1
15, N_3L_2[NBD]	9.6 ± 0.5	77 ± 7.7
16, N_4L_3[NBD]	8.3 ± 0.2	100 ± 10
17, N_5L_4[NBD]	8.6 ± 0.3	156 ± 16
18, N_6L_5[NBD]	5.4 ± 0.2	224 ± 22

Table 5-2: Correlation of Diffusion Coefficients of Labelled Macrocyclic Polyamides with Surface Areas at 30 mN/m determined by Monolayer Techniques

‡ Mean diffusion coefficient ± standard error of the mean

§ Errors in surface area measurements are reported ± 10% based on the reproducibility of monolayer experiments (Chapter 4)

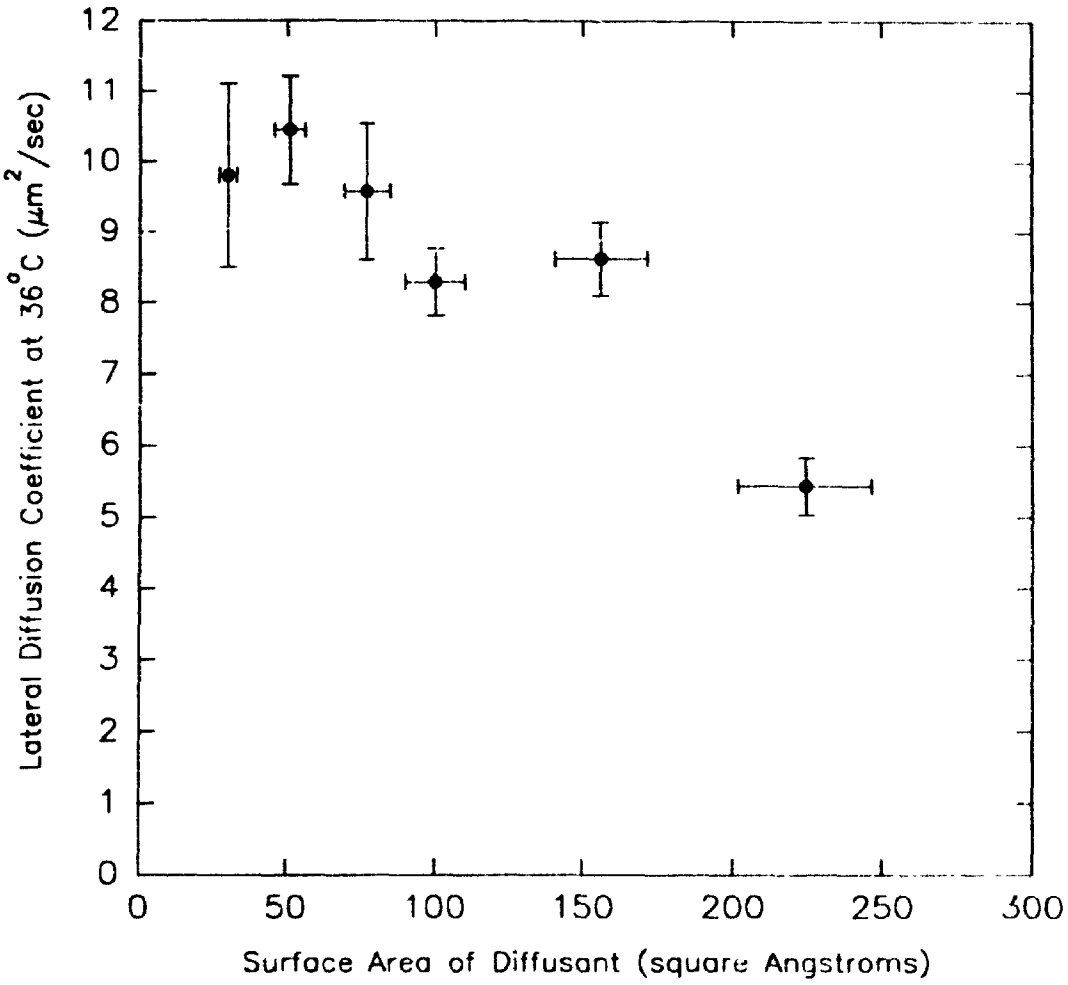

Figure 5-6: Correlation of Diffusion Coefficients with Surface Areas at 30 mN/m based on uncorrected experimental FPR data

The vertical error bars represent 95% confidence limits calculated based on the statistical spread of data for each amphiphile. The horizontal error bars represent the reproducibility of surface area measurements made using monolayer techniques.

This analysis is the first systematic study of lateral diffusion coefficients for molecules with intermediate surface areas. The most important finding of this study is the fact that the lateral diffusion coefficient for the largest amphiphile, labelled penta-amide **18** (N_6L_5[NBD]), is 55% of the lateral diffusion coefficient for the smallest amphiphile in the series, labelled mono-amide **14** (N_2L[NBD]). This variation of lateral diffusion coefficients is good evidence that the amphiphiles are incorporated in the lipid bilayer. Lateral diffusion coefficients for labelled di-amide **15** (N_3L_2[NBD]), labelled tri-amide **16** (N_4L_3{NBD]) and labelled tetra-amide **17** (N_5L_4[NBD]) also exhibit size dependence, and this data therefore reenforces the conclusion that lateral diffusion does vary with the surface area of labelled macrocyclic polyamides.

5.5 Implications for Theories of Lateral Diffusion

It is important to note that because the diffusion data were measured using a series of mono-NBD-labelled macrocyclic polyamides, every data point obtained is significant. In the past, comparison of the lateral diffusion properties of small amphiphiles (with surface areas $\leq 50Å^2$) and large amphiphiles (with surface areas greater than $300Å^2$) necessarily required comparing the lateral diffusion of two completely different types of molecules. The diffusion properties of phospholipid analogues and phospholipids was described using Free Area theory, and the lateral diffusion of proteins, which

span the lipid bilayer was described using Continuum theory. Our experimental data is the first set of results where the lateral diffusion coefficients of one type of molecule can be used to investigate lateral diffusion for molecules which are both smaller than phospholipids and much larger than phospholipids.

As stated previously, our mean value for the diffusion coefficient for NBD−PE was larger than the value reported by Vaz which was used to construct the graphical comparison of Free Area theory and Continuum theory.[7] Accordingly, our experimental lateral diffusion coefficients were adjusted by a scalar factor of 8.0 μm^2/10.4 μm^2. This correction factor corresponds to an actual beam spot diameter of 1.1μm, which is 8% smaller than our estimated value. The corrected diffusion coefficients were used to construct a graphical comparison of our experimental results with existing theories for lateral diffusion in lipid bilayer membranes (Figure 5-7).

In the case of labelled mono-amide **14** (N_2L[NBD]), the measured diffusion coefficient is approximately equal to the diffusion coefficient measured for NBD-PE. This result is in agreement with Free Area theory which states that molecules which have surface areas less than or equal to that of the phospholipids which comprise the bilayer will diffuse at the rate of lipid self-diffusion. This result is also in agreement with the recently published results for ubiquinone derivatives in model membrane systems, which were

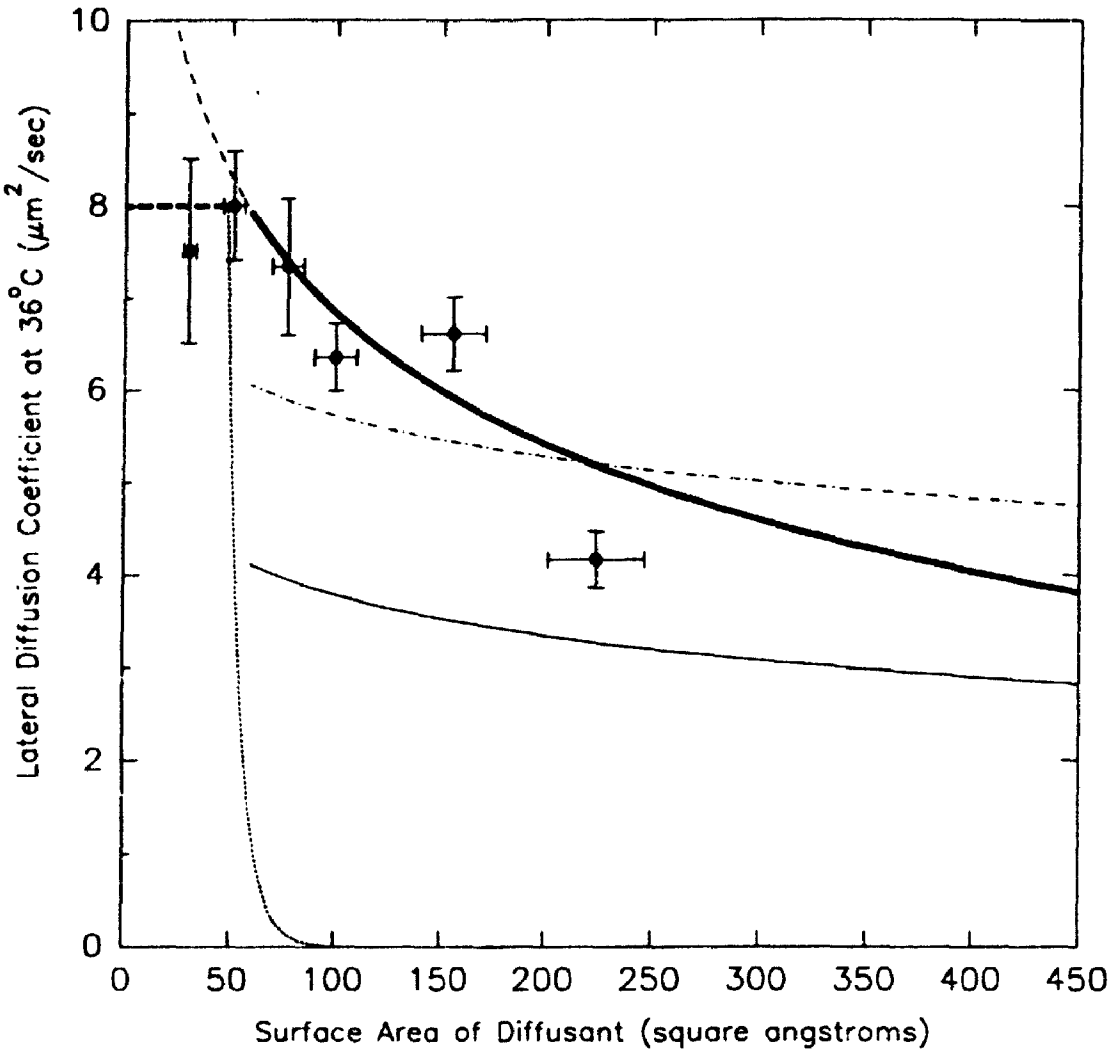

Figure 5-7: Graphical Comparison of Corrected Experimental Results with Theories for Lateral Diffusion in Lipid Bilayer Membranes

All theories for lateral diffusion in bilayer membranes are shown; Free Area theory (- - - - , ——), Saffman-Delbruck theory (—·—·—), Sackman-Evans theory for a diffusant which spans the membrane (——), and Sackman-Evans theory for molecules which do not span the membrane (——, - - - -). The curves for Continuum theories were calculated using a viscosity of 0.01 Poise for water, and 0.75 Poise for the viscosity of the membrane which is assumed to be 35 angstroms thick.

The best agreement with experimental results is obtained assuming that Free Area theory is obeyed until the size of the diffusant exceeds the size of phospholipids in the bilayer. Once the size of the diffusant is greater than 50 square angstroms, the best agreement is obtained if one assumes that the diffusant has a height of 10 angstroms, and the frictional force exterted by the substrate on the membrane (b_2) is 1.65×10^6 Poise/cm (this value was also used in the calculation of the Sackman-Evans prediction for a diffusant which spans the bilayer membrane).

also reported to diffuse at the rate of lipid self-diffusion.[10]

Within experimental error, the lateral diffusion of labelled di-amide **15** (N_3L_2[NBD]) can also be considered equivalent to the rate of lipid self-diffusion since the horizontal line defining the rate of lipid self-diffusion would pass through the error bar representing 95% confidence for this data point. This result can probably attributed to the fact that though the measured surface area of labelled di-amide **15** (N_3L_2[NBD]) is larger than that NBD-PE (77 vs 51 Å^2), both amphiphiles contain two alkyl chains.

In contrast, a graphical comparison of our results for labelled tri-amide **16** (N_4L_3{NBD]), labelled tetra-amide **17** (N_5L_4[NBD]) and labelled penta-amide **18** (N_6L_5[NBD]) with predictions from Free Area theory and Continuum theory for amphiphiles which span the membrane clearly indicates that our experimental results do not agree with the predictions of either theory (Figure 5-7). The exhibited dependence of lateral diffusion on surface area is much weaker than predicted by Free Area theory, but much stronger than the prediction of Continuum theories for molecules which span the membrane.

The graphical analysis (Figure 5-7) of the lateral diffusion coefficients of labelled macrocyclic polyamides is based on the surface areas of labelled macrocyclic polyamides which were determined using monolayer experiments. However, it should be noted that even if these surface areas deviate from the actual surface areas which the amphiphiles exhibit in bilayer membranes, one

can still discuss the dependence of lateral diffusion on the minimum surface area per molecule based on the number of alkyl chains in each amphiphile. The area per alkyl chain for each macrocyclic polyamide can be estimated based on the surface area of DMPC (50 $Å^2$) which has two alkyl chains.

If one assumes a minimum surface area of 25$Å^2$ per alkyl group, then the minimum surface areas of labelled macrocyclic polyamides **14**, **15**, **16**, **17**, **18** (N_2L[NBD], N_3L_2[NBD], N_4L_3[NBD], N_5L_4[NBD], N_6L_5[NBD]) are 25, 50, 75, 100, and 125 $Å^2$ respectively. These surface area values span only half the size regime of interest (50-300$Å^2$), but extend beyond the size limit that corresponds to a prediction of zero lateral diffusion according to Free Area theory. Therefore, even based on the minimum surface area per alkyl chain, one can conclude that the lateral diffusion of macrocyclic polyamides exhibits a size dependence which is much weaker than that predicted by Free Area theory and stronger than that predicted by Continuum theories for amphiphiles which span the bilayer.

If the amphiphiles do assume conformations with the macrocyclic ring parallel to the plane of the bilayer (Figure 3-10) with surface areas comparable to the values measured in monolayer experiments, then the maximum depth which the amphiphiles can penetrate into the membrane is approximately 15Å, if the alkyl chains are in the all trans-conformation and normal to the plane of the bilayer. Alternatively, if one assumes that each methylene group occupies

a volume of 35Å^3 (25Å^2 cross sectional area x 1.4Å vertical distance) then it is possible to calculate the minimum height for each amphiphile by dividing its minimum volume (based on the number of methylene groups) by the surface area of the amphiphile. These calculations yield an average height of 11Å for the series of amphiphiles. The thickness of a model DMPC liquid crystalline bilayer membrane is estimated to be 30-40Å. Therefore, we chose to compare our experimental diffusion coefficients with the predictions of the Sackman-Evans model for diffusants which do not span the bilayer membrane.

Tamm has recently applied Sackman-Evans theory to the lateral diffusion of a signal peptide which does not span the lipid bilayer.[11] According to the Sackman-Evans model for lateral diffusion, the lateral diffusion coefficient for an amphiphile which partially penetrates the lipid bilayer is given by Equation 5-5;[12]

Equation 5-5
$$D=\frac{kT}{4\pi\eta_m}\times\left[\frac{\varepsilon^2}{4}\times\left(1+\frac{b_1}{b_2}\right)+\varepsilon\times\frac{K_1}{K_0}\right]^{-1}$$

η_m is the viscosity of the membrane multiplied by the height of the diffusant and ϵ is related to the radius of the diffusant (a) according to Equation 5-6;

Equation 5-6
$$\varepsilon=a\sqrt{\frac{b_2+b_3}{\eta_m}}$$

K_1 and K_0 are first and second order modified Bessel functions of ϵ.

Most of the parameters for the equations describing Sackman-Evans model of lateral diffusion can be obtained from the literature. Estimates of membrane viscosity range from 0.75 to 1.5 Poise; our data were fit assuming a membrane viscosity of 0.75 Poise. The viscosity of water is generally accepted to be 0.01 Poise. The value for the frictional force between layers of the bilayer membrane, b_1, was set equal to 3×10^5 Poise/cm according to the calculation of the frictional coefficient between two fluid lipid monolayers reported by Merkel et al.[13] The frictional force applied by the aqueous phase on the membrane and diffusant, b_3, can be approximated as $b_3 \approx \mu_w^2/\eta_m$ (1.33×10^2 Poise/cm) where μ_w is the viscosity of water.

The best agreement of Sackman-Evans theory with our experimental data for amphiphiles with surface areas greater than 50Å^2 was obtained if one assumes that the height of the diffusant in the monolayer is 10Å, and drag of the membrane on the diffusant, b_2, is 1.65×10^6 Poise/cm, which is 5.5 times the drag between the two layers of the membrane (Appendix II).

Though the correspondence is not exact, it is clear that the Sackman-Evans model for a partially penetrating amphiphile agrees with the observed correlation between lateral diffusion coefficients and surface areas better than Free Area theory or Continuum theories based on amphiphiles which span the lipid bilayer. From this we can conclude that lateral diffusion coefficients of molecules which are only two times larger than the phospholipids are best

described using the Sackman-Evans model of lateral diffusion. It is also interesting to note that the mean value for the data point obtained for labelled di-amide **15** (N_3L_2[NBD]) also agrees well on the curve calculated using Sackman-Evans theory applied to a diffusant which does not span the membrane.

The fact that the Sackman-Evans theory agrees with our experimental data reasonably well represents a significant finding because it suggests that lateral diffusion of amphiphiles which are only slightly larger than phospholipids can be described using a model which treats the phospholipid bilayer as a continuous fluid sheet.

5.6 Conclusions

Each of the five NBD-labelled macrocyclic polyamides were incorporated in DMPC lipid bilayer membranes, and the lateral diffusion coefficient of each labelled amphiphile was determined at 36°C. The lateral diffusion coefficient for NBD-PE was also determined, and found to be in agreement with the results of research performed elsewhere.

The lateral diffusion coefficients of the labelled macrocyclic polyamides were correlated with the surface areas of the molecules which were determined using monolayer experiments. The results of this correlation demonstrate the first example of size dependence of lateral diffusion for a series of structurally similar amphiphiles.

Within experimental error, the lateral diffusion of labelled mono-amide **14** (N_2L[NBD]) and labelled di-amide **15** (N_3L_2[NBD]) are equal to the rate of lateral diffusion of NBD-PE. This result is in agreement with Free Area theory which states that diffusants which have areas smaller than or comparable to phospholipids will diffuse at the rate of lipid self-diffusion.

Our experimental results for labelled tri-amide **16** (N_4L_3{NBD]), labelled tetra-amide **17** (N_5L_4[NBD]) and labelled penta-amide **18** (N_6L_5[NBD]) were compared with those predicted by theories of lateral diffusion in lipid bilayer membranes. This analysis has indicated that the observed dependence of lateral diffusion on surface area is much weaker than the result predicted by

Free Area theory, and much stronger than the result predicted by Continuum theory when it is applied to a diffusant which spans the bilayer membrane.

However, if one assumes that the diffusant partially penetrates the membrane, reasonable agreement was found between the predictions of Sackman-Evans theory and our experimental results. This novel finding suggests that Continuum theory can be applied to the diffusion of molecules which are only slightly larger than the molecules which form the continuum.

5.7 Experimental

5.7.1 Preparation of Lipid Vesicles

Coverslips were cleaned by sonication in 95% ethanol for 30 minutes and dried in an oven at 70°C. Samples were handled in subdued light. Dimyristoylphosphatidylcholine (DMPC) was purchased from Fluka, New York. Nitrobenzoxadiazole labelled phosphatidylethanolamine was purchased from Avanti Polar Lipids, Alabama. Labelled macrocyclic polyamides were prepared as described in Chapter 2. Solutions of DMPC (~1 mM) and labelled amphiphiles (~ 1 μM) were prepared in glass-distilled chloroform.

DMPC lipid vesicles were prepared by a modification of the method of Balcolm and Petersen.[14] Typically 500 nmol of DMPC (500 μL of ~1 mM solution in chloroform) was combined with 0.5 nmol of labelled amphiphile. The solution of labelled amphiphile and lipid was allowed to mix for at least 10 minutes at room temperature, then heated in a water bath at 80°C until the total volume of the solution was ~50-100 μL. The solution was cooled to room temperature, then deposited as a single drop in the centre of a 22 mm clean, dry glass coverslip which had been heated to 70°C. The chloroform was allowed to evaporate at 70°C then the sample was dried under house vacuum at room temperature for at least 2 hours.

The sample of dry lipid and labelled amphiphile was then heated to 70°C, and a 200 μL drop of doubly distilled deionized water was placed on

top of the dry lipid. An 18 mm clean, dry glass coverslip was carefully placed on top of the water droplet, then the sample was heated in an oven at 70°C for 15 minutes. The sample was removed from the oven, allowed to cool for ~ 5 minutes, then the water and lipid were sealed between the two coverslips with paraffin wax which had been heated to 120°C. The sample was transferred to a 40°C oven which contained a pan of water, heated for at least 18 hours, then allowed to cool slowly in the oven over a period of several hours. Finally, a second coat of hot wax was applied to ensure the sample was sealed to prevent dehydration. Samples were stored in the dark for 2−15 days prior to experimentation.

5.7.2 Selection of Vesicles for FPR Experiments

All of the samples prepared by the above method contained large amounts of hydrated lipid. Approximately 50% of the samples contained numerous vesicles with diameters in the range of 40-100 μm.

When viewed under a phase contrast microscope, vesicles have the appearance of soap bubbles. Multilamellar vesicles have well defined edges, whereas the edges of vesicles which contain fewer layers are very thin and barely visible. FPR experiments were performed on both types of vesicles. Symmetrical, circular or elliptical vesicles were selected for all experiments. and the vast majority of the vesicles prepared by the above were stationary.

Immediately after each experiment, vesicles were examined with the eyepiece to ensure that no movement had occurred during the experiment. In cases where it was determined that the vesicle had moved during the experiment, the results were discarded.

Occasionally, large vesicles were found to contain smaller vesicles within them or on top of them. These vesicles could be identified using the laser beam because the projection of the laser beam on these vesicles did not produce a single circular spot. Instead, the fluorescent spot appeared to be very bright along the edge of the smaller vesicle. This phenomenon occurs because the sample irradiated by the laser beam extends $\sim$ 6 μm above and below the optical plane, and the edges of vesicles contain more fluorescent material within the sampled region than the apex of curvature of a single vesicle.

In general, the monitor, bleach, recovery sequence was performed on a single spot 4-10 times to obtain a single diffusion coefficient measurement. For each fluorescently labelled amphiphile, 1-6 measurements were made on at least ten different vesicles within a single sample, to yield at least 35 separate diffusion coefficient measurements.

5.7.3 FPR Hardware

The sample holder for FPR experiments was a hollow copper disk that contained an axially symmetric hole in the centre which was covered with an 18 mm glass coverslip and sealed with wax or silicone sealant. The copper sample holder was filled with water, then the sample was placed in the holder lipid-side-down. The bottom of the sample holder was covered with a thin layer of thermally conducting grease and the sample and holder were placed on a temperature controlled stage equipped with a Cambion Bipolar temperature controller. The temperature of the sample was set to 36 ± 1 °C, and the temperature of the sample was monitored by dipping a small 100 kΩ thermistor into the water near the focal point of the microscope and calculating the temperature from a resistance vs temperature calibration curve which was provided by the manufacturer (Yellow Springs Instrument Co.).

A Coherent Inc. Innova 70 Four Watt Argon Ion laser was used as the light source for the bleach and monitor beam. The laser was operated at 476.5 nm in current regulation mode with an output of approximately 50 mW. Timing of the bleach and monitor beams was controlled by a custom- made bleach box control unit. The intensity of the bleach and monitor beams was attenuated using neutral density filters of 0.6-1.4 O.D., depending on the sample. The fluorescence intensity incident on the detector was lowered further by placing neutral density filters (0.56-1.13 O.D.) in the optical path

after the sample.

The microscope used in these experiments was a Zeiss Universal model fitted for epi−illumination. Fluorescent emission was detected using an RCA 31034A photo multiplier tube which was fitted to the top of the optical column and cooled with dry ice. Data for FPR experiments were collected using a custom−made data acquisition microcomputer then transferred to an XT personal computer and processed using a BASIC computer program written by Dave Bjarneson. The data files were saved in ASCII format, then transferred to the VAX 6330 mainframe computer, where the fluorescence recovery curves were fit and the diffusion coefficients were extracted from the recovery curve of best fit.

5.8 References

1. Petersen, N.O., Felder, S., and Elson, E.L., Measurement of Lateral Diffusion by Fluorescence Photobleaching Recovery, in *Handbook of Experimental Immunology*, **1986**, Weir, D.M. Editor, Blackwell, Edinburgh, 24.1-24.3.
2. Axelrod, D., Fluorescence Photobleaching Techniques and Lateral Diffusion, in *Spectrosc. Dyn. Mol. Biol. Syst.*, **1985**, Bayley, P., and Dale, R., Editors, Academic Press, Toronto, 163-175.
3. Vaz, W.C., Derzko, Z.I., and Jacobsen, K.A., Photobleaching Measurements of the Lateral Diffusion of Lipids and Proteins in Artificial Phospholipid Bilayer Membranes, *Cell Surf. Rev*, **1982**, *8* (Membr. Reconst.), 83-135.
4. Frye, C.D., and Edidin, M., The Rapid Intermixing of Cell Surface Antigens After Formation of Mouse-Human Heterokaryons, *J.Cell. Sci.*, **1970**, *7*, 319-335.
5. Peters, R., Lateral Mobility of Proteins in Membranes, in *Struct. Prop. Cell Membr., VI*, **1985**, Benga, G., Editor, CRC Press, 35-50.
6. Wade, G., The Lateral Diffusion of Lipids, in *Struct. Prop. Cell Membr., VI*, **1985**, Benga, G., Editor, CRC Press, 51-66.
7. Vaz, W.L.C., Goodsaid-Zalduondo, F., and Jacobson, K., Lateral Diffusion of Lipids and Proteins in Bilayer Membranes, *FEBS Letters*, **1984**, *174*, 199-207 and references therein.

8. Vaz, W.L.C., Ciegg, R.M., and Hallman, D., Translational Diffusion of Lipids in Liquid Crystalline Phase Phosphatidylcholine Multibilayers. A Comparison of Experiment with Theory, *Biochemistry*, **1985**, *24*, 781-786.

9. Almeida, P.F., Vaz, W.L.C., and Thompson, T.E., Lateral Diffusion in the Liquid Phases of Dimyristoylphosphatidylcholine/Cholesterol Lipid Bilayers, *Biochemistry*, **1992**, *31*, 6739-6747.

10. Rajarathnan, K., Hochman, J., Schindler, M., and Ferguson-Miller, S., Synthesis, Location and Lateral Mobility of Fluorescently Labelled Ubiquinone 10 in Mitochondrial and Artificial Membranes, *Biochemistry*, **1989**, *28*, 3168-3176.

11. Evans, E., and Sackman, E., Translational and Rotational Drag Coefficients for a Disk Moving in a Liquid Membrane Associated with a Rigid Substrate, *J. Fluid Mech.*, **1988**, *194*, 553-561.

12. Tamm, L, Membrane Insertion and Lateral Mobility of Synthetic Amphiphilic Signal Peptides in Lipid Model Membranes, *Biochim. Biophys. Acta*, **1991**, *1071*, 123-148.

13. Merkel, R., Sackman, E., and Evans, E., Molecular Friction and Epitactic Coupling Between Monolayers in Supported Bilayers, *J. de Physique*, **1989**, *50*, 1535-1555.

14. Balcolm, B.J., and Petersen, N.O., Lateral Diffusion in Model Membranes is Independent of the Size of the Hydrophobic Region of Molecules, *Biophys. J.*, **1993**, *65*, 630-637.

Chapter 6

CONCLUSIONS

6.1 Summary of Experimental Results

We have successfully synthesized two series of polylauroyl macrocyclic polyamides derived from macrocyclic polyamines with the empirical formula $(CH_2CH_2NH)_n$ n=2,3,4,5,6. All of the macrocyclic polyamides are solids at room temperature. Unlabelled macrocyclic polyamides; di-amide **6** (N_2L_2), tri-amide **7** (N_3L_3), tetra-amide **8** (N_4L_4), penta-amide **9** (N_5L_5) and hexa-amide **10** (N_6L_6) were synthesized by a modification of Lehn's method,[1] which allows for faster and easier preparation without decreases in experimental yield. Mono-NBD-labelled polylauroyl macrocyclic polyamides; labelled mono-amide **14** (N_2L[NBD]), labelled di-amide **15** (N_3L_2[NBD]), labelled tri-amide **16** (N_3L_2[NBD]), labelled tetra-amide **17** (N_3L_2[NBD]), and labelled penta-amide **18** (N_3L_2[NBD]), were prepared by a novel, statistically-based, two step method. Traditionally, asymmetrically substituted derivatives of macrocyclic polyamines are difficult to prepare, therefore, our new method, which requires minutes for complete reaction, may have applications for the synthesis of other asymmetrically substituted macrocyclic polyamine derivatives.

Variable temperature ^1H NMR analysis of the smallest labelled and unlabelled macrocyclic polyamides (labelled mono-amide **14** (N_2L[NBD]) and di-amide **6** (N_2L_2), respectively) has indicated that both the N-C(O) bond of the amide group and the N-NBD bond of nitrogen derivatives exhibit partial double bond character. The partial double bond character of amide bonds in well known; however, our research is the first evidence that the NBD-N bond in nitrogen derivatives of NBD also exhibit partial double bond character. The activation energies for bond rotation have been calculated to be 40-41 kJ/mol for the C(O)-N bond and 59 kJ/mol for the NBD-N bond respectively. This finding will have significant impact in the field of biochemistry, where the geometry and electron configuration of NBD-N derivatives are used as the basis for numerous biochemical experiments. Owing to this partial double bond character, both the amide groups and the NBD-N groups can be viewed as rigid, planar moieties. It follows that the macrocyclic rings in all of the macrocyclic polyamides (labelled and unlabelled) can also be considered as rigid and predominantly planar structures.

Taking this information into account, computer molecular models of the labelled and unlabelled macrocyclic polyamides were generated. The molecules were constructed in conformations in which the alkyl chains are oriented normal to the plane of the macrocyclic ring, i.e. conformations which the amphiphiles are predicted to exhibit in monolayer and bilayer structures.

The surface areas of the two dimensional projections of the hydrophilic surfaces of the computer molecular models were measured based on these models.

Seelig has calcuated the bilayer equivalent pressure in a monolayer[2] to be 30 mN/m. The surface areas of labelled and unlabelled macrocyclic polyamides in monolayers at the air-water interface were measured as a function of surface pressure using a Langmuir film balance, and the surface area per molecule at 30 mN/m for each compound was determined graphically by interpolation or extrapolation where required. The surface area values thus obtained were compared with the results from surface areas calculated using computer molecular models. In general, all of the labelled macrocyclic polyamides which contain three or more nitrogen atoms in the macrocyclic ring exhibited surface areas which were approximately equal to the surface areas of their unlabelled analogues within experimental error. The smallest labelled macrocyclic polyamide, labelled mono-amide **14** (N_2L[NBD]), exhibited a surface area which was smaller than its unlabelled counterpart, di-amide **6** (N_2L_2). This smaller surface area is attributed to the fact that the macrocyclic ring of labelled mono-amide **14** (N_2L[NBD]) is normal to the air−water interface, whereas the macrocyclic ring of all other macrocyclic polyamides is parallel to the air-water interface. From these experiments we conclude that a minimum of two amide groups are required for the macrocyclic ring to assume

an orientation parallel to the air-water interface.

Labelled macrocyclic polyamides and NBD-PE were incorporated into DMPC phospholipid vesicles, and the diffusion coefficients of the fluorescent amphiphiles were determined using FPR. The diffusion coefficient for each labelled amphiphile was then correlated with its predicted surface area at 30 mN/m (based on monolayer experiments). This correlation has shown that there is a significant dependence of lateral diffusion on the surface areas of amphiphiles with surface areas between 30-250Å^2, and is the first demonstrated dependence of lateral diffusion on surface area for amphiphiles in this size regime.

Within experimental error, the lateral diffusion of the smallest labelled macrocyclic polyamides, labelled mono-amide **14** (N_2L[NBD]) and labelled di-amide **15** (N_3L_2[NBD]), are equal to the rate of lateral diffusion of NBD-PE. This result constitutes experimental evidence for Free Area theory which states that diffusants which have areas smaller than or comparable to phospholipids will diffuse at the rate of lipid self-diffusion.

Our experimental results for labelled tri-amide **16** (N_4L_3[NBD]), labelled tetra-amide **17** (N_5L_4[NBD]) and labelled penta-amide **18** (N_6L_5[NBD]) were compared with those predicted by theories of lateral diffusion in lipid bilayer membranes. This analysis has indicated that the observed dependence of lateral diffusion on surface area is in agreement with the predictions of

Sackman-Evans theory applied to a diffusant which extends ~10Å into the lipid bilayer which is at least 30Å thick. This novel finding suggests that Continuum theory can be applied to the diffusion of molecules which are only slightly larger than the molecules which form the continuum.

6.2 Directions for Further Research

For the most part, the significance of this study of lateral diffusion in lipid bilayers can be attributed to the macrocyclic polyamides which were used to study the process. These amphiphiles have allowed for the investigation of the lateral diffusion of structurally similar molecules which are both smaller and much larger than phospholipids. In contrast, previous analyses of lateral diffusion have been based on comparing the properties of phospholipid analogues with labelled proteins and peptides.

The utility of the probe molecules should also extend to the study of other factors which affect lateral diffusion in lipid bilayer membranes, including concentration dependence and temperature dependence. In addition, other probe molecules which are based on labelled macrocyclic polyamides but have larger surface areas may be useful to obtain more evidence in support of the application of Sackman-Evans model of lateral diffusion to diffusants with intermediate surface areas.

One of the most interesting findings of this research project is the

relevance of the Sackman-Evans model, which predicts that the rate of lateral diffusion has a strong dependence on the height of the diffusant rather than the thickness of the membrane. Our results indicate good agreement between theory and experiment if one assumes a height of 10Å. This value is 50% smaller than the maximum height of the probe estimated using computer molecular models. The difference between the estimated height, and the height which corresponded to the best agreement with the Sackman-Evans model may be attributed to the fact that the alkyl chains of the probe molecules are not necessarily in an all-trans conformation and normal to the plane of the bilayer. If the alkyl chains are angled, perhaps towards the geometric centre of the macrocyclic ring, then a decrease in predicted height is anticipated.

On the other hand, the value of 10Å for the height of the diffusant may have significance which can be attributed to the properties of lipid bilayers themselves, and not necessarily the diffusant. Numerous NMR studies on the structure of lipid bilayers have indicated that the region of the lipid bilayer from the carbonyl group of phospholipids to the 6th-8th methylene group is more ordered than the region of the bilayer corresponding to the termini of the alkyl chains.[3] If one assumes a projected height of 1.4Å per carbon-carbon bond,[4] the ordered region of the lipid bilayer corresponds to the first 9-11Å. The implication is that the viscosity near the hydrophilic surface of the lipid bilayer membrane may be greater than the viscosity of the hydrophobic core.

This analysis of the lipid bilayer as a three dimensional structure which contains a less viscous (oil-like) core 10-40Å thick between two more viscous (paraffin-like) sheets which are each 9-11Å thick is consistent with experimentally determined lateral diffusion coefficients of different types of probe molecules.

Balcolm and Petersen have recently reported that large changes in the length of the alkyl chains of fluorescently labelled isoprenoid alcohols do not affect their rates of lateral diffusion in lipid bilayer membranes.[5] These results are consistent with the three-layer model of the lipid bilayer described above if one assumes that the fluorescent probe used in this study resides in the more viscous, paraffin-like layer, while the hydrocarbon chains reside in the less viscous hydrocarbon core. In the same study, Balcolm and Petersen report that the diffusion of tetracene, a polyaromatic molecule which does not contain a polar group is faster than the rate of lipid self-diffusion.[5] This results is also consistent with a model of the lipid membrane which has a less viscous hydrocarbon core, assuming that the tetracene probe resides completely within this less vicous layer. Both of these finding support the model of a lipid bilayer where lateral diffusion of amphiphiles is limited by the region of the membrane near the hydrophilic surface which is more viscous than the hydrophobic core.

In the future, researchers may be able to use macrocyclic polyamides to investigate this membrane property and its effect on lateral diffusion. By synthesizing labelled macrocyclic polyamides which contain alkyl chains which are shorter or longer than the lauroyl groups used in this study, it may be possible to determine the exact nature of the height dependence of lateral diffusion in lipid bilayer membranes.

In summary, the results of this research project have demonstrated that there is a size dependence of lateral diffusion in lipid bilayer membranes for amphiphiles which are larger than the phospholipids which comprise the bilayer, and that this dependence can be modelled using Sackman-Evans theory which treats the bilayer as a continuous fluid sheet. Further investigation may provide evidence as to whether the entire bilayer determines the hydrodynamic properties of membranes, or whether it is the surface of the bilayer, which is known to be more ordered than the hydrophobic core.

6.3 References

1. Malthête, J., Poupinet, D., Vilanove, R, and Lehn, J.M., Monolayers of Macrocyclic Polyamides at the Air-Water Interface, *J. Chem. Soc. Chem. Comm.*, **1989**, 1016-1019.
2. Seelig, A., Local Anesthetics and Pressure: A Comparison of Dibucaine Binding to Lipid Monolayers and Bilayers, *Biochim. Biophys. Acta*, *899*, **1987** 196-205.
3. Lenaz, G., and Castelli, G.P., Membrane Fluidity: Molecular Basis and Physiological Significance, in *Struct. Prop. Cell Membr., Vl*, **1985**, Benga, G., Editor, CRC Press, 93-136. and refererces therein
4. Pink, D.A., Theoretical Studies of Phospholipid Bilayers and Monolayers, *Can. J. Biochem. Cell. Biol.*, **1984**, *62*, 760-777.
5. Balcolm, B.J., and Petersen, N.O., Lateral Diffusion in Model Membranes is Independent of the Size of the Hydrophobic Region of Molecules, *Biophys. J.*, **1993**, *65*, 630-637.

Appendix I

THEORETICAL AND EXPERIMENTAL ANALYSES OF OPTICAL TRANSITIONS OF NITROBENZOXADIAZOLE (NBD) DERIVATIVES

Paprica, P.A., Baird, N.C., and Petersen, N.O., *J.Photochem. Photobiol. A: Chemistry*, **1993**, *70*, 51-57.

Theoretical and experimental analyses of optical transitions of nitrobenzoxadiazole (NBD) derivatives

P. A. Paprica, N. C. Baird and N. O. Petersen*
Department of Chemistry, University of Western Ontario, London, Ont., N6A 5B7 (Canada)

(Received July 16, 1992; accepted August 28, 1992)

Abstract

Several nitrobenzoxadiazole (NBD) derivatives were synthesized using nitrobenzoxadiazole chloride as the starting material. The UV absorption maxima of the compounds were obtained experimentally and compared with predicted values from STO-3G *ab initio* CIS (configuration interaction with single excitation) calculations and Pariser–Pople–Parr (PPP) calculations. It was found that there was good agreement between the experimental and PPP-calculated λ_{max} values, which implies that the permanent and transition dipole moments calculated by the PPP method are also meaningful. These dipole moments of NBD derivatives are significant because a knowledge of their magnitude and orientation improves the utility of NBD derivatives in fluorescence depolarization and energy transfer experiments.

1. Introduction

Nitrobenzoxadiazole (NBD) derivatives are used extensively for the study of biological systems [1]. Typically, non-fluorescent nitrobenzoxadiazole chloride (NBD-Cl, 1) is reacted with a free amino or thiol group on a drug, protein or lipid to form a fluorescent NBD derivative. NBD derivatives undergo a characteristic red shift when they are transferred from a non-polar to a polar environment [2], and this shift in λ_{max} is used to probe the environment of biological molecules with respect to polarity. NBD derivatives are also widely used in fluorescence depolarization and energy transfer studies [3]. The interpretation of data for all of these techniques requires some knowledge or assumptions about the magnitude and orientation of the transition dipole moment associated with the fluorophore, and it is therefore surprising that very little information is available on the subject. Molecular orbital calculations can be used to obtain information about the energy required for chromophores to absorb light and about where the electron density is located in the molecular orbitals involved in the electronic transitions associated with absorption. Therefore the aim of this project was to use molecular orbital calculations to account for the λ_{max} values associated with different NBD derivatives, and to obtain some semi-empirical quantitative information about the transition dipole moments of NBD derivatives.

2. Experimental procedures

7-Chloro-4-nitrobenz-2-oxa-1,3-diazole (NBD-Cl, 1) was purchased from Sigma Chemical Co., St. Louis, MO and was used without additional purification. All other reagents were purchased from Aldrich Chemical Co., Milwaukee, WI, or British Drug House, Toronto, Ont.

Proton nuclear magnetic resonance (^{1}H NMR) spectra were recorded on a Varian Gemini 200 MHz spectrometer. ^{13}C APT (attached proton test) spectra were acquired with a Varian XL-300 300 MHz spectrometer. All NMR spectra were obtained using deutero-(d_6)-acetone or $CDCl_3$ as solvent, and chemical shifts are reported in parts per million relative to tetramethylsilane (TMS) as an internal standard. Mass spectroscopy analyses were performed on a Finnigan MAT 8320 by the chemical ionization (CI) technique. Purification of compounds was performed by preparative thin layer chromatography (TLC) using glass-backed silica gel UV/254 plates (Merck, 2.0 mm silica gel) as the stationary phase. UV spectra were obtained using a Shimadzu UV-160 UV–visible recording spectrophotometer.

*Author to whom correspondence should be addressed.

1010-6030/93/$6.00

Ab initio equilibrium geometry optimizations were performed using the Gaussian 90 computer program with 3-21G and STO-3G basis sets. *Ab initio* singlet excitation energies and dipole moments were calculated using the Gaussian 90 program with the CIS (configuration interaction with single excitations) option and the STO-3G basis set. The CIS option considers all single substitutions from the Hartree–Fock reference determinant. Pariser–Pople–Parr (PPP) singlet excitation energies and dipole moments were calculated using the Quantum Chemistry Program Exchange 314 computer program, and parameters obtained from tables included with the Quantum Chemistry Program Exchange QCMP054 computer program. All calculations were performed on a VAX 6430 mainframe computer.

2.1. NBD-methyl ether (NBD-OCH_3, 2)

This compound was prepared by dissolving 179.7 mg (0.901 mmol) of NBD-Cl in 25 ml of anhydrous methanol (dried over molecular sieves) with 96.6 mg (0.986 mmol) of potassium acetate. The solution was placed in a sonicator for 8 h and stirred for 48 h at room temperature; the methanol was then removed under reduced pressure. Acetic acid was removed from the crude product by twice adding 20 ml of cyclohexane (which forms an azeotrope with acetic acid) and removing all solvents by rotary evaporation. The mass of the crude product was 167.3 mg. In a typical purification procedure 80 mg of the acetone-soluble components of the crude product mixture (including unreacted NBD-Cl) were purified by loading the crude mixture in 0.5 ml of acetone on a preparative silica TLC plate and eluting with chloroform three times. The yellow–orange band (which eluted more slowly than the pale yellow unreacted NBD-Cl) was scraped off the plate and the product was extracted in acetone by stirring the solid silica gel in acetone at room temperature for 6 h. Filtration and removal of acetone from the filtrate by rotary evaporation furnished 41 mg of NBD-methyl ether (2) (overall yield, 51%). ^{1}H NMR (d_6-acetone): δ 4.30 (O-CH_3), 7.07, 7.12, 8.69, 8.73 (-CH=CH-, AB pattern). ^{13}C NMR ($CDCl_3$): δ 57.88 (OCH_3), 104.02, 134.12 (-CH=CH-), 129.91, 143.95, 145.20, 155.40 (quaternary carbons). Mass spectrum *m/e* 195.028, found 195.028 (M^+).

2.2. NBD-dodecyl thiol ether (NBD-SR, 3)

The sulphur derivative of NBD was prepared by dissolving 149 mg (0.736 mmol) of dodecane thiol in 3 ml of ethyl acetate, followed by the addition of 79.1 mg (0.396 mmol) of NBD-Cl (1) and 250 μl (1.798 mmol) of triethylamine. The solution was stirred for 1 h and then the solvent was removed by rotary evaporation, leaving 212.9 mg of crude product. In a typical purification procedure, a solution of 69.3 mg of crude product in 0.5 ml of acetone was loaded on a preparative silica TLC plate and eluted with dichloroethane–hexane (3:1). The product (40.4 mg), which appeared as a bright yellow–green band on the plate, was purified by the same method as compound 2 (overall yield, 58%). ^{1}H NMR (d_6-acetone): δ 0.88 (t, 3H, $-CH_2CH_3$), 1.27 (broad s, 16H, $(-CH_2-)_8$), 1.54 (m, 2H, $-SCH_2CH_2CH_2-$), 1.86 (quint., 2H, $-SCH_2CH_2-$), 3.27 (t, 2H, S-CH_2-), 7.13, 7.17, 8.39, 8.43 (-CH=CH-, AB pattern). ^{13}C NMR ($CDCl_3$): δ 14.13 ($-CH_2CH_3$), 22.69, 27.80, 28.89, 29.08, 29.35, 29.42, 29.62, 31.90 (CH_2 carbons), 120.14, 130.71 (-CH=CH-), 132.45, 142.21, 142.49, 149.21 (quaternary carbons). Mass spectrum *m/e* 365.177, found 365.177 (M^+).

2.3. NBD-N'-dodecylamine (NBD-NHR, 4)

The nitrogen derivative of NBD was prepared by dissolving 102.6 mg (0.553 mmol) of laurylamine in 20 ml of dichloromethane, followed by the addition of 99.4 mg (0.497 mmol) of NBD-Cl (1) and stirring of the reaction mixture for 3½ h at room temperature. The solvent was removed by rotary evaporation, leaving 176.5 mg of crude product. In a typical purification procedure, a solution of 70.3 mg of crude product in 1 ml of acetone was loaded on a preparative silica TLC plate and eluted with dichloroethane–hexane (3:1). The product (39.8 mg), which appeared as a bright yellow band around the edge and orange–brown in the centre, was purified by the same method as compound 2 (overall yield, 79%). ^{1}H NMR ($CDCl_3$): δ 0.88 (t, 3H, $-CH_2CH_3$), 1.26 (broad s, 16H, $(-CH_2-)_8$), 1.41 (m, 2H, $-NCH_2CH_2CH_2CH_2-$), 1.82 (quint., 2H, $-NCH_2CH_2CH_2-$), 3.49 (doublet of triplets, 2H, $-HN-CH_2CH_2-$), 6.15, 6.19, 8.48, 8.52 (-CH=CH-, AB pattern). ^{13}C NMR ($CDCl_3$): δ 14.15 ($-CH_2CH_3$), 22.71, 26.97, 28.58, 29.24, 29.36, 29.48, 29.56, 29.63, 29.73, 31.93, 44.04 (CH_2 carbons), 98.52, 136.52 (-CH=CH-), 124.01, 143.88, 143.92, 144.29 (quaternary carbons). Mass spectrum *m/e* 348.216, found 348.216 (M^+).

3. Results and discussion

Compounds 2, 3 and 4 (see Fig. 1) were synthesized as described in Section 2 by modification of standard methods described elsewhere [4]. The

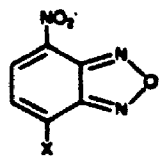

1: X = Cl
2: X = OCH_3
3: X = $S(CH_2)_{11}CH_3$
3a: X = SCH_3
4: X = $NH(CH_2)_{11}CH_3$
4a: X = $NHCH_3$

Fig. 1. Structures of relevant NBD compounds.

TABLE 1. Wavelength (in nm) at the absorption maxima for NBD derivatives in various solvents (in order of increasing polarity)

Solvent	NBD-Cl (1)	NBD-OCH_3 (2)	NBD-SR (3)	NBD-NHR (4)
Hexane	332	358	411	444
Diethylether	335	365	415	449
Dichloromethane	340	373	425	459
Acetonitrile	338	374	422	465
2-Propanol	336	369	417	466
Ethanol	336	373	420	466
Methanol	337	372	419	467

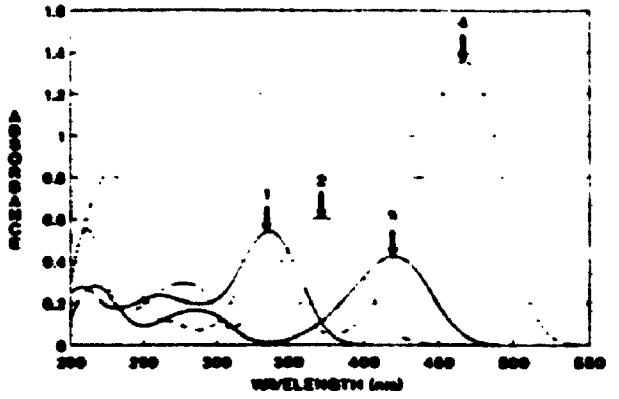

Fig. 2. Wavelength at the absorption maxima for 55 μM solutions of NBD compounds.

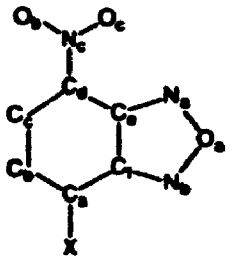

Fig. 3. Framework for geometry optimization of NBD derivatives.

syntheses of compounds 3 and 4 were straightforward and the product was obtained in reasonable yield. Derivatives with dodecyl alkyl chains were chosen as the target molecules because the long alkyl chain facilitated purification of the product from unreacted NBD-Cl by preparative TLC. The dodecyl ether derivative of NBD could not be synthesized because of the low nucleophilicity of dodecyl alcohol and the fact that it was not possible to obtain adequate concentrations of the alcohol in solvents suitable for S_N2 reactions. Moreover, the desired ether product could not be obtained via S_N2 attack of an alkoxide on NBD-Cl since the NBD moiety was not stable in the presence of alkoxides. Accordingly, the methyl ether of NBD (2) was chosen as the representative oxygen-substituted NBD derivative since it could be prepared by allowing NBD-Cl to react in neat methanol in the presence of a weak base.

Each of the compounds 1–4 exhibited distinct colours in the solid phase (NBD-Cl (1) was pale yellow, NBD-methyl ether was orange-yellow, NBD-dodecyl thiol ether was bright yellow and NBD-*N'*-dodecylamine was bright orange) and each compound had a characteristic λ_{max} value in solution (see Table 1, Fig. 2). The initial goal of our research was to account for the different colours of the various NBD derivatives by determining the energies of the molecular orbitals involved in the lowest energy, non-forbidden transitions.

Initially *ab initio* molecular orbital calculations were performed on the benzoxadiazole ring without substituents (see Fig. 3, C_a, C_b, C_c, C_d, C_e, C_f, N_g, O_h, N_i) using the 3-21G basis set to determine the extent of conjugation in the carbon ring. The initial bond lengths for these and all subsequent optimizations were obtained from published sets of data [5]. Two geometry optimizations were performed using the Gaussian 90 computer program [6], one optimizing the bond length of a fully delocalized benzoxadiazole ring (all carbon–carbon bond lengths were initially set to the same value), and one optimizing both the C–C bond length and the C=C bond length of the structure containing fixed alternating double bonds (C_a=C_b, C_c=C_d) and single bonds (C_b–C_c, C_d–C_e, C_e–C_f, C_f–C_a) around the perimeter of the bicyclic NBD ring structure. These calculations indicated that the relative energy for the structure with fixed single and double bonds (as drawn in Fig. 1) was more stable than the energy for the completely delocalized benzoxadiazole by 21 kJ mol^{-1}, and therefore all molecules are expected to have the localized electron conformation.

It was not possible to optimize the geometry of substituted benzoxadiazoles using *ab initio* calculations and the 3-21G basis set due to time, cost and memory constraints. Consequently, the

bond lengths and angles associated with the nitro group and all other substituents on the benzoxadiazole ring were obtained using *ab initio* calculations and the STO-3G basis set. Compounds 3a and 4a were chosen as the respective nitrogen and sulphur derivatives for these calculations since it was too expensive to include the entire dodecyl chain. It was assumed that neither the length of the C–X bond, nor the absorption spectrum, should vary significantly with the length of the alkyl chain on the electron-donating substituents.

Geometry optimization was performed in several stages. First, bonds and angles in the benzoxadiazole ring were optimized, followed by the bonds and angles of the nitro group. With the nitrobenzoxadiazole geometry fixed, the C–N and C–O bond lengths were determined. Because the STO-3G basis set does not adequately calculate equilibrium bond lengths for second row elements [7], the C–X bond lengths for the sulphur and chlorine derivatives were obtained from the literature [8, 9]. The optimized geometries of compounds 1, 2, 3a and 4a are available as supplementary material. The optimized geometry of NBD-Cl (1) was in close agreement with a recently published crystal structure of the molecule which also exhibited alternating single and double bonds in the carbon ring of the benzoxadiazole [8]. Crystal structures of other NBD derivatives have not been published.

The absorption maxima values obtained via *ab initio* STO-3G calculations with the CIS option did not agree well with experimental values (see Table 2). These results were disappointing, but not surprising given the fact that calculations performed using the STO-3G basis set generally do not provide good estimates of excitation energies [7]. Because the predicted absorption maxima from the STO-3G CIS calculations did not correlate well with the experimental results, it was difficult to assess the validity of the molecular orbital coefficients generated with the STO-3G basis set. However, from the calculations it was apparent that, for every molecule, all molecular orbitals involved in allowed visible transitions were π orbitals. Based on this information, we hoped to obtain better prediction of absorption maxima for the NBD derivatives using PPP semi-empirical calculations which consider only the π system of conjugated molecules [9, 10].

TABLE 2. Predicted and experimental wavelengths of the absorption maxima (in nm)

	NBD-OCH$_3$ (2)	NBD-SR (3, 3a)	NBD-NHR (4, 4a)
STO-3G	216	230	225
PPP	380	421	466
Ethanol	373	420	468
Hexane	358	411	444

PPP calculations were performed on compounds 1, 2, 3a and 4a using the optimized geometries obtained from the *ab initio* STO-3G calculations. The semi-empirical parameters for these calculations were taken directly from published sets of data [9]. The oxygen, sulphur and nitrogen substituents were considered part of the π system (*i.e.* as "π-excessive" species) and the chlorine atom was treated as both part of the π system and as a weakly electron-donating substituent.

The PPP results obtained from NBD-Cl (1) were not as conclusive as those for the other derivatives. When the chlorine atom was included in the π system, the calculated λ_{max} value was 380 nm, and the predicted lowest energy transition involved the transfer of electron density from carbon atoms near the chlorine to the nitro group and benzoxadiazole ring. Conversely, when chlorine was treated as a weakly electron-donating substituent (which is not part of the π system), the calculated absorption maximum energy was 323 nm, but the lowest energy transition involved the transfer of electron density from the nitro group to the benzoxadiazole ring. The fact that the experimental λ_{max} values for NBD-Cl (1) (see Table 1) are intermediate between the two calculated values may indicate that chlorine acts both as part of the π system and as an electron-donating substituent in NBD-Cl.

In general, the molecular orbitals predicted to participate in the lowest energy, non-forbidden transition by the PPP calculations were very similar to those predicted by the STO-3G *ab initio* method (see Figs. 4 and 5). The lowest energy transition for all three NBD derivatives appears to be an intramolecular charge transfer-type transition, with a net movement of electron density from the electron-donating substituent to the NBD ring and nitro substituent. This result is consistent with other conjugated amino–nitro systems which also undergo intramolecular charge transfer transitions [9, 11, 12].

The absorption maxima predicted by the PPP calculations showed very good agreement with the experimental results (see Table 2). Given that molecular orbital calculations should predict absorption maxima for molecules in a vacuum [7], it is surprising that the PPP-predicted values agree better with the experimental λ_{max} values obtained

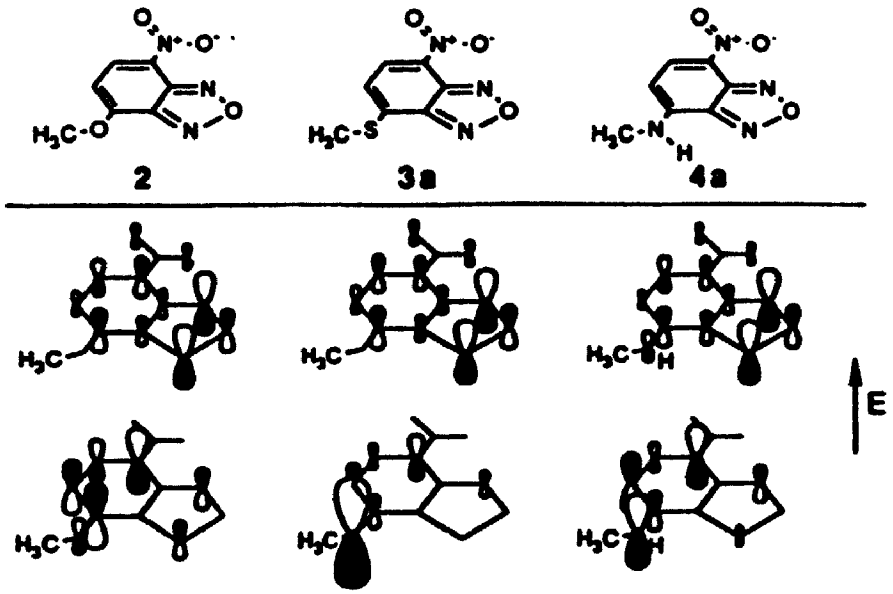

Fig. 4. STO-3G *ab initio* molecular orbital coefficients for lowest energy, non-forbidden transitions of NBD derivatives. Compound 2 transition is from the highest occupied molecular orbital (HOMO) to the lowest unoccupied molecular orbital (LUMO); compounds 3a and 4a transition is from HOMO−1 to LUMO.

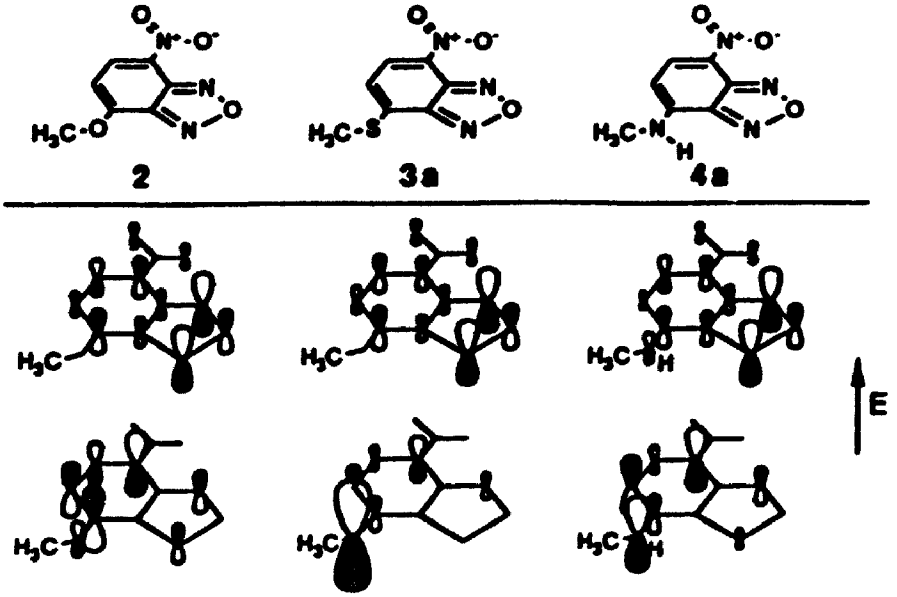

Fig. 5. PPP molecular orbital coefficients for lowest energy, non-forbidden transitions of NBD derivatives. All transitions are HOMO to LUMO.

in ethanol (a polar solvent) than with those results obtained using non-polar hexane. Nevertheless, it is remarkable that all of the PPP-predicted absorption maxima of the NBD derivatives are within 7 nm of the experimental λ_{max} values obtained in ethanol, especially since the parameters used as input were not designed for complex heterocyclic systems such as the benzoxadiazoles. These results illustrate the power of the PPP method for the prediction of absorption maxima.

The agreement between the experimental λ_{max} values and the PPP predictions suggests that other values generated by the program (which were used to calculate the absorption maxima) are also accurate. Of particular interest are the permanent and transition dipole moments associated with the chromophore. The magnitude and orientation of the dipole moments are given in Table 3. For each derivative the permanent dipole moment (of the ground state) and the transition state dipole moment (of the lowest energy, non-forbidden transition) are aligned along axes which deviate by 13° or less from the axis defined by the C–X bond. This result is in agreement with previously published data on NBD nitrogen derivatives [13]. The permanent dipole moments of the first excited state (which are not included) can be calculated as the resultant vector when the transition dipole moment is added to the ground state dipole moment.

Since the lowest energy transitions for compounds 2, 3a and 4a are of an intramolecular charge transfer type, the first excited state of each molecule is expected to have a larger dipole moment than the ground state [9]. Consequently, on moving any of these derivatives from a non-polar to a polar environment, we would expect the first excited state to be stabilized more than the ground state, the result being a decrease in the energy gap between the two states and a corresponding increase in the wavelength of light required for excitation (*i.e.* a red shift). Therefore, according to the dipole moments of NBD derivatives as calculated by the PPP method, we can account qualitatively for the observed red shifts of these molecules which are used extensively in experiments (Table 1).

Also significant is the orientation of the transition dipole moments within the NBD nitrogen and sulphur derivatives. Figure 6 illustrates the magnitude and orientation of the permanent and transition state dipole moments for the sulphur and nitrogen derivatives of NBD. In fluorescence depolarization experiments, reorientation of the transition dipoles of molecules during the lifetime of the excited state causes depolarization of the emitted fluorescence. The extent of depolarization of the emitted light can be correlated with the movement of the fluorophore and/or the group to which it is chemically attached [14]. The transition dipole moments for the nitrogen and sulphur derivatives of NBD, calculated by the PPP method, are aligned along an axis approximately colinear with the bond connecting the nitrogen or sulphur to the ring system (*i.e.* the C–X bond, see Figs. 3 and 6). Therefore, when performing fluorescence depolarization experiments with NBD nitrogen and sulphur derivatives, we can conclude that any depolarization of the emitted light is due to motion of the group to which NBD is attached, and we can exclude the possibility of depolarization due to rotation of the NBD group around the C–X bond.

Energy transfer experiments are used in biological systems to estimate the distance between chemically reactive sites on large biological molecules. In energy transfer experiments, two different chromophores are chemically attached to two different reactive sites on the same molecule, and the energy transfer between the chromophores is measured by exciting one of the two chromophores (the donor) and monitoring for fluorescent emission from the second (the acceptor). For energy transfer to occur the emission transition dipole moment of the donor must be aligned with the absorption transition dipole moment of the acceptor [3]. Therefore, when estimating the distance between sites, we must take into account the freedom of the chromophores to undergo

TABLE 3. *Magnitude*[a] *and orientation*[b] *of permanent dipole moments* (μ) *and transition dipole moments* (μ^*) *of NBD derivatives*

	NBD-OCH$_3$ (2)	NBD-SR (3a)	NBD-NHR (4a)
μ magnitude	3.718	3.417	6.851
μ orientation	11.8	13.0	6.4
μ^* magnitude	0.753	0.734	0.828
μ^* orientation	−5.0	−0.9	9.5

[a]Magnitude is expressed in debyes.
[b]Orientation is expressed in degrees relative to the C–X bond (see Figs. 3 and 6). Positive values indicate rotation in the clockwise direction; negative values represent rotation in the counterclockwise direction.

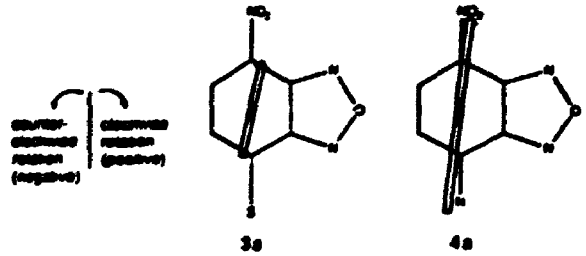

Fig. 6. Magnitude and orientation of dipole moments for nitrogen and sulphur NBD derivatives.

movement of their transition dipole moments. Our PPP results for the nitrogen and sulphur derivatives of NBD indicate that rotation about the C–X bond should not affect the energy transfer to or from NBD derivatives, since it does not change the position of the NBD transition dipole moment (see Fig. 6). Application of these results for NBD derivatives allows the simplification of the models of movement which are used to evaluate geometrical factors influencing energy transfer and more precise distance information can be obtained in energy transfer experiments.

4. Conclusions

The four compounds analysed each had distinct λ_{max} values. STO-3G *ab initio* calculations were not effective for the prediction of the absorption maxima for the four compounds, but gave geometries for the molecules which agreed well with experimental data. These geometries were used as input for semi-empirical PPP calculations which provided good predictions of the observed λ_{max} values. The transition dipole moments calculated by the PPP method account for the observed red shifts of NBD derivatives in polar solvents, and the PPP-predicted orientations of transition dipole moments will permit more precise interpretation of the results obtained when NBD derivatives are used in fluorescence depolarization and energy transfer experiments.

Acknowledgments

Funding for the work described in this paper was provided by a National Science and Engineering Research Council (NSERC) postgraduate fellowship (P.A.P.) and by an NSERC operating grant 3272 (N.O.P.). Special thanks are due to D. Bjarneson for his help with the modification of the PPP program to facilitate its use on our computer system.

References

1 R. P. Haugland, *Handbook of Fluorescent Probes and Research Chemicals*, Molecular Probes, Inc., Eugene, OR, 1989.
2 N. O. Petersen, *Can. J. Chem.*, *63* (1) (1985) 77.
3 D. J. Allen and S. J. Benkovic, *Biochemistry*, *28* (1989) 9506.
4 N. O. Petersen, *Spectrosc. Int. J.*, *2* (1983) 408.
5 L. E. Sutton (ed.), *Tables of Interatomic Distances*, The Chemical Society, London, 1965.
6 M. J. Frisch *et al.*, *Gaussian 90 Computer Program*, Gaussian Inc., Pittsburgh, PA, 1990.
7 W. J. Hehre, *Ab Initio Molecular Orbital Theory*, Wiley, Toronto, Ont., 1986.
8 H. Suzuki, T. Kurihara, T. Kaino and F. Ebisawa, *Acta Crystallogr. Sect. C 44* (1988) 484.
9 J. Griffiths, *Dyes Pigments*, *3* (1982) 211.
10 H. H. Greenwood, *Computing Methods in Quantum Organic Chemistry*, Wiley Interscience, New York, 1972.
11 S. Nagakura, *Pure Appl. Chem.*, *7* (1963) 79.
12 S. Nagakura, *J. Chem. Phys.*, *23* (8) (1955) 1441.
13 H. Suzuki and H. Hiratsuka, *Proc. SPIE Int. Soc. Opt. Eng., Nonlinear Optical Properties of Organic Materials*, Vol. 971, 1988, pp. 97–105.
14 J. Dunyushi, A. Dupuis, B. Lux and P. V. Vignais, *Biochemistry*, *27* (1988) 6288.

PROGRAM FOR CALCULATION OF SACKMAN-EVANS MODEL OF LATERAL DIFFUSION

```
;;z = column to write data to
z=32
;;a = area of diffusant
a=col(31)
r=sqrt(a/3.14)*10^-10
;;converted viscosities x 0.1 to obtain SI units
;;w=viscosity of water
;;h=height of diffusant/membrane thickness
;;m=membrane viscosity
w=0.001
h=10*10^-10
m=0.075
nm=m*h
b1=3*10^6
b2=b1*5.5
b3=(w^2)/nm
;;ep=epsilon defined by Sackman-Evans Theory
ep=r*sqrt((b2+b3)/nm)
;;;;;;;;;;;;;;;;;;;;;;;;;;;;;;;;;;;;;;;;;;;;;;;;;;;;;;;;;;;;;;;;;;;;;;;;;;;;;;;;;;
;;Calculation of Bessel Functions
;;Formulas from Numerical
;;Recipees for Fortran 2nd ed.
;;;;;;;;;;;;;;;;;;;;;;;;;;;;;;;;;;;;;;;;;;;;;;;;;;;;;;;;;;;;;;;;;;;;;;;;;;;;;;;;;;
x=ep
y=(x/3.75)^2
i0=1+y*(3.5156229+y*(3.0899424+y*(1.2067492+y*(0.2659732+y*(0.0360768
+y*( 0.0045813))))))
```

```
;;;;;;;;;;;;;;;;;;;;;;;;;;;;;;;;;;;;;;;;;;;;;;;;;;;;;;;;;;;;;;;;;;;;;;;;;;;;;;;;;
y2=x*x/4
k0=((-ln(x/2))*(i0))+
  (-0.57721566+y2*(0.42278420+y2*(0.23069756+y2*(0.03488590
+y2*(0.00262698+y2*(0.00010750+y*0.0000074))))))
;;;;;;;;;;;;;;;;;;;;;;;;;;;;;;;;;;;;;;;;;;;;;;;;;;;;;;;;;;;;;;;;;;;;;;;;;;;;;;;;;
i1=x*(0.5+y*(0.87890594+y*(0.51498869+y*(0.1508493
+y*(0.02658733+y*(0.00301532+y*0.00032411))))))
;;;;;;;;;;;;;;;;;;;;;;;;;;;;;;;;;;;;;;;;;;;;;;;;;;;;;;;;;;;;;;;;;;;;;;;;;;;;;;;;;
k1=(ln(x/2)*(i1))+(1/x)*(1+y2*(1.5443144+y2*(-0.67278579+y2*
  (-0.18156897+y2*(-0.01919402+y2*(-0.00110404+y2*-0.00004686))))))
;;;;;;;;;;;;;;;;;;;;;;;;;;;;;;;;;;;;;;;;;;;;;;;;;;;;;;;;;;;;;;;;;;;;;;;;;;;;;;;;;
;;;;;;;;;;;;;;;;;;;;;;;;;;;;;;;;;;;;;;;;;;;;;;;;;;;;;;;;;;;;;;;;;;;;;;;;;;;;;;;;;
;;Transform to Calculate Sackman-Evans model of Diffusion
;;;;;;;;;;;;;;;;;;;;;;;;;;;;;;;;;;;;;;;;;;;;;;;;;;;;;;;;;;;;;;;;;;;;;;;;;;;;;;;;;
;;;;;;;;;;;;;;;;;;;;;;;;;;;;;;;;;;;;;;;;;;;;;;;;;;;;;;;;;;;;;;;;;;;;;;;;;;;;;;;;;
k=1.38066*10^-23
T=273.15+36
;;Q=Bessel Function Factor
Q=k1/k0
;;C is the pre-bracket constant
C=k*T/(4*3.14*nm)
;;Calculation of diffusion coefficient
d1=C/(((ep^2)/4)*(1+(b1/b2))+ep*Q)
;;Convert to micrometers per second
col(z)=d1*10^12
```